JLAB-THY-02-??
WM-02-104
nucl-th/02????

Covariant description of inelastic electron–deuteron scattering: predictions of the relativistic impulse approximation

J. Adam, Jr.[1,2], Franz Gross[1,3], Sabine Jeschonnek[1,4], Paul Ulmer[5] and J. W. Van Orden[1,5]

[1] *Jefferson Lab, 12000 Jefferson Avenue, Newport News, VA 23606*
[2] *Nuclear Physics Institute, Řež near Prague, CZ-25068, Czech Republic*
[3] *Department of Physics, College of William and Mary, Williamsburg, VA 23185*
[4] *The Ohio State University, Physics Department, Lima, OH 45804*
[5] *Department of Physics, Old Dominion University, Norfolk, VA 23529*

(Dated: April 19, 2002)

Abstract

Using the covariant spectator theory and the transversity formalism, the unpolarized, coincidence cross section for deuteron electrodisintegration, $d(e,e'p)n$, is studied. The relativistic kinematics are reviewed, and simple theoretical formulae for the relativistic impulse approximation (RIA) are derived and discussed. Numerical predictions for the scattering in the high Q^2 region obtained from the RIA and five other approximations are presented and compared. We conclude that measurements of the unpolarized coincidence cross section and the asymmetry A_ϕ, to an accuracy that will distinguish between different theoretical models, is feasible over most of the wide kinematic range accessible at Jefferson Lab.

PACS numbers: 21.45.+v,25.10.+s,25.30.Fj

I. INTRODUCTION

Inelastic scattering of electrons from the deuteron is an important source of information about the nuclear current, deuteron structure, and the NN force. The exclusive scattering cross section, $d(e,e'p)n$, was first measured almost forty years ago [1], and since then it has been measured under a wide variety of kinematic conditions [2]. There is a substantial body of data for this reaction, including cross section measurements [3–6] as well as separations of various response functions [7–16] which differentiate between absorption of longitudinal and transverse photons.

In this paper we survey results that might be expected from a new generation of $d(e,e'p)n$ coincidence measurements proposed for Jefferson Laboratory (JLab). At JLab it is possible to carry out a comprehensive program of measurements at both high Q^2 and large W (where W is the invariant mass of the final np state). A broad program of such measurements offers the best hope of independently determining effects of final state interactions and the nuclear current, permitting the extraction of important new information about the short range NN interaction.

Electrodisintegration of the deuteron has been studied theoretically by many groups. Recently, Arenhövel, Beck, and Wilbois [17] have emphasized that the relativistic effects in inelastic scattering can be very large, even at modest momenta, and it is therefore particularly important to have a fully relativistic theory available for the analysis of the higher momenta data that will be measured at JLab. Relativistic calculations of this reaction date back to the early work of Durand [18] and McGee [19] and lead up to more recent work by Tjon [20]. One of the goals of this paper is to present a fully modern, covariant treatment of this process suitable for the analysis of JLab data.

This paper imbeds the dynamical calculation in the general formalism developed in Ref. [21], where a covariant, systematic treatment of most of the polarization observables that can be measured in the $d(e,e'p)n$ reaction were classified and defined. There it was found that the use of transversity amplitudes (closely related to helicity amplitudes) gave a very efficient description of the reaction. Transversity amplitudes were discussed by Moravcsik [22], who found that they build in the constraints imposed by parity and rotational invariance in the most efficient way. In a transversity basis, the constraints imposed by these symmetries insure that half of the possible amplitudes vanish identically, so that the cumbersome linear relations needed in other formalisms [23] are unnecessary. This economy will be essential some time in the future when large data sets exist, and it may be important to know whether or not a proposed new measurement will really be independent of amplitudes already measured.

The details of the calculation are carried out using the covariant spectator theory, which has been successfully applied to the description of NN scattering [24] and the electromagnetic form factors of the deuteron [25]. One feature of this theory is that the deuteron bound state is described by the covariant dnp vertex with one nucleon on mass-shell, and this is precisely the amplitude that is needed for the relativistic impulse approximation (RIA), making the theory well suited to the analysis of the $d(e,e'p)n$ coincidence reaction [26]. In this first application of the covariant spectator theory using the transversity basis, we present the RIA calculation only. This provides the opportunity to work out several new technical details for the simplest case, and to compare to other approximations. The inclusion of final state interactions and interaction currents will be the subject of future work.

A second purpose of this paper is to estimate the size of the unpolarized $d(e,e'p)n$ cross sections expected over the broad range of Q^2 and W accessible to JLab. In preparing this survey we found that relativistic and nonrelativistic predictions for $d(e,e'p)n$ at high Q^2, where the cross section is most sensitive to the theory, often differ by as much as an order of magnitude, extending the observations of Arenhövel, Beck, and Wilbois [17]. Since nonrelativistic calculations cannot be taken seriously at such high energies, we report our results for a variety of relativistic or semi-relativistic models only. In this first exploratory study the goal is to provide only a rough survey of the landscape. The simplicity of the RIA allows a uniform treatment over the entire kinematic range, but is, of course, very incomplete. It is our intention to follow up this study with complete calculations for cases where the theoretical effects look especially interesting.

Our notation for the cross section and the spectator theory for the RIA are reviewed briefly in Sec. II, numerical results presented in Sec. III, and conclusions given in Sec. IV. Many theoretical details are given in the several Appendices, which are an important part of this paper.

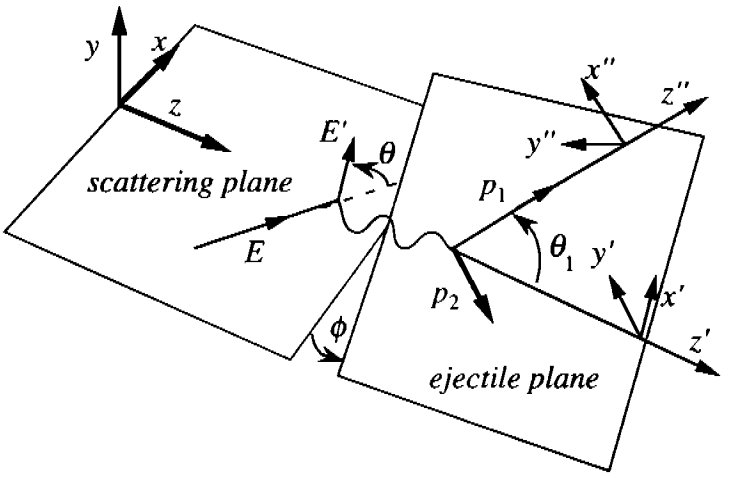

FIG. 1: The kinematics of electron scattering when the final hadronic state is broken into two fragments with momenta p_1 and p_2.

II. THEORY

In this section we define the coincidence cross section and the RIA matrix element. All other theoretical details can be found in the Appendices.

A. The Cross Section

Figure 1 shows the kinematics for the process $e + d \rightarrow e' + p + n$ (using the notation of Ref. [21]). The incident and scattered electron momenta form a plane called the "scattering plane" while the momenta of the proton and neutron in the final state form a second plane called the "ejectile plane." The virtual photon momentum is common to the two planes and is chosen as the direction of the z-axis. The two planes, which are represented by the (x, y, z) and (x', y', z') coordinate systems, are oriented at a relative azimuthal angle of ϕ. A rotation of the response tensor (defined below) from the unprimed to the primed frame can be used to extract all of the ϕ dependence from the tensor. Using this along with the explicit form of the electron tensor, the cross section can be shown to be of the form (c.f. Eq. (95) of Ref. [21])

$$\begin{aligned}\frac{d^5\sigma}{d\Omega' dE' d\Sigma} &= \frac{\sigma_M}{4\pi M_d}\frac{Q^2}{q_L^2}\Big\{\tilde{R}_L^{(\mathrm{I})} + s_T\tilde{R}_T^{(\mathrm{I})} - \frac{1}{2}\left[\cos 2\phi\tilde{R}_{TT}^{(\mathrm{I})} + \sin 2\phi\tilde{R}_{TT}^{(\mathrm{II})}\right] \\ &+ s_{LT}\left[\cos\phi\tilde{R}_{LT}^{(\mathrm{I})} + \sin\phi\tilde{R}_{LT}^{(\mathrm{II})}\right] + 2h\ s_{T'}\tilde{R}_{T'}^{(\mathrm{II})} \\ &+ 2h\ s_{LT'}\left[\sin\phi\tilde{R}_{LT'}^{(\mathrm{I})} + \cos\phi\tilde{R}_{LT'}^{(\mathrm{II})}\right]\Big\} \end{aligned} \tag{2.1}$$

where

$$\sigma_M = \left[\frac{\alpha\cos\frac{1}{2}\theta}{2E\sin^2\frac{1}{2}\theta}\right]^2 \tag{2.2}$$

is the Mott cross section and $d\Sigma$ is defined below. The quantities θ, E, E', and Ω' are the electron scattering angle, the energies of the initial and final electron, and the solid angle of the final electron, all in the lab frame. The deuteron mass is M_d and $h = \pm 1/2$ is the helicity of the incident electron. The electron kinematical factors are

$$\begin{aligned} s_T &= \tfrac{1}{2} + \xi^2 & s_{LT} &= -\frac{1}{\sqrt{2}}\left(1+\xi^2\right)^{\frac{1}{2}} \\ s_{T'} &= \xi\left(1+\xi^2\right)^{\frac{1}{2}} & s_{LT'} &= -\frac{1}{\sqrt{2}}\xi \end{aligned} \tag{2.3}$$

where

$$\xi = \frac{q_L}{Q}\tan\frac{\theta}{2} \tag{2.4}$$

with

$$q^2 = -Q^2 = \nu^2 - q_L^2 = \nu_0^2 - q_0^2 \tag{2.5}$$

the square of the virtual photon four-momentum, with $\{\nu, \mathbf{q}_L\}$ and $\{\nu_0, \mathbf{q}_0\}$ the energy and three-momentum of the virtual photon in the lab and c.m. systems, respectively, and $q_0 = |\mathbf{q}_0|$, etc.

There are two inertial reference frames that are of interest in the calculation of deuteron electrodisintegration: the laboratory frame which coincides with the rest frame of the target deuteron, and the center of momentum (c.m.) frame in which the total three-momentum of the final state proton-neutron pair (or of the initial virtual photon and the target deuteron) is zero. One of the virtues of Eq. (2.1) is that the response functions $\tilde{R}$ are *covariant*, and hence (2.1) can be used to describe the cross section in either the c.m. of the outgoing np pair or the laboratory frame by the replacement of $d\Sigma$ by

$$d\Sigma|_{cm} = \mathrm{p}\; d\Omega^* \tag{2.6}$$

in the c.m. frame or

$$d\Sigma|_{lab} = \mathrm{p}_1\; d\Omega_1\; \mathcal{R} \tag{2.7}$$

in the laboratory frame. [Except for special notation used in Eq. (2.5), we use a roman character for the magnitude of a three-momentum, so that $\mathrm{p}_1 = |\mathbf{p}_1|$, to distinguish it from the corresponding four-momentum, p_1.] The factor

$$\mathcal{R} = \frac{W}{M_d}\;\frac{1}{\left(1+\dfrac{\nu \mathrm{p}_1 - E_1 q\cos\theta_1}{M_d \mathrm{p}_1}\right)_L} \tag{2.8}$$

is the recoil factor, where W is the invariant mass of the outgoing pair and the subscript L means that each variable in the parentheses is to be replaced by its value in the lab frame (for example, $q \to q_L$ and p_1 is a function of θ_1, the angle between the outgoing proton and the $\hat{z}$ axis in the lab system). We will sometimes use an asterisk (*) to denote a variable in the c.m. system. Notation for some of the most important variables is summarized in Table I.

The c.m. frame (referred to as the "antilab" frame in Ref. [17]) is of interest for theoretical reasons because integrating over the final state kinematical variables is particularly convenient in this frame and the partial wave expansion of the final state is normally carried out in this frame. While this partial wave expansion is particularly convenient at low and

TABLE I: Notation for frequently used variables.

variable	Lab	c.m.
photon energy	ν	ν_0
magnitude of photon 3-momentum	q_L	q_0
deuteron 4-momentum	P	P^*
deuteron energy	M_d	D_0
proton 4-momentum	p_1	p_1^*
neutron 4-momentum	p_2	p_2^*
proton angle	θ_1	θ^*
neutron angle	θ_2	$\theta^* + \pi$
magnitude of proton 3-momentum	p_1	p
magnitude of neutron 3-momentum	p_2	p

medium energies of a few hundred MeV, we would like to point out that the partial wave approach becomes extremely tedious and/or impractical at GeV energies. At such energies Glauber theory [27], or the new so-called "three-dimensional" methods of calculating the NN amplitude directly without partial wave expansions [28], are better. In any case, since the final scattering state is by far the most complicated ingredient in the calculation of the transition matrix elements, it is important to be able to carry out calculations in this frame and to translate them to the lab frame. The necessity of boosting the calculation from the c.m. frame to the lab frame requires that the Lorentz properties of the matrix elements be understood. This goal is conveniently accomplished by using the Jacob and Wick helicity formalism [29] provided that it can be shown that the various ingredients in the calculation of the matrix elements, such as the wave functions, are covariant. We will assume for the moment that this is the case and will demonstrate later that it is true for the particular calculations which are described in this paper.

The nine response functions of (2.1) are related to sums over the squares of matrix elements of the deuteron current. In the helicity basis, with λ_γ the helicity of the virtual photon, λ_1 and λ_2 the helicities of particles 1 and 2 in the final state, and λ_d the helicity of the initial deuteron, the current operator is written $\left\langle \lambda_1 \lambda_2 \left| J_{\lambda_\gamma}(q) \right| \lambda_d \right\rangle$. Following the conventions of Jacob and Wick [29] we choose particle 1 in the final state to be the proton and particle 2 to be the neutron. The current operator conserves parity, which means that the matrix elements satisfy the condition

$$\left\langle \lambda_1 \lambda_2 \left| J_{\lambda_\gamma}(q) \right| \lambda_d \right\rangle = \pm \left\langle -\lambda_1, -\lambda_2 \left| J_{-\lambda_\gamma}(q) \right| -\lambda_d \right\rangle , \tag{2.9}$$

where the phase depends on the helicities (see Ref [21]). For this reason it is convenient to introduce symmetric and antisymmetric combinations of the $|\lambda_\gamma| = 1$ amplitudes

$$\begin{aligned} J^{\lambda_d}_{s\,\lambda_1\,\lambda_2}(p_1, p_2, q) \equiv \langle \lambda_1 \lambda_2 \left| J_s(q) \right| \lambda_d \rangle &= \frac{1}{2}\Big\{ \langle \lambda_1 \lambda_2 \left| J_1(q) \right| \lambda_d \rangle - \langle \lambda_1 \lambda_2 \left| J_{-1}(q) \right| \lambda_d \rangle \Big\} \\ J^{\lambda_d}_{a\,\lambda_1\,\lambda_2}(p_1, p_2, q) \equiv \langle \lambda_1 \lambda_2 \left| J_a(q) \right| \lambda_d \rangle &= \frac{1}{2}\Big\{ \langle \lambda_1 \lambda_2 \left| J_1(q) \right| \lambda_d \rangle + \langle \lambda_1 \lambda_2 \left| J_{-1}(q) \right| \lambda_d \rangle \Big\} , \end{aligned} \tag{2.10}$$

where, because of the phases, J_s is *symmetric* under the Y parity transformation (parity followed by rotation by π about the y axis) and J_a is *antisymmetric* (and we note for future

TABLE II: Response functions.

$\tilde{R}_L^{(\mathrm{I})} = R_{00}$	
$\tilde{R}_T^{(\mathrm{I})} = 2(R_{aa} + R_{ss})$	$\tilde{R}_{T'}^{(\mathrm{II})} = 4\mathrm{Re}\ R_{sa}$
$\tilde{R}_{TT}^{(\mathrm{I})} = 2(R_{aa} - R_{ss})$	$\tilde{R}_{TT}^{(\mathrm{II})} = -4\mathrm{Im}\ R_{sa}$
$\tilde{R}_{LT}^{(\mathrm{I})} = 4\mathrm{Re}\ R_{0s}$	$\tilde{R}_{LT}^{(\mathrm{II})} = 4\mathrm{Im}\ R_{0a}$
$\tilde{R}_{LT'}^{(\mathrm{I})} = 4\mathrm{Im}\ R_{0s}$	$\tilde{R}_{LT'}^{(\mathrm{II})} = 4\mathrm{Re}\ R_{0a}$

reference that $J^{\lambda_d}_{0\,\lambda_1\,\lambda_2} \equiv \langle \lambda_1 \lambda_2 \,|J_0(q)|\, \lambda_d \rangle$ is also *symmetric*). We then define the deuteron response tensors $R^{(\mathrm{I})}_{gg'}$ and $R^{(\mathrm{II})}_{gg'}$

$$R^{(\mathrm{I})}_{gg'} = \frac{m^2}{2\pi^2 W} \sum_{\substack{\lambda'_1\lambda_1\lambda_2 \\ \lambda'_d\lambda_d}} \sum_{\rho=\pm} \left\{ (\rho^\rho_N)_{\lambda'_1\lambda_1}\, J^{\lambda_d}_{g\,\lambda_1\lambda_2}(p_1,p_2,q)\, (\rho^\rho_D)_{\lambda_d\lambda'_d}\, J^{\dagger\,\lambda'_d}_{g'\,\lambda'_1\lambda_2}(p_1,p_2,q) \right\}$$

$$R^{(\mathrm{II})}_{gg'} = \frac{m^2}{2\pi^2 W} \sum_{\substack{\lambda'_1\lambda_1\lambda_2 \\ \lambda'_d\lambda_d\rho}} \sum_{\rho=\pm} \left\{ (\rho^\rho_N)_{\lambda'_1\lambda_1}\, J^{\lambda_d}_{g\,\lambda_1\lambda_2}(p_1,p_2,q)\, (\rho^{(-\rho)}_D)_{\lambda_d\lambda'_d}\, J^{\dagger\,\lambda'_d}_{g'\,\lambda'_1\lambda_2}(p_1,p_2,q) \right\}, \quad (2.11)$$

where g and $g' = \{0, s, a\}$, and ρ^ρ_N and ρ^ρ_D are the spin density matrices for one nucleon in the final state or the deuteron target, with ρ^+ being the part of the density matrix *symmetric* under Y parity and ρ^- the part *antisymmetric* under Y parity. Symmetry under the Y parity operation then insures that those observables of type (II) must include one, and only one factor of the antisymmetric current J_a (further details can be found in Ref. [21]). The relation between the nine response functions that appear in Eq. (2.1) and the tensors defined in (2.11) are given in Table II. The normalization of Eq. (2.11) and the density matrices is consistent, for unpolarized reactions, to summing over final state spins and averaging over the initial deuteron spin.

For unpolarized particles,

$$\begin{aligned} (\rho^+_N)_{\lambda'_1\lambda_1} &= \frac{1}{2}\delta_{\lambda'_1\lambda_1} \qquad (\rho^-_N)_{\lambda'_1\lambda_1} = 0 \\ (\rho^+_D)_{\lambda_d\lambda'_d} &= \frac{1}{3}\delta_{\lambda_d\lambda'_d} \qquad (\rho^-_D)_{\lambda_d\lambda'_d} = 0\,, \end{aligned} \quad (2.12)$$

so the observables of type (II) are zero. If we also limit discussion to unpolarized electrons, the terms proportional to the electron helicity h average to zero, and the cross section depends on only 4 response functions:

$$\frac{d^5\sigma}{d\Omega' dE' d\Sigma} = \frac{\sigma_M}{4\pi M_d}\frac{Q^2}{q_L^2}\left\{ \tilde{R}_L^{(\mathrm{I})} + s_T \tilde{R}_T^{(\mathrm{I})} - \frac{1}{2}\cos 2\phi\ \tilde{R}_{TT}^{(\mathrm{I})} + s_{LT}\cos\phi\ \tilde{R}_{LT}^{(\mathrm{I})} \right\} \quad (2.13)$$

A second, independent combination of the same four response functions gives the asymmetry

$$A_\phi = \frac{\frac{d^5\sigma}{d\Omega' dE' d\Sigma}(\phi=0) - \frac{d^5\sigma}{d\Omega' dE' d\Sigma}(\phi=\pi)}{\frac{d^5\sigma}{d\Omega' dE' d\Sigma}(\phi=0) + \frac{d^5\sigma}{d\Omega' dE' d\Sigma}(\phi=\pi)} = \frac{s_{LT}\tilde{R}_{LT}^{(\mathrm{I})}}{\tilde{R}_L^{(\mathrm{I})} + s_T\tilde{R}_T^{(\mathrm{I})} - \frac{1}{2}\tilde{R}_{TT}^{(\mathrm{I})}} \quad (2.14)$$

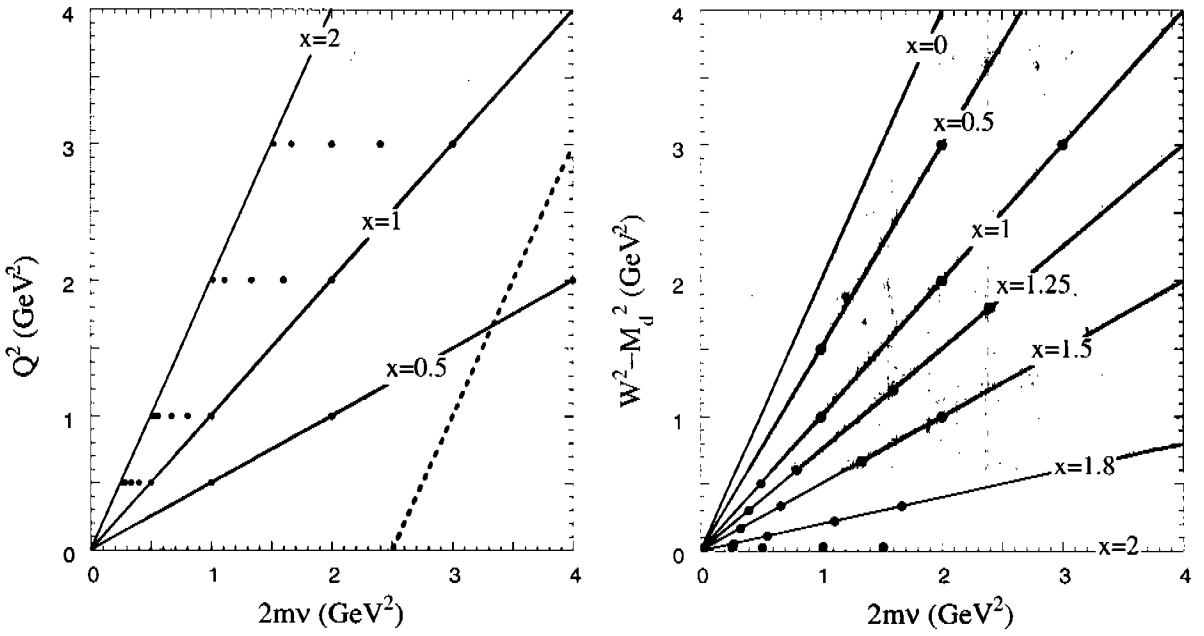

FIG. 2: Left panel is the $Q^2\nu$ plane, and the right panel the $W^2\nu$ plane. In each panel lines with constant x are shown, and the cases analyzed in the following section are shown as dots. The shaded area in each panel is the region where pion production is kinematically possible. Note that pions cannot be produced near the line $x = 2$, but that inelasticity sets in even at small Q^2 along the quasielastic ridge ($x = 1$) and at smaller values of x. The dashed line in the left panel corresponds to $W^2 = 9m^2$, just above the region shown in the right panel.

where the electron kinematics is held fixed and the outgoing proton is measured forward to the direction of the virtual photon momentum $\mathbf{q}$ (at $\phi = 0$) and backward (at $\phi = \pi$). The longitudinal contributions $\tilde{R}_L^{(\mathrm{I})} - \frac{1}{2}\tilde{R}_{TT}^{(\mathrm{I})}$ can be separated from the transverse response $\tilde{R}_T^{(\mathrm{I})}$ by measuring the cross section for the same kinematics at forward and backward electron scattering angles, but the transverse interference term $\tilde{R}_{TT}^{(\mathrm{I})}$ can be separated from $\tilde{R}_L^{(\mathrm{I})}$ only by an out-of plane measurement (for example, $\phi = \pi/2$).

These four unpolarized structure functions are only a small fraction of the structure functions which can be measured. With *polarized* electrons, targets, and recoiling nucleons many more can be studied [21, 23], but these observables tend to be very sensitive to final state interactions and interaction currents. In this first paper we have omitted final state interactions and interaction currents, and hence also limit the discussion to unpolarized observables.

B. Kinematics

The response functions $\tilde{R}$ depend on three variables: Q^2, ν, and the angle θ_1 between $\mathbf{p}_1$ and $\mathbf{q}$, where $\mathbf{p}_1$ is the three-momentum of the particle detected in coincidence with the final electron (assumed here to be the proton). The variables Q^2 and ν are fixed by the virtual photon, and we choose θ^* (the lab value of θ_1) rather than θ_1 because it is independent of Q^2 and ν and always varies between 0 and π. In place of ν, it is often convenient to use W^2 or $x = Q^2/2m\nu$, the Bjorken scaling variable. The mass of the final state, W, is related to

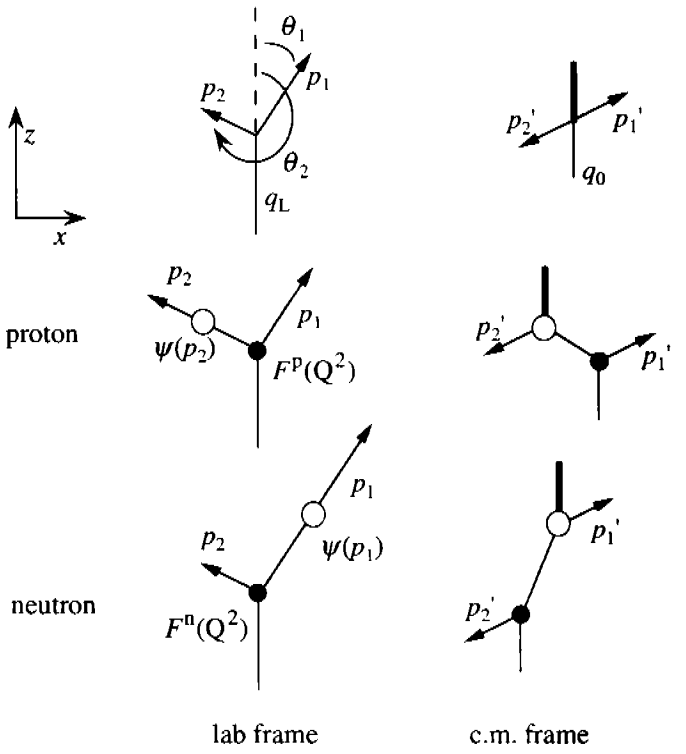

FIG. 3: The relativistic impulse approximation (RIA) to deuteron electrodisintegration in the lab frame and the c.m. frame. The open circle denotes the deuteron wave function, the filled circle the nucleon form factor, and the nucleon propagating between the two is off-shell. Note that the wave functions ψ always have one particle off-shell.

ν (or x) by

$$\begin{aligned} W^2 &= M_d^2 + 2M_d\nu - Q^2 \\ &= M_d^2 + 2M_d\nu\left(1 - \frac{mx}{M_d}\right) \end{aligned} \tag{2.15}$$

The region of allowed values of Q^2 and ν is shown in Fig. 2. If the scattering is elastic, so that the deuteron remains bound after the scattering, $x \simeq 2$, and this defines one boundary of the allowed scattering region. It is sometimes assumed that pions must necessarily be produced as Q^2 increases, but as long as x remains close to 2, the final state remains below the pion production threshold up to very large values of Q^2, and one may try to explain the large Q^2 behavior of these inelastic processes using a theory with no pion rescattering in the final state. The line $x = 1$ is the quasielastic peak; when Q^2 is large the region between $x = 1$ and $x = 0$ is the region where y (or x) scaling is observed. If x is small, pions will be produced more and more easily as Q^2 increases (penetrating further and further into the shaded region in Fig. 2), and explicit treatment of the pion degrees of freedom will be necessary.

The variables Q^2, ν (or x or W^2), and θ^* are convenient for thinking about final state interactions. However the RIA depends primarily on only two variables, Q^2 and $p_{\rm miss}$, where $p_{\rm miss}$ is the value of the *spectator* momentum in the lab system. The spectator momentum $p_{\rm miss}$ may be either $\rm p_1$ or $\rm p_2$ depending on which of the two nucleons was struck by the virtual photon (in the absence of final state interactions or interaction currents, this is all that can

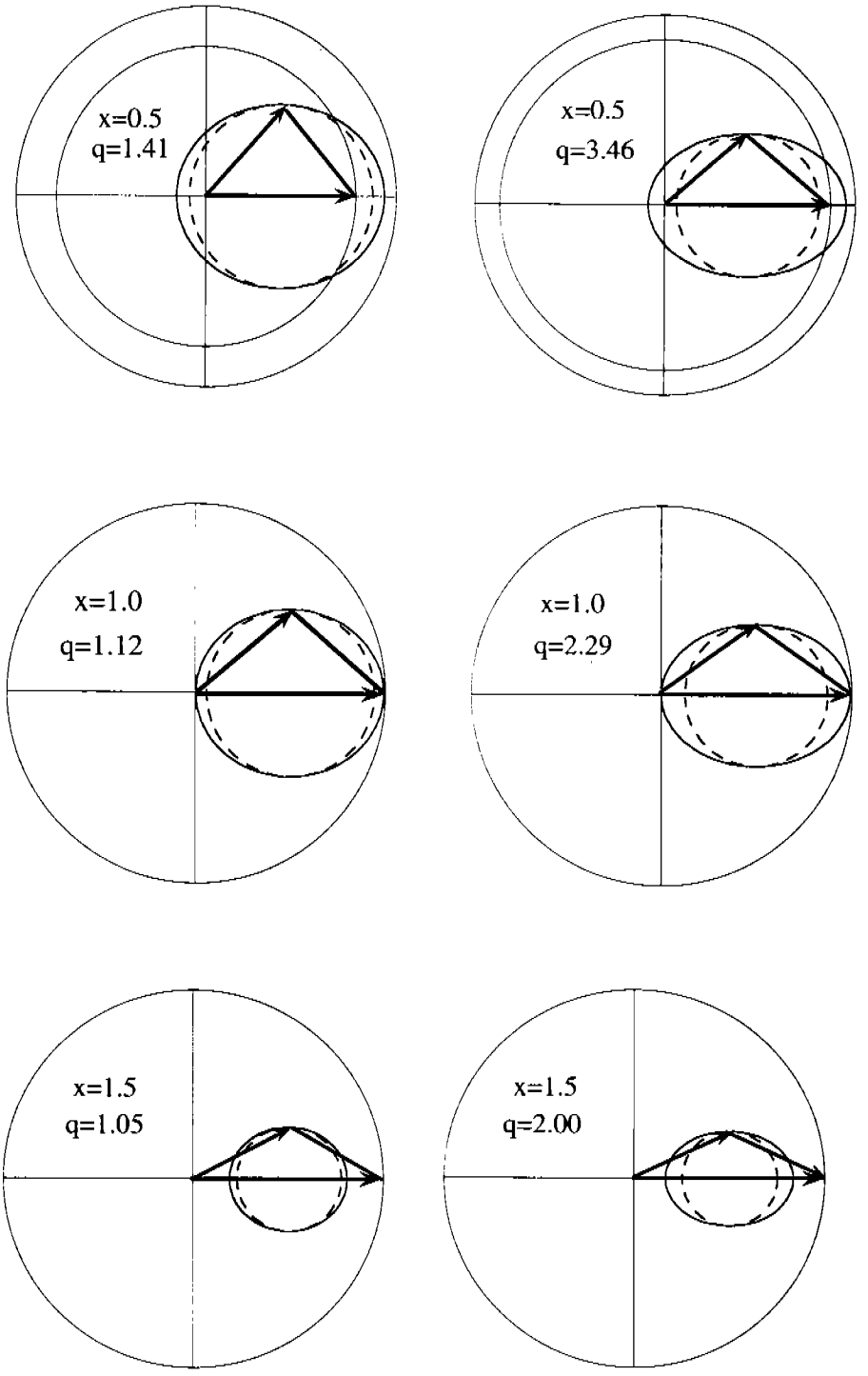

FIG. 4: Polar plots showing the locus of the momentum vector $\mathbf{p}_1$ in the lab system (solid lines are relativistic; dashed lines nonrelativistic). The horizontal axis in each panel is $\hat{z}$; the vertical is $\hat{x}$. The three left hand panels have $Q^2 = 1$ GeV^2 and the various values of x and q shown on each panel; the right hand panels are for $Q^2 = 3$ GeV^2. In all panels the $\mathbf{q}$ vector points to the right along the $\hat{z}$ axis and sets the scale. The other two vectors are $\mathbf{p}_1$ and $\mathbf{p}_2$ for the symmetry case discussed in the text.

happen), and the cross section is therefore the coherent sum of two terms. Symbolically, the RIA current is

$$J_{\rm RIA}(p_1,p_2,q) = \left| F^p(Q^2)\psi(\mathrm{p}_2) \pm F^n(Q^2)\psi(\mathrm{p}_1) \right|^2 , \tag{2.16}$$

where explicit formulae for the magnitudes of the rest frame three momenta, p_1 and p_2, are given in Eq. (2.19) below. The two terms contributing to this sum are illustrated in Fig. 3. Since $\psi(\mathrm{p})$ is normally a rapidly decreasing function of p, these two terms are normally dominated by the one with the smallest $p_{\rm miss}$.

The momenta $\mathbf{p}_1$ and $\mathbf{p}_2$ are most easily obtained by boosting from the c.m. frame. Their x and z components are

$$\begin{aligned} \mathbf{p}_i^x &= \pm \mathrm{p} \sin\theta^* \\ \mathbf{p}_i^z &= \frac{q_L}{2} \pm \mathrm{p}\frac{E_W}{W}\cos\theta^* \end{aligned} \tag{2.17}$$

where the upper (lower) sign is for $i = 1$ ($i = 2$). p is the magnitude of the nucleon momenta in the c.m. frame, E_W is the energy of the outgoing pair in the lab frame, with

$$\begin{aligned} \mathrm{p} &= \sqrt{\frac{[W^2-(m_1+m_2)^2][W^2-(m_1-m_2)^2]}{4W^2}} \simeq \frac{1}{2}\sqrt{W^2-4m^2} \\ E_W &= \sqrt{W^2+q_L^2} = M_d + \nu \,, \end{aligned} \tag{2.18}$$

and the other variables were previously defined (recall Table I). Hence

$$\mathrm{p}_i^2 = \left(\frac{q_L}{2} \pm \mathrm{p}\frac{E_W}{W}\cos\theta^*\right)^2 + \mathrm{p}^2\sin^2\theta^* \tag{2.19}$$

The behavior of the magnitudes of p_1 and p_2, and the angles θ_1 and θ_2, for six choices of Q^2 and x, can be inferred from Fig. 4. The solid lines in each panel are the locus of points swept out by Eq. (2.17), and the dashed lines by (2.17) with $E_W = W$ (for a Galilean boost). For $x \geq 1$ the two vectors $\mathbf{p}_1$ and $\mathbf{p}_2$ always lie in the first or third quadrant, but for $x < 1$ the vectors may lie in any quadrant.

The restriction of both momenta $\mathbf{p}_1$ and $\mathbf{p}_2$ to the first and third quadrant, which happens for $x > 1$, produces a curious singularity in the lab cross section. Under these conditions, the lab angle θ_1 will reach a maximum value less than 90° at a c.m. angle $\theta^* = \theta^*_{\rm crit}$. At this point

$$\left.\frac{d\theta_1}{d\theta^*}\right|_{\theta^*_{\rm crit}} = 0 \,. \tag{2.20}$$

The differential cross section in the c.m. is always finite, but the lab cross section, defined by the transformation

$$d\sigma = d\theta^*\,|M_{\rm c.m.}(\theta^*_{\rm crit})|^2 = d\theta_1\,|M_{\rm lab}(\theta^*_{\rm crit})|^2 \equiv d\theta_1\,\frac{|M_{\rm c.m.}(\theta^*_{\rm crit})|^2}{d\theta_1/d\theta^*} \,, \tag{2.21}$$

has a singularity at the critical point because of the vanishing of the Jacobian (2.20). This singularity is analyzed in detail in Appendix C. In this paper we present c.m. cross sections only, so we do not encounter this singularity.

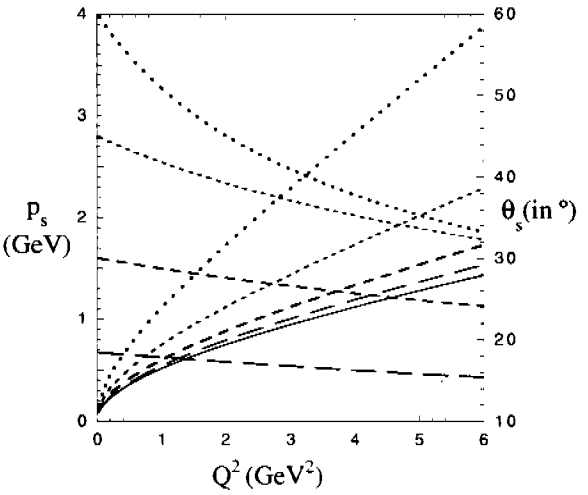

FIG. 5: The symmetry momenta p_s and the symmetry angles θ_s as functions of Q^2 for five values of x: $x = 2$ (solid line), 1.8 (long dashes), 1.5 (medium dashes), 1.0 (dashes) and 0.5 (dots). The momenta rise with Q^2 and the angles fall with Q^2. For $x = 2$ the angle $\theta_s = 0$ and is not shown.

For the special case when $\theta^* = \pi/2$ (where the relativistic ellipse touches the nonrelativistic circle) the magnitudes of $\mathbf{p}_1$ and $\mathbf{p}_2$ are equal, and the RIA depends uniquely on the wave function at only one momentum point. We will refer to this as the *symmetry point*. Since the angle between $\mathbf{p}_1$ and $\mathbf{p}_2$ is 90° in the nonrelativistic limit, this is referred to as perpendicular kinematics. Were there no final state interactions or interaction currents, the symmetry point would be an optimal place to measure the wave function. The symmetry point momenta $p_s = |\mathbf{p}_1| = |\mathbf{p}_2|$ and angles $\theta_s = \theta_1 = -\theta_2$ are

$$\begin{aligned} p_s = &\quad \sqrt{\mathrm{p}^2 + q^2} \simeq \frac{Q}{4mx}\sqrt{8m^2x + Q^2} \\ \theta_s = &\quad \tan^{-1}\left[\frac{2\mathrm{p}}{q}\right] \simeq \tan^{-1}\left[\sqrt{\frac{4m^2x(2-x)}{4m^2x^2 + Q^2}}\right] . \end{aligned} \tag{2.22}$$

These are shown in Fig. 5 as a function of Q^2 for several fixed values of x. The figure shows that if we wish to measure the wave function at large p_s (near one GeV) and at large x where pion production is not large, we must go to large Q^2 (about 2 to 3 GeV^2).

We now turn to a discussion of the RIA.

C. Matrix Element for the Relativistic Impulse Approximation

The RIA approximation used in this paper is based on the simple pole diagrams shown in Fig. 3. We use a (standard but unfamiliar) notation in which matrix elements of an operator between *two outgoing* Dirac particles are written in the form

$$\langle \mathcal{O} \rangle = \bar{u}(\mathbf{p}_1, \lambda_1)\, \mathcal{O}\, \mathcal{C}\, \bar{u}^T(\mathbf{p}_2, \lambda_2)\,, \tag{2.23}$$

where $\mathcal{C} = -i\gamma^0\gamma^2$ is the Dirac charge conjugation matrix. This notation is very convenient because $\mathcal{C}\,\bar{u}^T$ transforms like an incoming v spinor (but is *not* to be interpreted as an antipar-

ticle in this application), and therefore the most general operator $\mathcal{O}$ can be constructed from the standard 16 independent Dirac bilinear covariant operators. The matrix representation (2.23) is equivalent to a direct product representation

$$\bar{u}_\alpha(\mathbf{p}_1,\lambda_1)\,[\mathcal{O}\,\mathcal{C}]_{\alpha\beta}\,\bar{u}^T_\beta(\mathbf{p}_2,\lambda_2) \leftrightarrow \bar{u}_\alpha(\mathbf{p}_1,\lambda_1)\bar{u}_\beta(\mathbf{p}_2,\lambda_2)\,[\mathcal{O}\,\mathcal{C}]_{\alpha\beta}\,, \tag{2.24}$$

but is more convenient for relativistic calculations. [Note that the RHS and LHS of this equation are *identical* as long as the Dirac indices are shown explicitly, but only the LHS can be turned into Eq. (2.23) by dropping explicit reference to the indices. Beware that the order of the momenta in (2.23) and (2.24) is opposite from that used in a previous reference [30] where $\bar{u}(\mathbf{p}_2,\lambda_2)$ was multiplied from the left and $u(\mathbf{p}_1,\lambda_1)$ from the right; see Appendix A.]

Including the isospin factor $\left\langle \frac{1}{2}\frac{1}{2}, \frac{1}{2}-\frac{1}{2} \,|\, 00 \right\rangle = \frac{1}{\sqrt{2}}$ the Feynman amplitudes for the RIA in *any* frame can be written

$$\begin{aligned}\langle \lambda_1\lambda_2\,|J_g(q)|\,\lambda_d\rangle \;=\; & \frac{1}{\sqrt{2}\,N_d}\Big[\bar{u}_1(\mathbf{p}_1,\lambda_1)j^{(1)}_g(p_1,p_1-q)\psi^{(2)}_{\lambda_2,\lambda_d}(p_2,P) \\ & -\bar{u}_2(\mathbf{p}_2,\lambda_2)j^{(2)}_g(p_2,p_2-q)\psi^{(1)}_{\lambda_1,\lambda_d}(p_1,P)\Big]\,,\end{aligned} \tag{2.25}$$

where λ_i are the nucleon helicities and λ_d the helicity of the deuteron, and N_d is a normalization constant defined and discussed below. The subscript on the nucleon helicity spinor, $\bar{u}_i$ [suppressed in Eq. (2.23)], refers to whether it is particle 1 or particle 2, in the sense of Jacob and Wick [29] (see the discussion in Appendix A). The nucleon current is

$$j^{(i)}_g(p,p-q) = \varepsilon^\mu_g j^{(i)}_\mu(p,p-q)\,, \tag{2.26}$$

where p and $p-q$ are nucleon four-momenta with p on-shell ($p^2=m^2$) and $p-q$ off-shell, the superscript $i=1$ (proton) or 2 (neutron), and the virtual photon has polarization vector ε_g, where $g=\{0,s,a\}$ with s and a the linear combination of photon helicities introduced in Eq. (2.10) [for more details, see Eq. (B14)]. The relativistic deuteron wave function [30] for a nucleon with momentum $P-p$ off-shell and a nucleon with momentum p and helicity λ on-shell (so that $p^2=m^2$) is *defined* to be $\psi_{\lambda,\lambda_d}(p,P)$, and is related to the normalized *dnp* vertex function Γ by

$$\psi^{(i)}_{\lambda,\lambda_d}(p,P) \equiv \frac{m+\not{P}-\not{p}}{m^2-(P-p)^2}\,N_d\,\Gamma_\mu(p,P)\,\mathcal{C}\,\bar{u}^T_i(\mathbf{p},\lambda)\,\xi^\mu_{\lambda_d}(P)\,. \tag{2.27}$$

where the normalization constant

$$N_d = \left[2M_d\,(2\pi)^3\right]^{-1/2} \tag{2.28}$$

is chosen to give the defined wave function ψ a convenient normalization [see Eq. (A15)]. The superscript (i) labels the choice of helicity convention (particle 1 or 2) for the on-shell particle, $\Gamma_\mu(p,P)$ is the normalized *dnp* deuteron vertex (with the off-shell particle on the left) first defined by Blankenbecler and Cook [31], and $\xi^\mu_{\lambda_d}(P)$ is the deuteron polarization vector for a state with helicity λ_d and four-momentum P. We use the notation of Ref [30] for Γ. Note that the normalization constant in (2.25) and (2.27) cancel; the Feynman amplitude depends only on the normalization of Γ and not on the convention used to normalize ψ. For further details, see Appendix A.

D. The issue of gauge invariance

The RIA is not gauge invariant by itself. This issue must be dealt with before we can proceed with the calculation. Here we discuss how this is done.

Using the method of Ref. [32], the RIA, together with final state interactions (FSI) and interaction currents (IntC), is part of a gauge invariant calculation. Once all of these pieces have been calculated and assembled, the result will be gauge invariant. Here we describe a convenient prescription that is (i) covariant, (ii) renders each of the individual contributions (RIA, FSI, and IntC) *separately* gauge invariant without altering their sum, and (iii) modifies each of the individual contributions as little as possible. The method was introduced in Ref. [33], where it was also shown that the prescription guarantees that the RIA also gives the correct asymptotic result for deep inelastic scattering.

If the individual contributions to the total current are denoted $J_{\rm RIA}$, $J_{\rm FSI}$, and $J_{\rm IntC}$, then the prescription calls for each to be modified by the replacement

$$\tilde{J}^\mu_{\rm X} = J^\mu_{\rm X} - \frac{q^\mu}{q^2}\, q\cdot J_{\rm X} \tag{2.29}$$

where X is any of the RIA, FSI, or IntC terms. Since the total current is gauge invariant, $q\cdot J_{\rm total}=0$, and

$$\tilde{J}^\mu_{\rm total} = J^\mu_{\rm total} \tag{2.30}$$

so the prescription does not modify the total current. Furthermore, since the photon helicity vectors are all orthogonal to q, $\varepsilon_\lambda\cdot q=0$,

$$\varepsilon_\lambda\cdot\tilde{J}_{\rm x} = \varepsilon_\lambda\cdot J_{\rm x} \tag{2.31}$$

and the prescription has *no effect on the contribution of each of the terms in the current.* This prescription meets all three of the conditions listed above.

Unfortunately, there is no uniquely correct way to modify the RIA so that it is gauge invariant. The choice proposed here is only one of many possibilities.

E. Calculation of the structure functions

The structure functions are obtained by squaring the matrix element (2.25) and summing over spins. There will be three terms: the two "diagonal" terms coming from the square of the proton term and the square of the neutron term, and the interference term. The diagonal terms can be calculated by expanding the density matrices

$$\mathcal{N}^{(i)}(p) = \sum_{\lambda_d\lambda} \psi^{(i)}_{\lambda\lambda_d}(p,P)\otimes\psi^{(i)\,\dagger}_{\lambda\lambda_d}(p,P) \tag{2.32}$$

in terms of independent Dirac spin invariants, and then performing the sum over the off-shell particle degrees of freedom using Feynman trace techniques. The final result, given in Ref. [34], is a sum of squares of invariant functions and scalar products of four vectors, and is manifestly covariant.

In this paper we present an alternative method in which the structure functions are calculated by first expanding the off-shell nucleon in terms of on-shell nucleon degrees of freedom, and then computing the squares of the matrix elements. It is possible that this method will simplify the calculation of polarization observables planned for future work. Unfortunately, the results obtained using this method are not manifestly covariant (but they are, nevertheless, covariant), and, unless one is extremely careful, it is easy to make sign mistakes by dropping one of the many phases that arise when transforming helicity amplitudes. As a check of the results presented here, we have shown explicitly that our final analytical result for the diagonal term is *identical* to the result obtained in Ref. [34].

The discussion of this method begins by noting that the physical content of the matrix element (2.25) can be displayed by decomposing the off-shell nucleon into positive energy (u spinor) and negative energy (v spinor) states. For example, if we choose a four-momentum $k = \{E_k, \mathbf{k}\}$, then the states $u(\mathbf{k}, \lambda)$ and $\gamma^5 u(\mathbf{k}, \lambda)$ (which we use in place of the v spinors), with helicity $\lambda = \pm\frac{1}{2}$, are complete, and

$$\mathbb{1} = \sum_{\lambda} \Big\{ u(\mathbf{k}, \lambda)\, \bar{u}(\mathbf{k}, \lambda) + \gamma^5\, u(\mathbf{k}, \lambda)\, \bar{u}(\mathbf{k}, \lambda)\gamma^5 \Big\} \,. \tag{2.33}$$

(The definitions and normalization of the helicity states are discussed in Appendix A.) It is important to realize that while this decomposition can be carried out *in any frame* using nucleon states with *any on-shell four-momentum*, the result may *appear* very different depending on the frame and the spinor states used to do the decomposition (even though the final numerical result will always be independent of these choices).

In this subsection we record the results for the current Eq. (2.25) if the decomposition is made in terms of the states of the *spectator* nucleon (with four-momentum p_2 for the proton term and four-momentum p_1 for the neutron term). The final result in the c.m. frame [see Eq. (B4)] is

$$\begin{aligned}
\langle \lambda_1 \lambda_2 \,|J_g(q^*)|\, \lambda_d \rangle = \sqrt{\frac{3}{16\pi}}\, \frac{1}{N_d} \sum_{\lambda\,\rho} \sum_{\lambda_1' \lambda_2'} \\
\Big\{ \eta_\rho(2\lambda_1')\, j^{(1)\,\rho}_{\lambda_1' \lambda, g}(\mathrm{p}, \theta^*, q_0)\, \phi^\rho_{|\Lambda|}(\mathrm{p}_2)\, d^{(1)}_{\Lambda, \lambda_d}(\theta_2 - \pi)\, d^{(1/2)}_{\lambda_2' \lambda_2}(\omega_2)\, d^{(1/2)}_{\lambda_1' \lambda}(\omega_2) \\
- \eta_\rho(2\lambda_2')\, j^{(2)\,\rho}_{\lambda_2' \lambda, g}(\mathrm{p}, \theta^*, q_0)\, \phi^\rho_{|\Lambda|}(\mathrm{p}_1)\, d^{(1)}_{-\Lambda, \lambda_d}(\theta_1)\, d^{(1/2)}_{\lambda_1' \lambda_1}(\omega_1)\, d^{(1/2)}_{\lambda_2' \lambda}(\omega_1) \Big\} \,,
\end{aligned} \tag{2.34}$$

where the d's are the rotation matrices, $\Lambda = \lambda_1' + \lambda_2'$, ω_j are the Wigner rotation angles resulting from the boost of the spectator nucleons with four-momentum p_j from the lab to the c.m. frame, and p_j and θ_j are the magnitudes of the on-shell spectator three-momenta and polar angles in the rest frame of the deuteron [i.e. the lab frame; recall Table I]. The phase $\eta_\rho(x)$ is

$$\eta_\rho(x) = \begin{cases} 1 & \text{if } \rho = + \\ -x & \text{if } \rho = - \end{cases} \tag{2.35}$$

and the matrix elements of the single nucleon current, in the c.m. system, are

$$j^{(i)\,\rho}_{\lambda_i \lambda, g}(\mathrm{p}, \theta^*, q_0) = \begin{cases} \bar{u}_i(\mathbf{p}_i^*, \lambda_i)\, j_g^{(i)}(p_i^*, p_i^* - q^*)\, u_j(\mathbf{p}_j^*, \lambda) & \text{if } \rho = + \\ \bar{u}_i(\mathbf{p}_i^*, \lambda_i)\, j_g^{(i)}(p_i^*, p_i^* - q^*)\, \gamma^5\, u_j(\mathbf{p}_j^*, \lambda) & \text{if } \rho = - \end{cases} \,, \tag{2.36}$$

TABLE III: Wave function combinations that enter the current.

$\phi_0^+(\mathrm{p}) = \frac{1}{\sqrt{3}}\frac{E}{m}\Big(u(\mathrm{p}) + \sqrt{2}\,w(\mathrm{p})\Big)$	$\phi_0^-(\mathrm{p}) = \frac{1}{\sqrt{3}}\left\{\frac{\mathrm{p}}{m}\Big(u(\mathrm{p}) + \sqrt{2}w(\mathrm{p})\Big) - \sqrt{3}\,v_s(\mathrm{p})\right\}$
$\phi_1^+(\mathrm{p}) = \frac{1}{\sqrt{3}}\frac{E}{m}\Big(\sqrt{2}\,u(\mathrm{p}) - w(\mathrm{p})\Big)$	$\phi_1^-(\mathrm{p}) = \frac{1}{\sqrt{3}}\left\{\frac{\mathrm{p}}{m}\Big(\sqrt{2}\,u(\mathrm{p}) - w(\mathrm{p})\Big) + \sqrt{3}\,v_t(\mathrm{p})\right\}$

with $j = 1$ or 2, but $j \neq i$. The deuteron matrix elements are defined in the deuteron rest frame using the expansion (2.33), and are written

$$\psi^{(i)}_{\lambda_i',\lambda_d}(p_i,P) = \sqrt{\frac{3}{8\pi}}\sum_{\lambda_j'}\Big\{u_i(\mathbf{p}_i,\lambda_j')\;\phi^+_{|\Lambda|}(\mathrm{p}_i) - 2\lambda_j'\,\gamma^5 u_i(\mathbf{p}_i,\lambda_j')\;\phi^-_{|\Lambda|}(\mathrm{p}_i)\Big\} \times \begin{cases} d^{(1)}_{-\Lambda\,\lambda_d}(\theta_1) & \text{if } i=1 \\ d^{(1)}_{\Lambda\,\lambda_d}(\theta_2-\pi) & \text{if } i=2\ . \end{cases} \tag{2.37}$$

The ϕ's are combinations of the four scalar deuteron wave functions defined by Eq. (2.27). These are the S-state u, the D-state w, and the two P-state wave functions v_t and v_s, and expressions for the ϕ's are given in Table III. The final result (2.34) was obtained by boosting this result to the c.m. frame, as shown in Appendix A.

This form of the Born term makes it easy to examine polarization observables, and gives a simple form for the unpolarized response tensors (2.11). Squaring the proton term [with $(i) = (1)$] and summing over spins (averaging over the initial deuteron polarization) gives

$$\begin{aligned} R_{gg'} &= \frac{m^2}{12\pi^2 W}\left\langle J_g\,J_{g'}^\dagger\right\rangle = \frac{m^2}{12\pi^2 W}\sum_{\lambda_1\lambda_2\lambda_d} J^{(1)\,\lambda_d}_{g\,\lambda_1\,\lambda_2}(p_1^*,p_2^*;P^*)\,J^{(1)\lambda_d\,\dagger}_{g'\,\lambda_1\,\lambda_2}(p_1^*,p_2^*;P^*) \\ &= \frac{m^2 M_d}{W}\Big\{J^+_{gg'}\Big[\Big\{\phi_0^+(\mathrm{p}_2)\Big\}^2 + \Big\{\phi_1^+(\mathrm{p}_2)\Big\}^2\Big] + J^-_{gg'}\Big[\Big\{\phi_0^-(\mathrm{p}_2)\Big\}^2 + \Big\{\phi_1^-(\mathrm{p}_2)\Big\}^2\Big] \\ &\quad + \Big(J^c_{gg'}\cos\omega_2 + J^s_{gg'}\sin\omega_2\Big)\Big[\phi_0^+(\mathrm{p}_2)\phi_0^-(\mathrm{p}_2) + \phi_1^+(\mathrm{p}_2)\phi_1^-(\mathrm{p}_2)\Big]\Big\} \end{aligned} \tag{2.38}$$

where the currents are

$$\begin{aligned} J^+_{gg'} &= j^{(1)+}_{1g}\,j^{(1)+}_{1g'} + j^{(1)+}_{2g}\,j^{(1)+}_{2g'} \\ J^-_{gg'} &= j^{(1)-}_{1g}\,j^{(1)-}_{1g'} + j^{(1)-}_{2g}\,j^{(1)-}_{2g'} \\ J^c_{gg'} &= j^{(1)+}_{1g}\,j^{(1)-}_{1g'} + j^{(1)+}_{1g'}\,j^{(1)-}_{1g} - j^{(1)+}_{2g}\,j^{(1)-}_{2g'} - j^{(1)+}_{2g'}\,j^{(1)-}_{2g} \\ J^s_{gg'} &= j^{(1)+}_{1g}\,j^{(1)-}_{2g'} + j^{(1)+}_{2g'}\,j^{(1)-}_{1g} + j^{(1)+}_{2g}\,j^{(1)-}_{1g'} + j^{(1)+}_{1g'}\,j^{(1)-}_{2g}\ . \end{aligned} \tag{2.39}$$

Recall that g and g' can be either $0, s$, or a. The 12 individual current matrix elements are given in Table IV. These exact expressions are easily evaluated, and the response functions determined from Table II. The square of the neutron term [with $(i) = (2)$] is obtained by replacing $1 \leftrightarrow 2$, and the result for the interference term is given in Appendix B.

TABLE IV: Matrix elements of the current. All variables are in the c.m. frame, and $E = \sqrt{m^2 + \mathrm{p}^2}$, $\mathrm{p}_\perp = \mathrm{p}\sin\theta^*$, and $\mathrm{p}_z = \mathrm{p}\cos\theta^*$. For the proton current, $j^{(1)}$, substitute proton form factors for F_1 and F_2 and set the phase $\delta = +$. For the neutron current, $j^{(2)}$, substitute neutron form factors and set $\delta = -$.

$j_1^{+0} = \frac{1}{Q}\left(F_1 q_0 - \delta\, 2\tau F_2 \mathrm{p}_z\right)$	$j_2^{+0} = F_1 \frac{\nu_0\, \mathrm{p}_\perp}{mQ}$
$j_1^{+s} = -\delta \frac{1}{\sqrt{2}} F_2 \frac{\nu_0\, \mathrm{p}_\perp}{2m^2}$	$j_2^{+s} = \frac{1}{\sqrt{2}\, m}\left(F_1 \mathrm{p}_z + \delta\, \frac{1}{2} F_2\, q_0\right)$
$j_1^{+a} = \delta \frac{1}{\sqrt{2}} F_2 \sin\theta^* \frac{q_0 E}{2m^2}$	$j_2^{+a} = \frac{1}{\sqrt{2}\, m}\left(\delta\, F_1 \mathrm{p} + \frac{1}{2} F_2\, q_0 \cos\theta^*\right)$
$j_1^{-0} = -\delta \frac{\cos\theta^*}{Q}\left(F_1 \nu_0 - 2\tau F_2 E\right)$	$j_2^{-0} = \frac{\sin\theta^*}{mQ}\left(F_1 \nu_0 E - 2\tau F_2 m^2\right)$
$j_1^{-s} = \delta \frac{\sin\theta^*}{\sqrt{2}}\left(F_1 + F_2 \frac{\nu_0 E}{2m^2}\right)$	$j_2^{-s} = \frac{\cos\theta^*}{\sqrt{2}\, m}\left(F_1 E + \frac{1}{2} F_2 \nu_0\right)$
$j_1^{-a} = -\delta \frac{1}{\sqrt{2}} F_2 \frac{q_0\, \mathrm{p}_\perp}{2m^2}$	$j_2^{-a} = \delta \frac{1}{\sqrt{2}\, m}\left(F_1 E + \frac{1}{2} F_2 \nu_0\right)$

F. The cross section in the quasielastic limit

We may use expression (2.38) to look at the cross section at the quasielastic peak, where $\mathrm{p}_2 = 0$ and $x \simeq 1$ (we assume here that $M_d = 2m$). Near $\mathrm{p}_2 = 0$ the minus components of the wave functions are both suppressed, and the leading contribution to the cross section comes only from the term proportional to

$$\left(\phi_0^+\right)^2 + \left(\phi_1^+\right)^2 = \frac{E^2}{m^2}\left[u^2 + w^2\right] \simeq \left[u^2 + w^2\right] \equiv 4\pi\, n(\mathrm{p}_2)\,, \tag{2.40}$$

where the momentum density is approximately normalized to

$$\int n(\mathrm{p})\, d^3p = \frac{1}{4\pi}\int d^3p\left[u^2(\mathrm{p}) + w^2(\mathrm{p})\right] \approx 1 \tag{2.41}$$

[the exact relativistic normalization is given in Eq. (A15)]. At the quasielastic peak $\theta^* = 0$ and the c.m. momentum p that enters the current matrix elements given in Table IV is fixed. From Eq. (2.17) and the condition $x = 1$ we obtain

$$\mathrm{p} = \frac{W q_{_L}}{2E_W} = \frac{W^2 q_0}{2E_W M_d} \simeq \frac{q_0}{2}\,. \tag{2.42}$$

This gives $R_{TT} = 0$ and $R_{LT} = 0$, and the following simple formula for the coincidence cross section

$$\frac{d^5\sigma}{d\Omega' dE' d\Sigma} = \sigma_M \frac{m^2}{W}\, n(0)\left\{\frac{G_E^2(Q^2) + \tau G_M^2(Q^2)}{1+\tau} + 2\tau G_M^2(Q^2)\tan^2\theta/2\right\} \tag{2.43}$$

This can be compared to the cross section for scattering from a free proton, which is

$$\frac{d^2\sigma}{d\Omega'} = \sigma_M \frac{E'}{E}\left\{\frac{G_E^2(Q^2)+\tau G_M^2(Q^2)}{1+\tau} + 2\tau G_M^2(Q^2)\tan^2\theta/2\right\} \tag{2.44}$$

In both of these formulae, $\tau = Q^2/(4m^2)$, and G_E and G_M are the familiar electric and magnetic form factors, related to F_1 and F_2:

$$\begin{aligned} G_E &= F_1 - \tau F_2 \\ G_M &= F_1 + F_2 \,. \end{aligned} \tag{2.45}$$

III. PREDICTIONS OF THE RELATIVISTIC IMPULSE APPROXIMATION

A. How good is the RIA?

The low energy Bernheim (1981) data [3] are shown in Fig. 6. This figure shows (i) that the relativistic effects are large and (ii) at these low missing momenta there is no evidence for relativistic effects of higher order in v/c, nor for model dependencies coming from the difference between the Argonne V18 and Model IIB wave functions. The importance of relativistic effects in the $d(e,e'p)n$ reaction has already been emphasized in Ref. [17], and is confirmed in our calculations. For this reason we will dispense with further nonrelativistic calculations, and present only calculations with relativistic effects included.

Figure 6, and the accompanying Figs. 7 and 8, also show that the low energy cross section is reasonably well approximated by the (relativistic) RIA. The agreement is at the level of $\pm 50\%$ for a drop in the cross section of four orders of magnitude. We take this as evidence that the RIA is sufficient for the kind of crude survey carried out in this paper.

B. Covariant RIA predictions for high Q^2

We surveyed the $d(e,e'p)n$ reaction over the wide range of kinematical conditions summarized in Table V. We did calculations at 4 different four-momentum transfers $Q^2 = 0.5$, 1, 2, and 3 GeV^2, and 6 different values of the Bjorken variable $x = 0.5$, 1.0, 1.25, 1.5, 1.8, and just below 2, near the highest value accessible in the $d(e,e'p)n$ reaction at a given Q^2. [The value of x=2 can be reached only in the elastic reaction, not in electrodisintegration.] In addition to Q^2 and x, Table V gives the transferred energy ν, the magnitude of the transferred 3-momentum $q_L = |\mathbf{q}_L|$, and the range in missing momentum, where p_2^{min} corresponds to a value of $\theta^* = 0°$, and p_2^{max} corresponds to a value of $\theta^* = 180°$. In addition, we list the value of the final state np relative energy (in the c.m. system), E_{np}, which is

$$E_{np} = \sqrt{(\nu + M_d)^2 - q_L^2} - m_p - m_n \,, \tag{3.1}$$

and the kinetic energy of the pn system in the Lab frame,

$$T_{pn}^{Lab} = \frac{M_d^2}{2m} - 2m + \frac{Q^2}{2m}\left(\frac{M_d}{m\,x} - 1\right) . \tag{3.2}$$

The highest accessible value of x for a certain Q^2 is given by

$$x_{max} = \frac{Q^2\, M_d}{m\,(4m^2 - M_d^2 + Q^2)} \,, \tag{3.3}$$

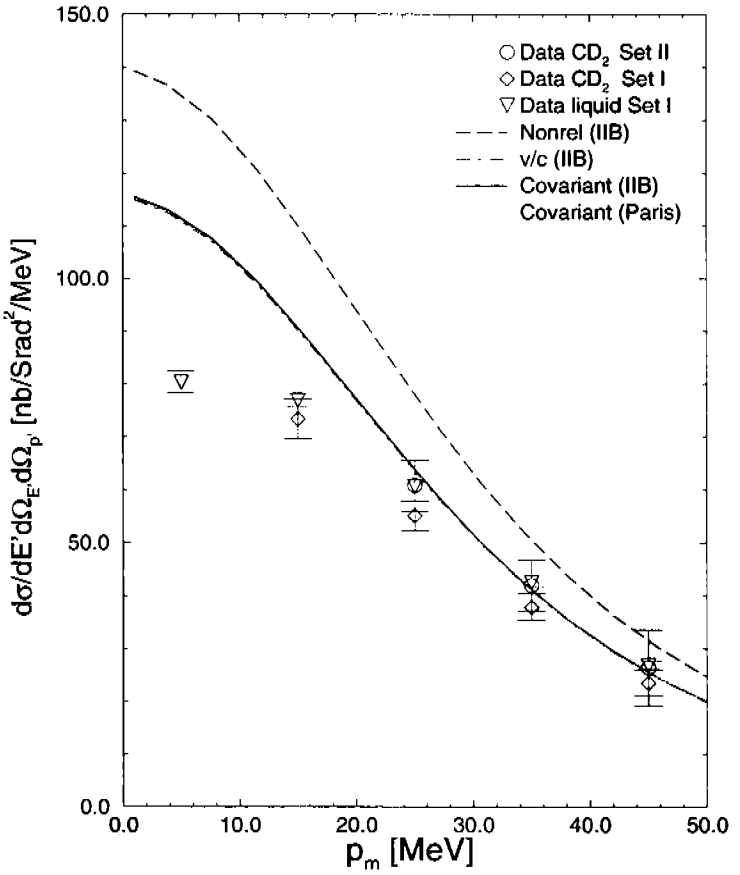

FIG. 6: The Bernheim data at low missing momentum. Note that the relativistic effects (mostly from the current operator) are significant. [Three of the lowest p_m data points, possibly contaminated by bremstrahluung, have been omited from the figure.]

which comes from the requirement that $T_{pn}^{Lab} > 0$. In Table V, we list the kinematic variables for $x = x_{max}$ in the last line for each Q^2. The closest x value to that is the highest one for which we present calculations later on; it is characterized by a kinetic energy in the Lab frame of roughly 10 MeV.

Table V shows that the values of the transferred energy and transferred three-momentum are closest for low x. In nonrelativistic reduction schemes one often assumes $\nu << q_L$, which is clearly not the case for low x. Note also that the np relative energy is highest for low x. These imply that relativistic effects should be very strong in this region. This is interesting as it allows for a description of final state interaction by Glauber theory [27]. Although final state interactions (FSIs) are not considered in this present study, it is useful to know that they can be calculated reliably in this kinematic region.

At high x, the np relative energy is very small, on the order of a few tens of MeV.

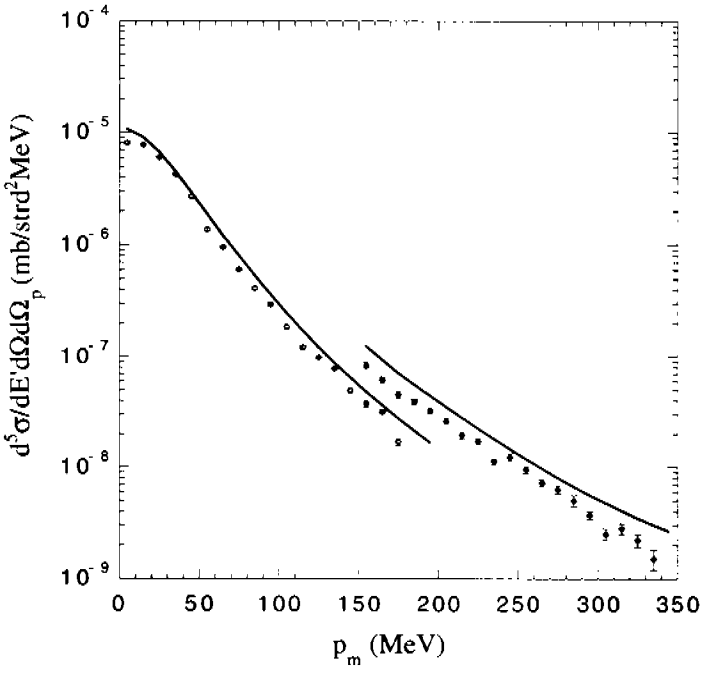

FIG. 7: The acceptance averaged relativistic RIA calculation compared to the Bernheim data.

Under these kinematic conditions, the system is reminiscent of a bound system, and one might realistically expect wave function physics to be important here, e.g. the presence of the relativistic P-waves. The calculation of final state interactions proceeds by including the lowest partial waves. So, we have reliable methods for the calculation of FSIs both at high x and at low x. In the region in between, the description of FSIs is more involved and accordingly more difficult.

The case of $x = 1$ roughly corresponds to the quasi-free case. Strictly speaking, the quasi-free case corresponds to

$$\nu = \frac{Q^2}{2m_N} - E_b\,, \tag{3.4}$$

where the binding energy E_b leads to a small deviation from $x = 1$. However, the binding energy for the deuteron is small and we will refer to $x = 1$ as the quasi-free case in the following discussion.

C. Six approximations

Six different theoretical approximations will be discussed in the following. The first three are based on the covariant spectator RIA presented in detail in this paper, and will be denoted "C-IIB", "C-IIB-noP", and "C-AV18".

- **C-IIB** is calculated using the covariant IIB deuteron wave function obtained from the successful IIB NN interaction [24]. This wave function and the relativistic spectator model have been previously used to successfully explain the elastic deuteron form factors [25]. The full wave function has 4 components: the familiar S- and D-states, and two small P-states of relativistic origin.

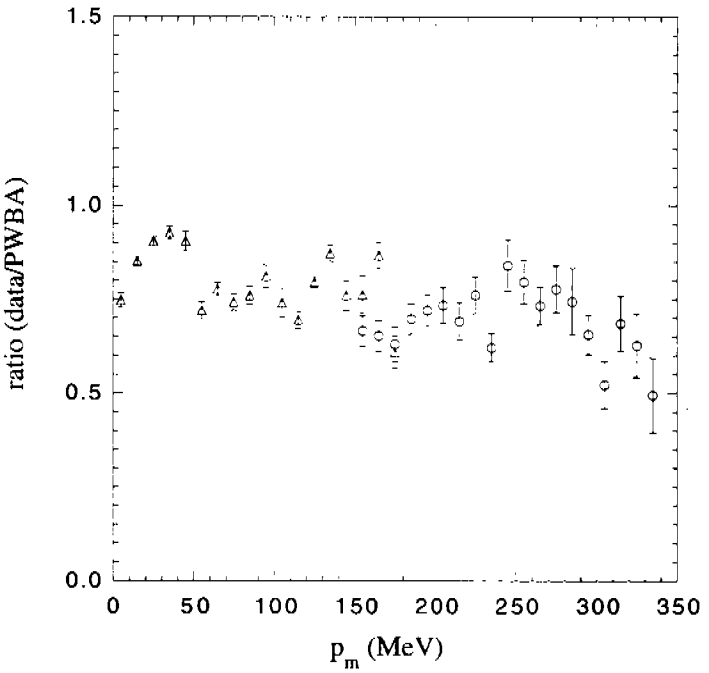

FIG. 8: The ratio of the Berheim data to the acceptance averaged relativistic RIA calculation shown in Fig. [7]. The triangles are the low p_m data set, and the circles the high p_m set.

- **C-IIB-noP** is calculated using covariant IIB S- and D-state wave functions, but setting the small relativistic P-state components to zero.

- **C-AV18** is calculated from the covariant spectator RIA formulae using the S- and D-state Argonne V18 deuteron wave functions [35] (instead of the wave functions derived from the IIB one boson exchange model) and setting the P-state components to zero. This is included among the covariant models even though, strictly speaking, the wave function is not consistent with the covariant formalism. This model is very similar to the "covariant model" previously discussed by Arenhövel [17], but they used ordinary spin instead of helicity, and the Paris deuteron wave functions instead of the (very similar) AV18 wave functions.

The next three calculations are not consistently covariant, but they do use relativistic current operators. They all use the nonrelativistic Argonne V18 wave function. The first of these is based on the work of Adam and Arenhövel [36].

- **AA-v/c** uses a current operator that results from a v/c-expansion of the intrinsic current [36, 37]. Matrix elements of this current are made frame independent by replacing the approximate noninvariant effective 3-momentum transfer derived in [36, 37] by its invariant extension, defined to be:

$$\vec{q}^{\,2}_{eff} = \frac{Q^2}{1+\frac{Q^2}{16m_N^2}} + (\epsilon_d - W)^2 \,. \tag{3.5}$$

where ϵ_d, W are energies of pn pair in its respective c.m. frame in the initial and final states. This prescription is similar to one proposed long ago for the elastic scattering by J. Friar [38], but differs from calculations by Arenhövel et al [17].

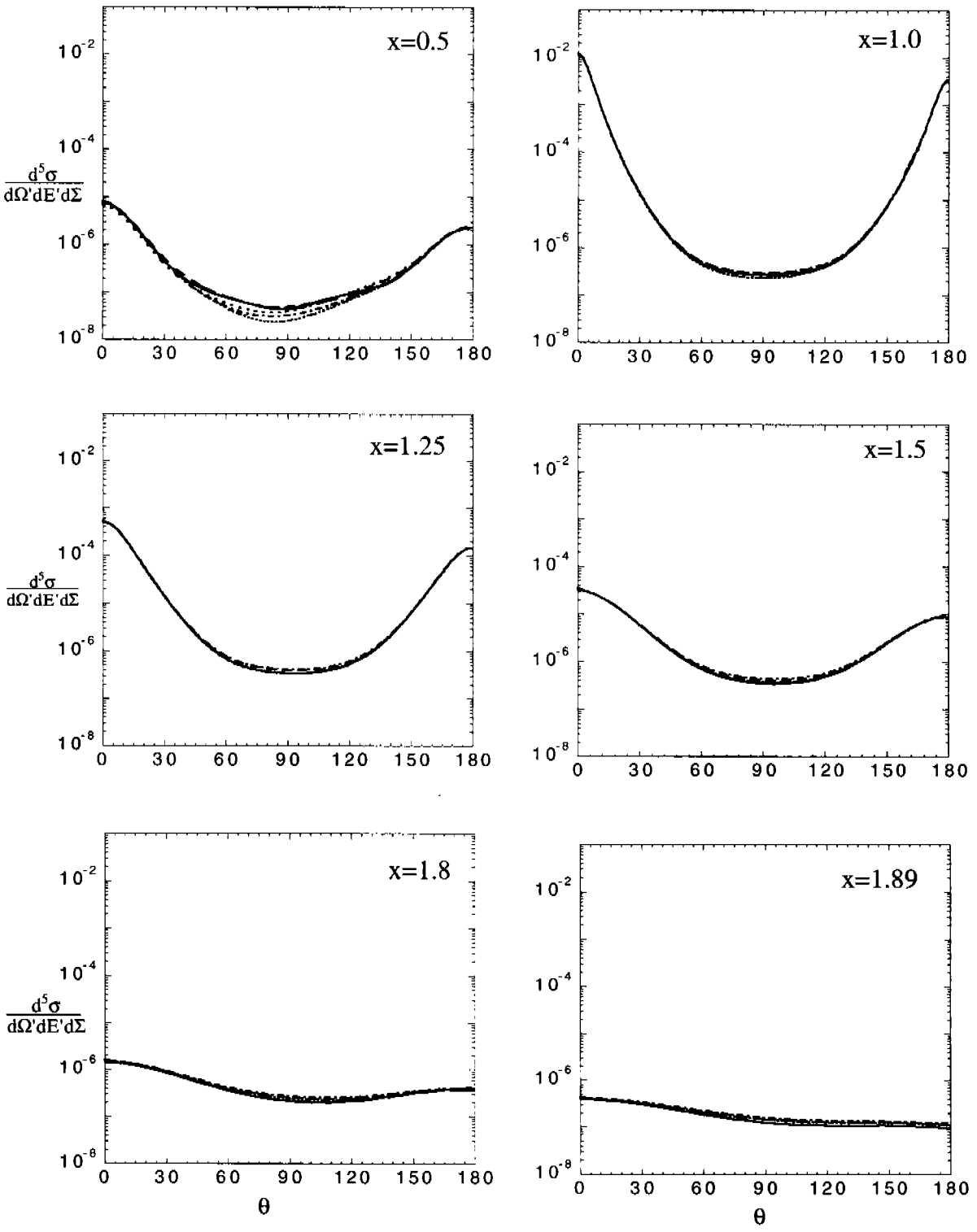

FIG. 9: The differential cross section *in the c.m. system* at $Q^2 = 0.5$ GeV^2 and for $x = 0.5, 1, 1.25, 1.5, 1.8$, and 1.89. Each panel shows the six calculations described in the text: C-IIB (solid line), C-IIB-noP (long-dashed line), C-AV18 (dashed line), AA-v/c (widely dotted line), JD-full (dash-dotted line), and JD-1st (closely dotted line). Note that the different approximations are hard to distinguish, as discussed in the text.

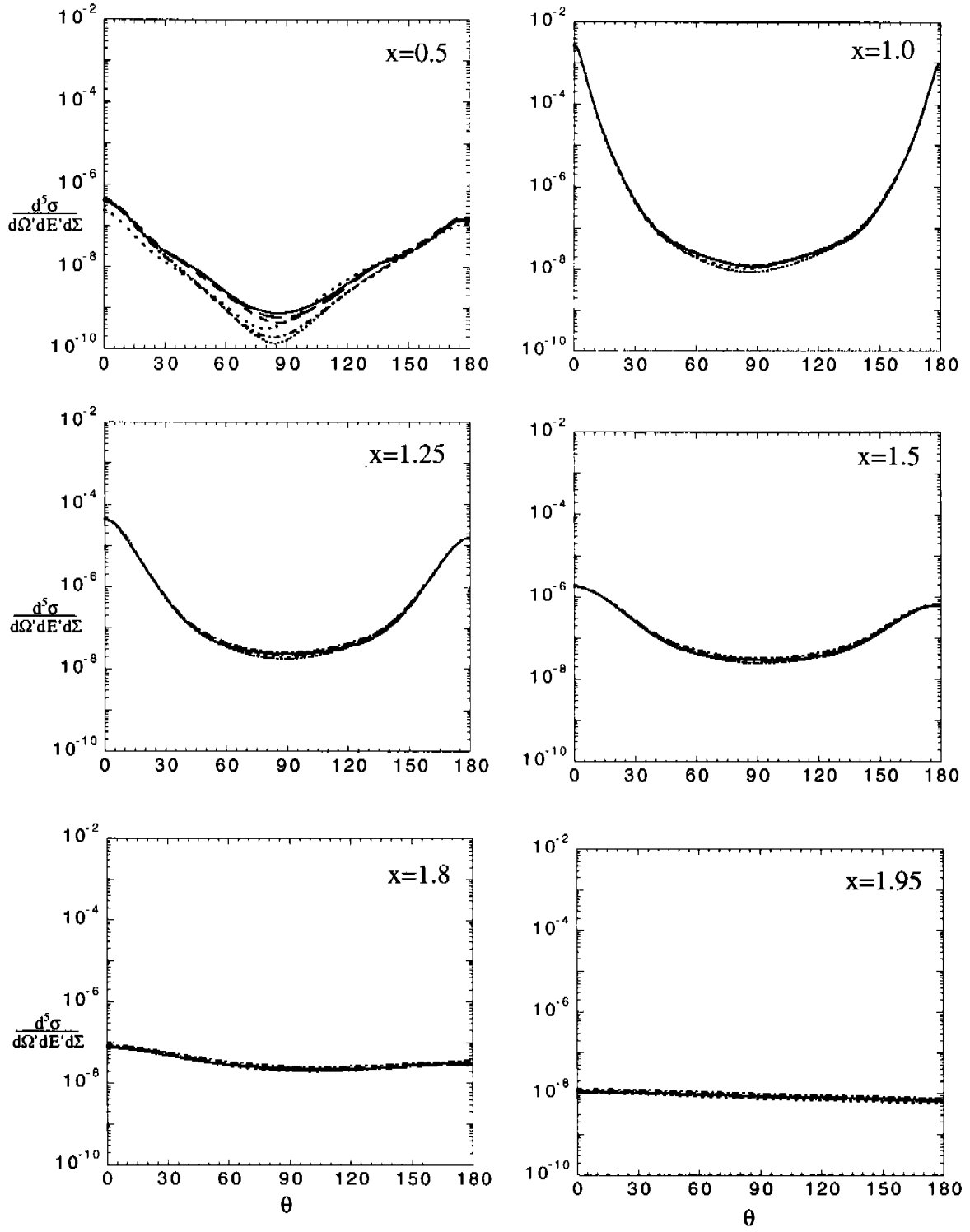

FIG. 10: The differential cross section at $Q^2 = 1$ GeV^2 and for various x. The meaning of the curves is the same as in Fig. 9.

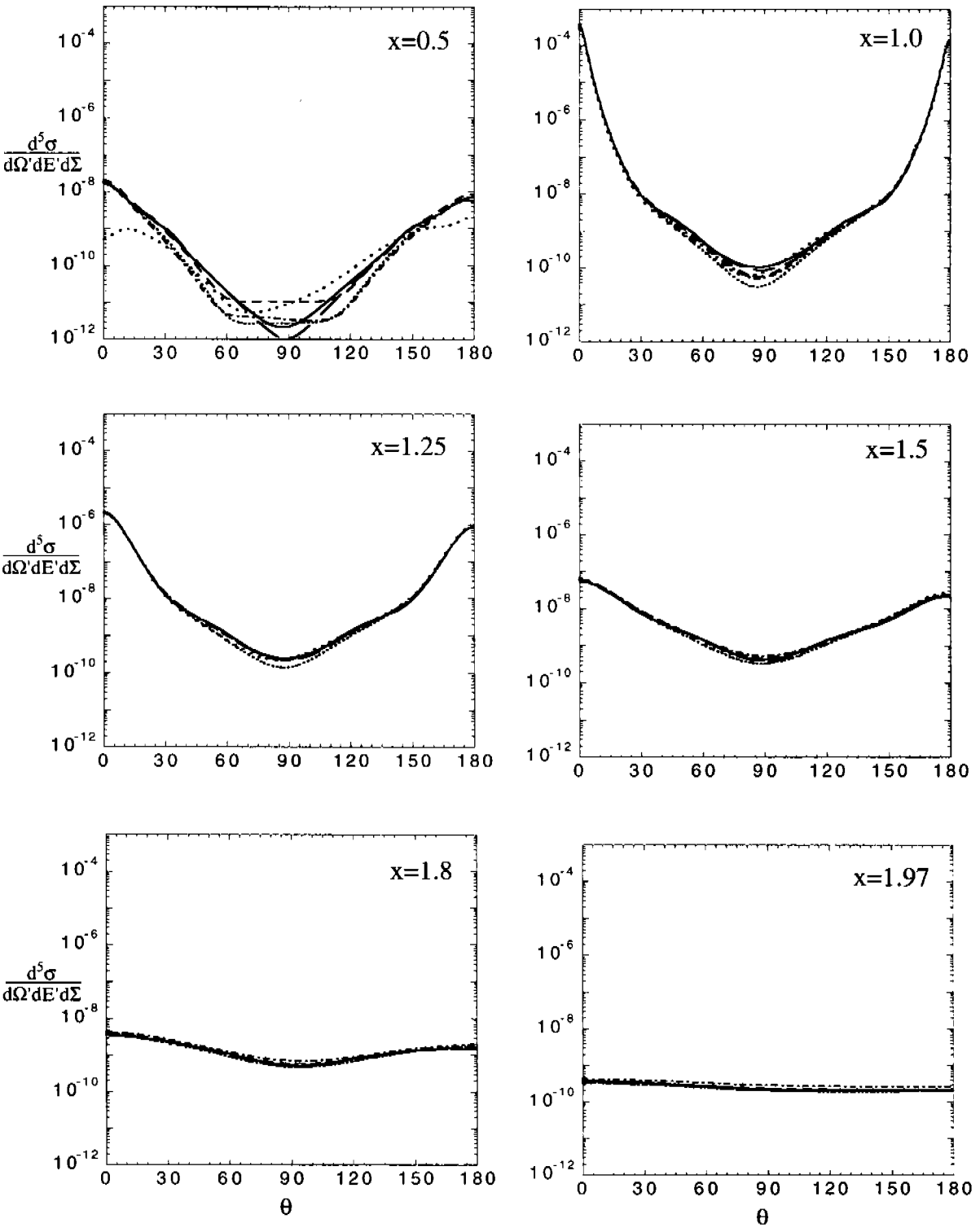

FIG. 11: The differential cross section at $Q^2 = 2$ GeV^2 and for various x. The meaning of the curves is the same as in Fig. 9.

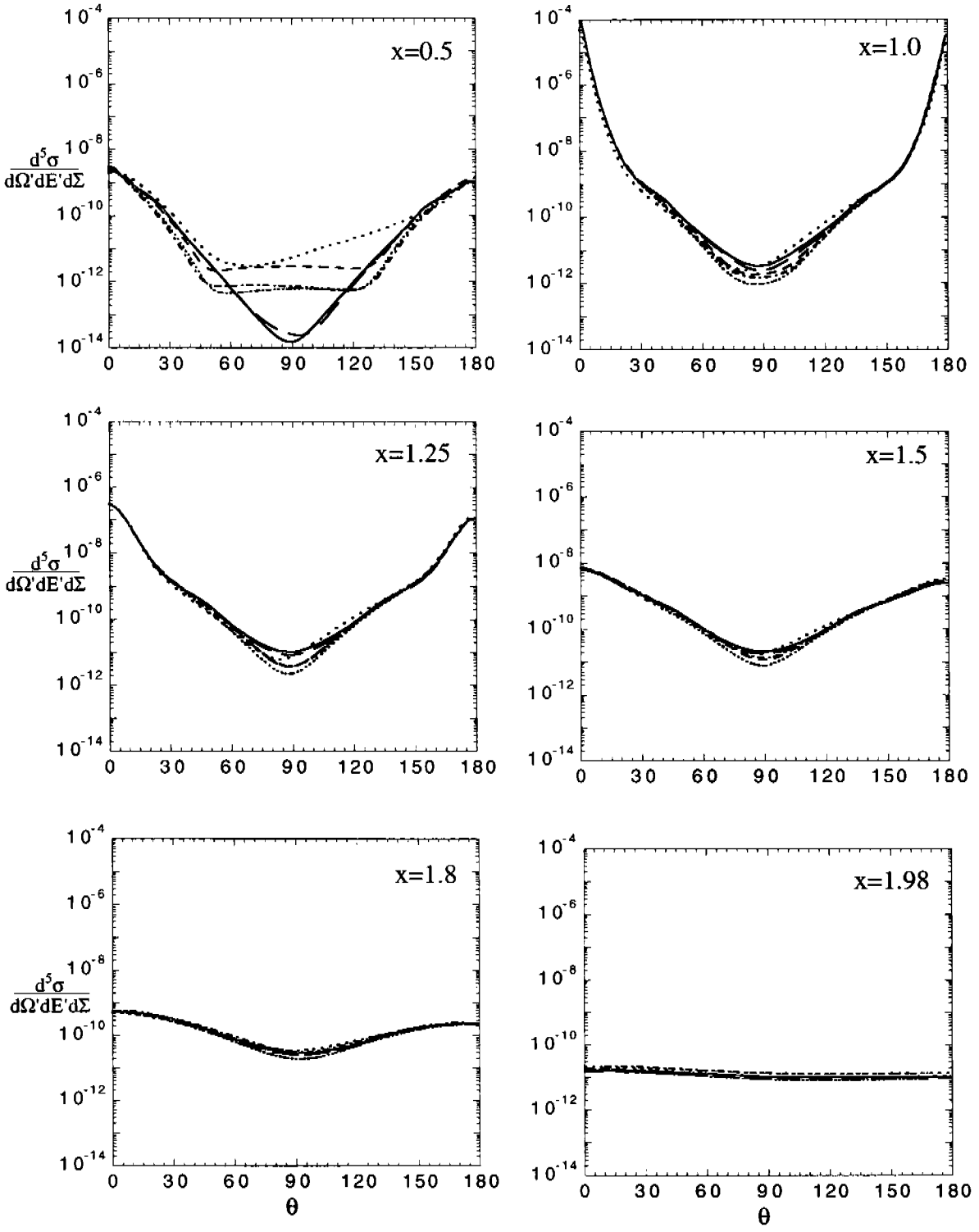

FIG. 12: The differential cross section at $Q^2 = 3$ GeV^2 and for various x. The meaning of the curves is the same as in Fig. 9.

TABLE V: Overview over the kinematics employed in the calculation of the differential cross section and asymmetry A_ϕ.

Q^2 (GeV ^{2})	x	q_L (GeV)	ν (GeV)	p_2^{min} (GeV)	p_2^{max} (GeV)	E_{np} (GeV)	T_{pn}^{Lab} (GeV)
0.5	0.5	0.885	0.533	0.214	1.099	0.362	0.793
0.5	1.0	0.756	0.266	0.004	0.752	0.126	0.261
0.5	1.25	0.738	0.213	0.081	0.657	0.076	0.155
0.5	1.5	0.729	0.178	0.152	0.577	0.041	0.084
0.5	1.8	0.722	0.148	0.246	0.477	0.012	0.025
0.5	1.89	0.721	0.141	0.285	0.436	0.005	0.011
0.5	1.97	0.720	0.136	0.360	0.360	0	0
1	0.5	1.461	1.065	0.265	1.726	0.674	1.591
1	1.0	1.133	0.533	0.003	1.130	0.247	0.527
1	1.25	1.087	0.426	0.108	0.979	0.151	0.314
1	1.5	1.061	0.355	0.207	0.854	0.084	0.172
1	1.8	1.043	0.296	0.340	0.703	0.027	0.054
1	1.95	1.037	0.273	0.446	0.590	0.004	0.009
1	1.98	1.035	0.269	0.518	0.518	0	0
2	0.5	2.557	2.130	0.310	2.867	1.206	3.186
2	1.0	1.770	1.065	0.003	1.768	0.470	1.058
2	1.25	1.651	0.852	0.141	1.510	0.293	0.633
2	1.5	1.582	0.710	0.280	1.303	0.167	0.349
2	1.8	1.533	0.592	0.473	1.060	0.055	0.112
2	1.97	1.514	0.541	0.667	0.847	0.005	0.010
2	1.99	1.512	0.535	0.756	0.756	0	0
3	0.5	3.634	3.195	0.331	3.966	1.658	4.781
3	1.0	2.356	1.598	0.002	2.354	0.673	1.589
3	1.25	2.153	1.278	0.162	1.991	0.427	0.951
3	1.5	2.033	1.065	0.329	1.704	0.247	0.526
3	1.8	1.946	1.946	0.574	1.372	0.084	0.171
3	1.98	1.911	0.807	0.859	1.052	0.005	0.010
3	1.99	1.909	0.802	0.954	0.954	0	0

The next two versions are from Jeschonnek and Donnelly [39].

- **JD-full** uses a fully relativistic, positive energy current operator. This covariant current differs from the spectator one by certain off-mass-shell extensions studied in a recent paper by two of the authors [34].

- **JD-1st** uses a current operator expanded to first order in the initial nucleon momentum, with all other terms retained fully. This approximate "first order" form should be closer to the covariant one than the traditional v/c current mentioned above, since an expansion is made only in terms of the moderate momenta of nucleons in the initial nucleus.

The relativistic one-nucleon current used here in the JD-full calculation has been recently employed by Donnelly [39] in studies of $(e, e'N)$ reactions. In these studies relativistic models appeared to be far more successful than nonrelativistic ones [17, 39]. It is, however, a nontrivial task to extend them beyond RIA.

Final state interaction and meson-exchange currents (MECs) have been so far included into realistic calculations mostly within approximate frameworks based on various expansions of the nuclear operators in terms of supposedly small momenta [39–41]. We do not intend to give an exhaustive survey of those techniques, neither do we dare to compete in completeness and consistency with recent elaborate calculations [40, 42]. We only show in our figures the results obtained with the various one-nucleon currents introduced above.

While a much more comprehensive study of relativistic effects, including relativistic expansions of π exchange currents and heavy meson exchange currents including boost terms, $\gamma\pi\rho$ and $\gamma\pi\omega$ currents, and isobar contributions, was performed by Ritz et al [40] for lower energies, we focus on high energies. Here, high energies mean the GeV region, accessible by CEBAF at Jefferson Lab and even the new kinematic regime opening up with the planned 12 GeV upgrade of CEBAF. Our C-IIB calculation given here is fully covariant, and part of a consistent treatment of the nuclear dynamics and the one-body current that does not rely on any kind of nonrelativistic expansion.

None of our calculations is complete, the purpose is rather to explore various experimentally feasible kinematical regions to find those for which the complete microscopic calculations and precise measurements would be worthwhile. Nevertheless, the variations between results obtained with versions of covariant currents and their approximations, as well as those between two covariant or two approximate formulations themselves, should provide some insight on the region of validity of the expansions and approximations used.

D. Differential cross section

The differential cross section (2.1) is given in Figs. 9–12. The six panels in each figure all have the same scale, so the relative size of the cross section may be seen at a glance. Examination of these figures shows that the magnitude of the cross section depends strongly on Q^2, x, and θ^* . The bulk feature of the differential cross section consists of the two peaks at $\theta^* = 0°$ and $\theta^* = 180°$. The first peak corresponds to the impulse approximation contribution, where the photon couples to the proton which is detected later on, and the second peak at 180° corresponds to the Born contribution, where the photon interacts with the neutron. For $x \leq 1.5$ the two peaks are well separated because (cf. Fig. 4) the nucleons have very different momenta at $\theta^* \simeq 0$ and 180°. In this case one of the two RIA contributions [recall Eq. (2.16) and Fig. 3] is much larger than the other.

However, if we wish to probe the deuteron wave function at high momentum, we will seek the region near $\theta^* \simeq 90°$, where both nucleons have nearly the same momenta and only high momentum components of the wave function can contribute. In this region the cross section is very small (and FSI will be large), reflecting the small size of the deuteron wave function at large momenta. At large x, and in particular near $x \simeq 2$, the two diagrams will always have large momenta (because the relative momentum of the final state is low), and the cross section shows no sharp forward or backward peak. Here high momentum components of the deuteron contribute over the whole angular range.

Figures 9–12 seem to suggest that, for $x > 0.5$, the differential cross section is relatively insensitive to the model used. However, this is largely an artifact of the log scales used in

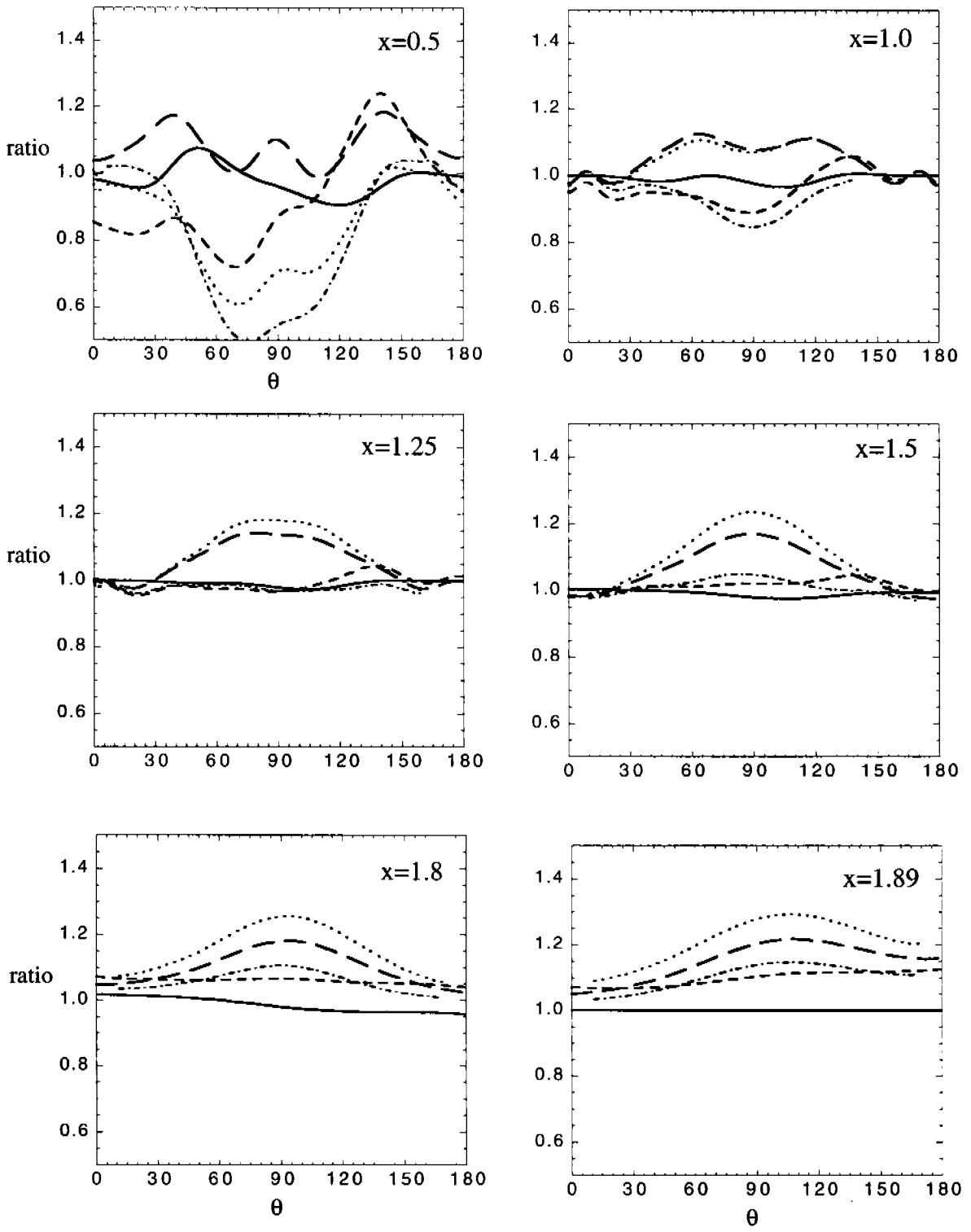

FIG. 13: Ratios of the differential cross section *in the c.m. system* for the cases shown in Fig. 9 (Q^2 =0.5 GeV^2). Here five of the calculations are divided by the C-IIB calculation: C-IIB-noP (solid line), C-AV18 (long dashed line), AA-v/c (short dashed line), JD-full (dotted line), and JD-1st (dash-dotted line).

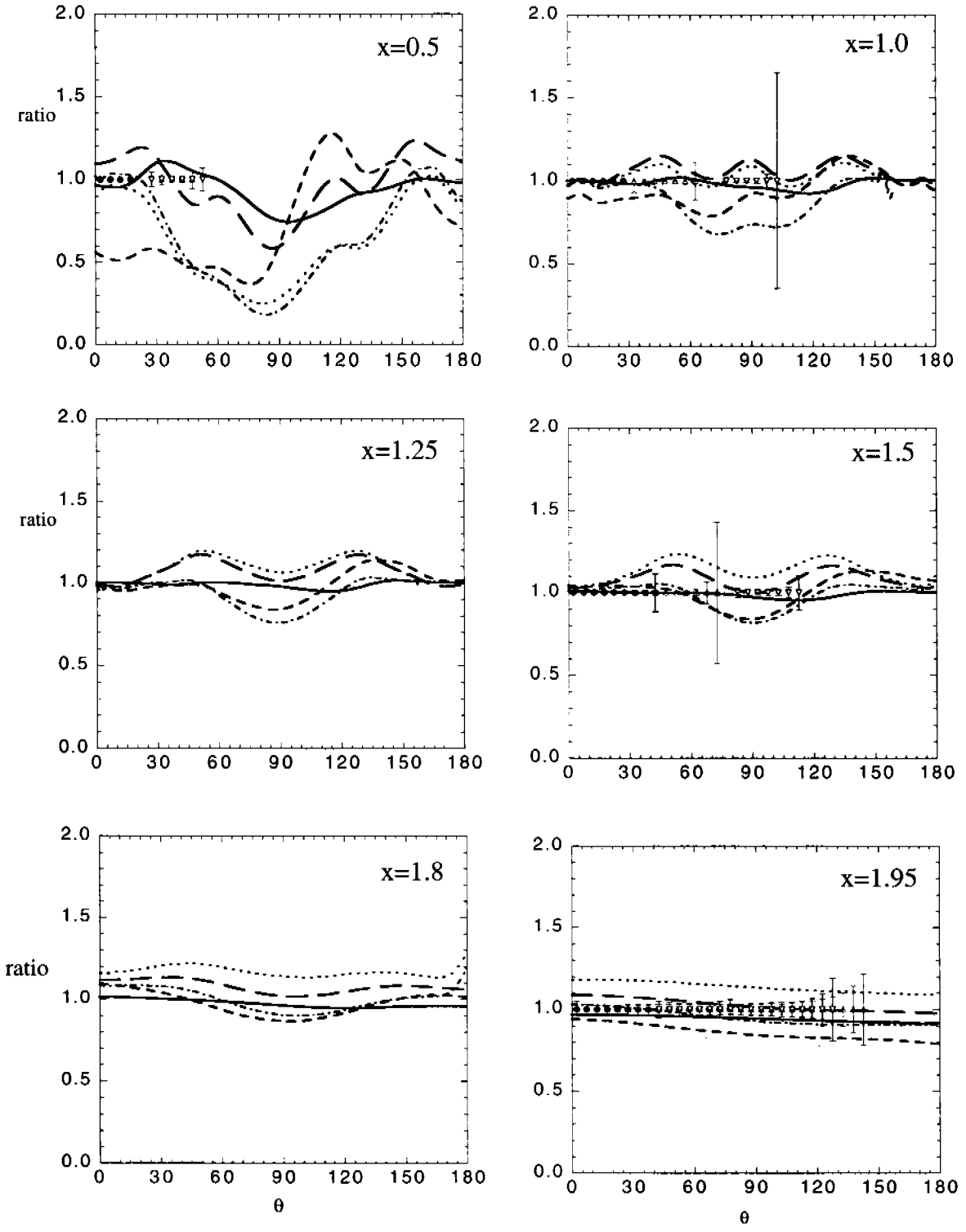

FIG. 14: Ratios of the differential cross section at $Q^2 = 1$ GeV^2 and for various x. The meaning of the curves is the same as in Fig. 13. The estimated errors for a JLab measurement using existing equipment, shown on panels for $x = 0.5, 1.0, 1.5$, and 1.95, are discussed in the text.

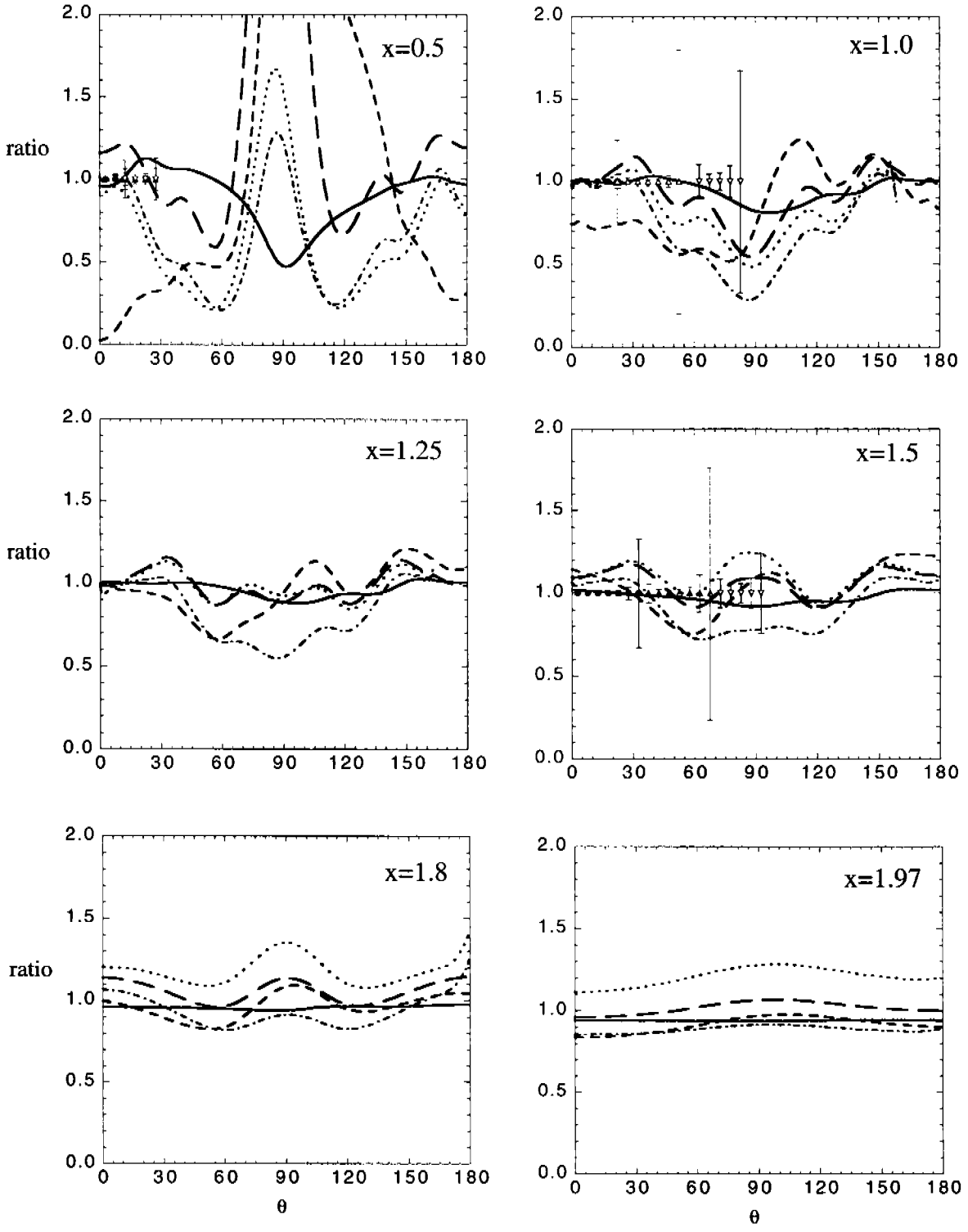

FIG. 15: Ratios of the differential cross section at $Q^2 = 2$ GeV^2 and for various x. The meaning of the curves is the same as in Fig. 13. The estimated errors for a JLab measurement using existing equipment, shown on panels for $x = 0.5, 1.0$, and 1.5 are discussed in the text.

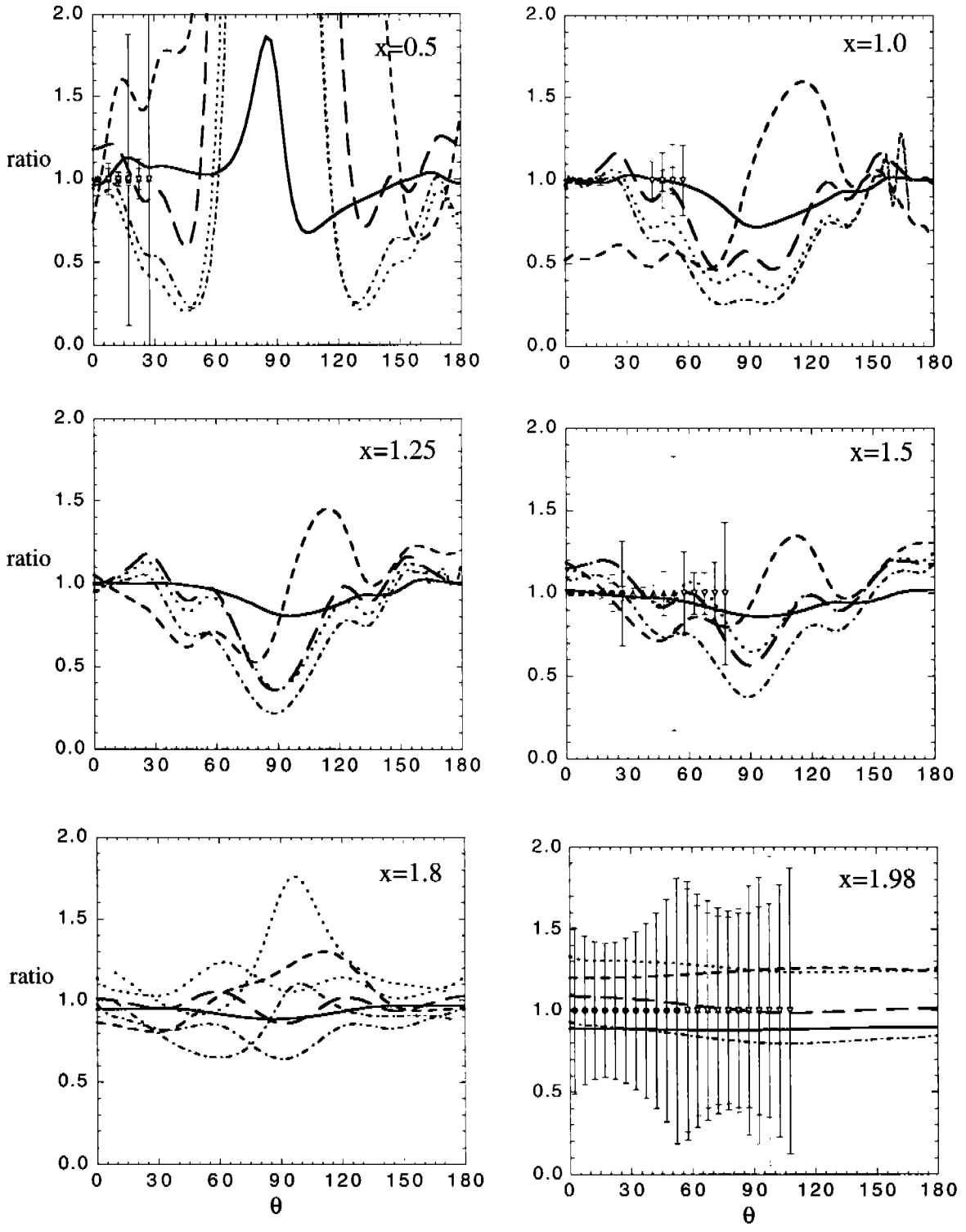

FIG. 16: Ratios of the differential cross section at $Q^2 = 3$ GeV^2 and for various x. The meaning of the curves is the same as in Fig. 13. The estimated errors for a JLab measurement using existing equipment, shown on panels for $x = 0.5, 1.0, 1.5$, and 1.98, are discussed in the text.

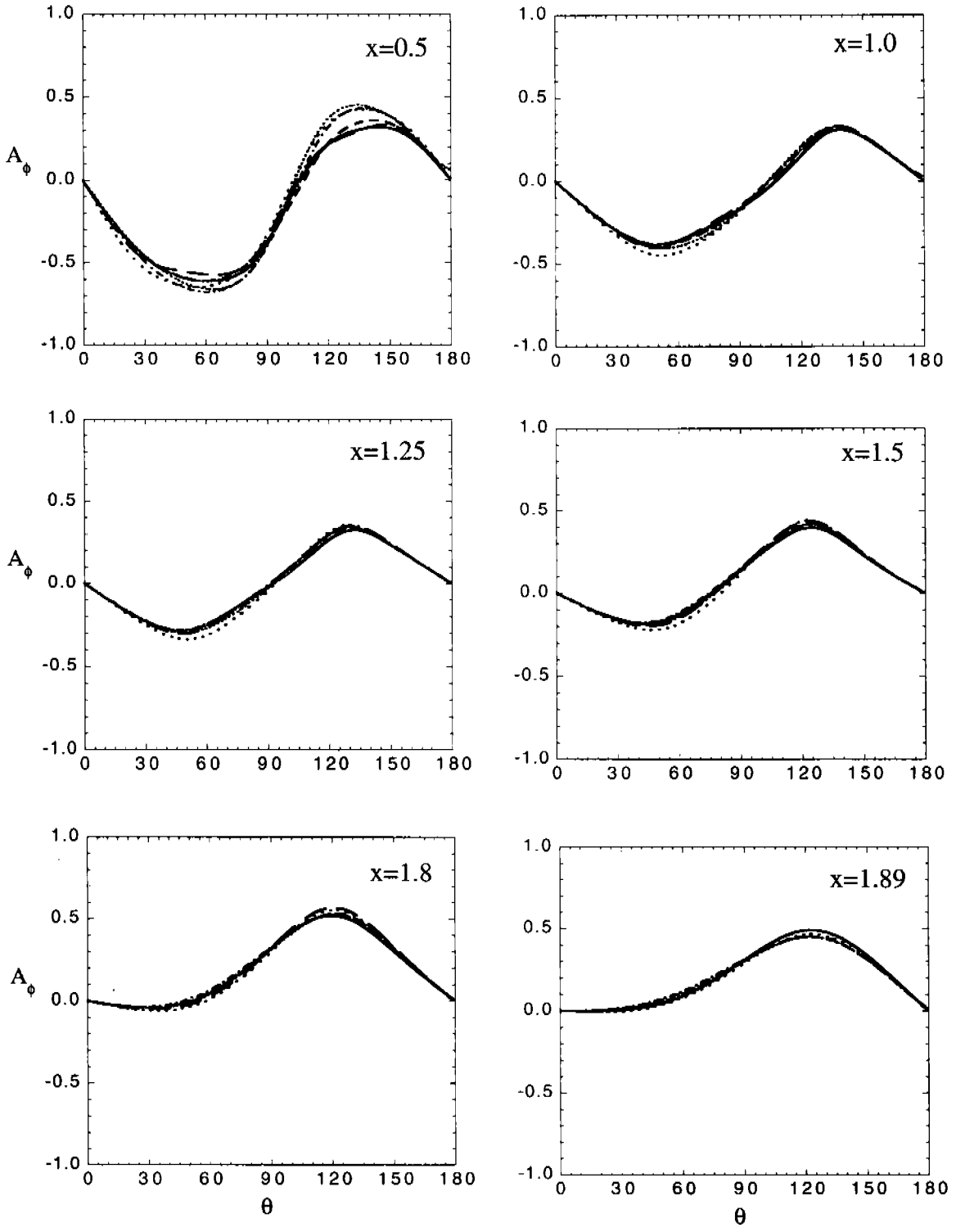

FIG. 17: The asymmetry A_ϕ at $Q^2 = 0.5$ GeV^2 and for various x. The meaning of the curves is the same as in Fig. 9.

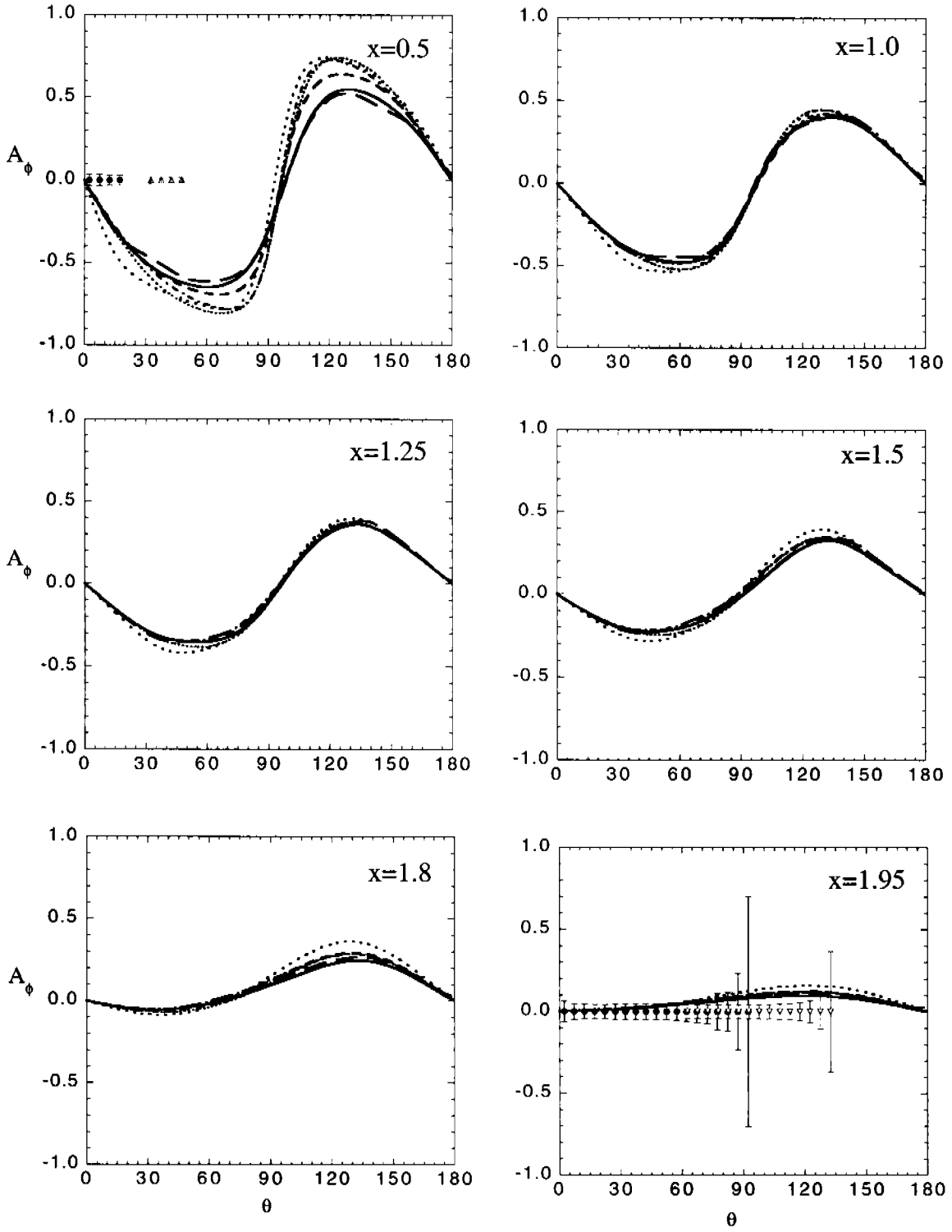

FIG. 18: The A_ϕ at $Q^2 = 1$ GeV^2 and for various x. The meaning of the curves is the same as in Fig. 9. The estimated errors for a JLab measurement using existing equipment, shown on panels for $x = 0.5$ and 1.95, are discussed in the text.

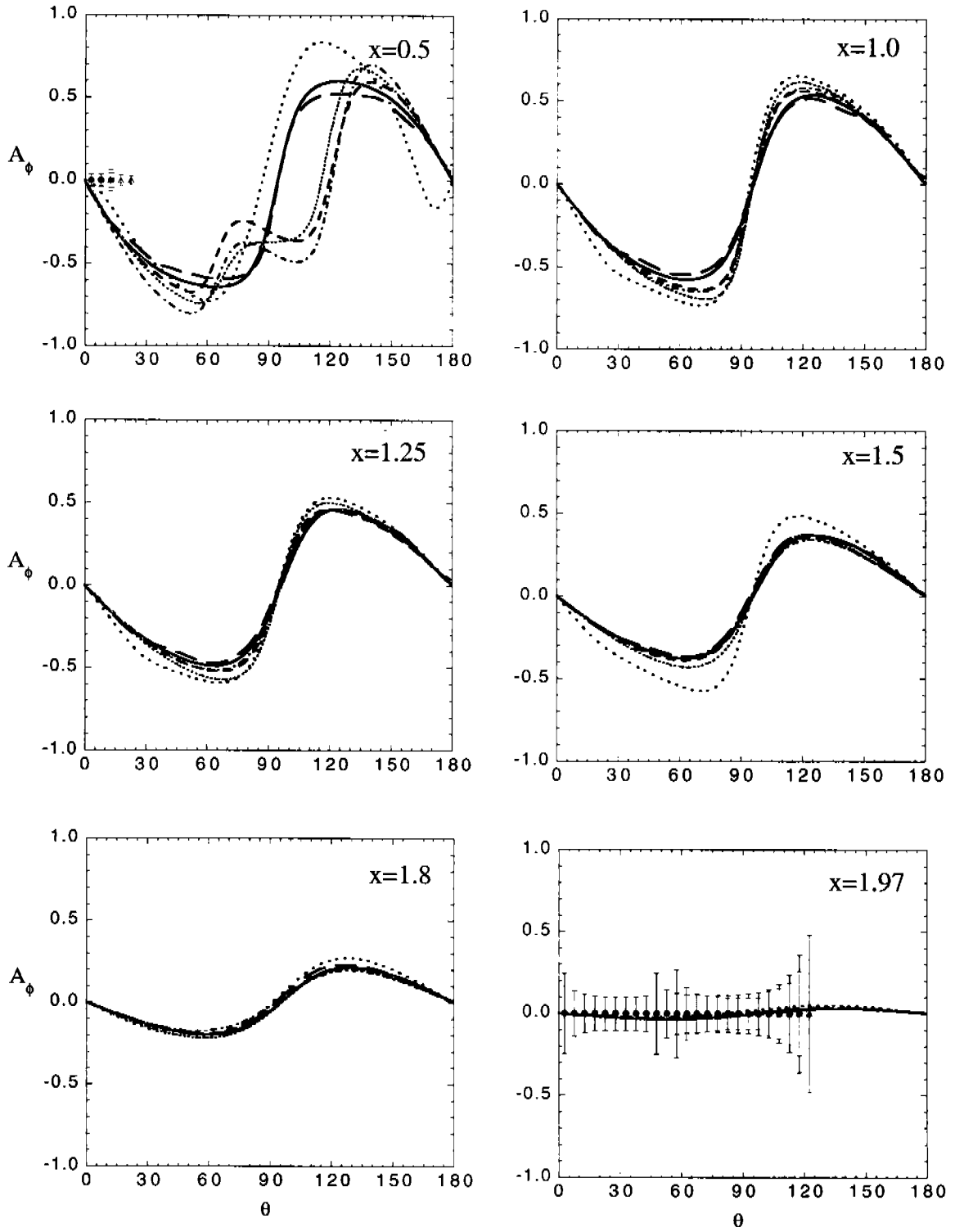

FIG. 19: The A_ϕ at $Q^2 = 2$ GeV^2 and for various x. The meaning of the curves is the same as in Fig. 9. The estimated errors for a JLab measurement using existing equipment, shown on panels for $x = 0.5$ and 1.97, are discussed in the text.

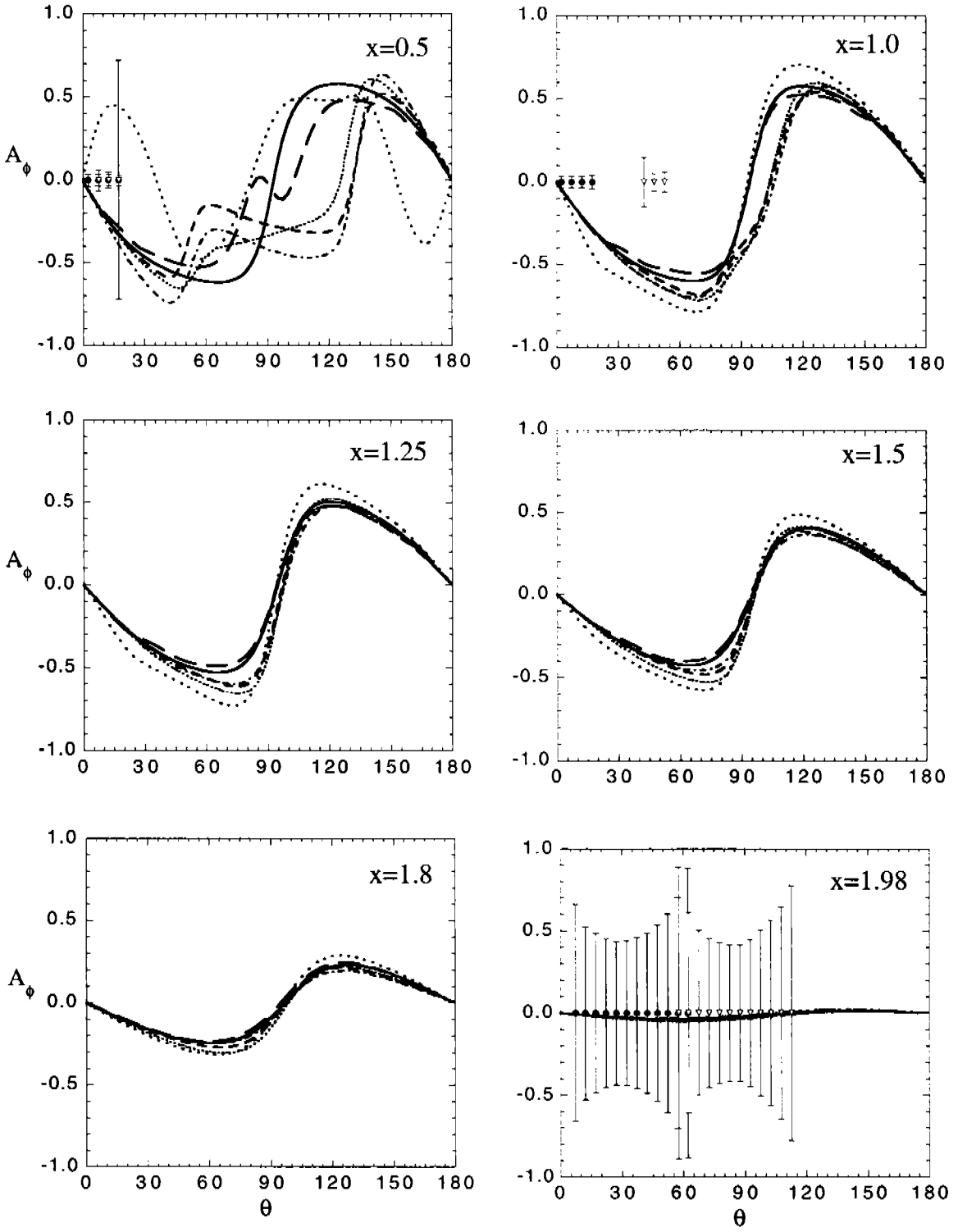

FIG. 20: The A_ϕ at $Q^2 = 3$ GeV^2 and for various x. The meaning of the curves is the same as in Fig. 9. The estimated errors for a JLab measurement using existing equipment, shown on panels for $x = 0.5, 1$, and 1.98 are discussed in the text.

TABLE VI: Sensitivity to relativistic effects (R) compared to estimated measurement errors (M) for selected Q^2 and x.

Q^2 (GeV)^2	1				2				3			
x	0.5	1.0	1.5	1.95	0.5	1.0	1.5	1.97	0.5	1.0	1.5	1.98
$d\sigma$ R (in %)	50	20	10	10	100	50	20	10	100+	50	50	20
$d\sigma$ M (in %)	1	1	1-3	5	5	1-10	1-10		10+	1-20	1-20	50
A_ϕ R (absolute)	0.1	<0.1	<0.1	<0.05	0.2	0.1	0.1	0.01	0.5	0.2	0.1	<0.05
A_ϕ M (absolute)	0.1-0.2			0.1	0.2-0.5			0.1-0.2	<0.1			>0.5

the figures, and to show more clearly the *relative size* of the different calculations, Figs. 13–16 show the *ratio* of each approximation to the C-IIB calculation (our most complete and consistent calculation). The *relative* variation is largest for low x (x=0.5), but is significant at all x, varying from about $\pm 10\%$ to $\pm 50\%$, particularly near $\theta^* \simeq 90°$, depending on the values of Q^2 and x. These variations are summarized in Table VI for the larger values of Q^2. Since the cross sections vary by many orders of magnitude, this model dependence is not large enough to prevent these calculations from providing a useful estimate of the size of the cross section over a wide range of kinematics.

For a few choices of kinematics, we have estimated the size of the experimental errors that can be expected from a measurement of this reaction at JLab using existing equipment. We find, for many kinematics, that the experimental errors would be small enough to distinguish between the different theoretical models shown in the figures. Our estimates of the experimental errors are shown in Figs. 13–16 and in Table VI. In all cases we have examined, except possibly at the largest values of x at the largest Q^2, we could distinguish these models from one another. Of course, the final state interactions and exchange current contributions must be calculated before one has a complete picture of this process, but our results suggest that such a calculation is likely to be worthwhile.

To estimate these errors we assumed the measurement would be carried out in Hall A with the hadron arm of the HRS spectrometer pair placed either in the direction of the momentum transfer vector $\mathbf{q}_L$ (data points with solid circles) or to the left (triangles) or right (inverted triangles) of $\mathbf{q}_L$. Each spectrometer setting is able to measure a range of angles θ^*, with the settings to the left and the right of $\mathbf{q}_L$ able to measure larger θ^*'s than the setting along $\mathbf{q}_L$ (which samples angles near $\theta^* \simeq 0$). The errors grow as θ^* gets close to the limit of the acceptance of the spectrometer, and this explains the large errors at certain angles shown in the figures (see for example, the case when $x = 1.5$ and $Q^2 = 3$, where there are large errors at $\theta^* \simeq 25°$, $\theta^* \simeq 50°$, and $\theta^* \simeq 80°$). This is clearly an artifact of our crude estimates, and could be removed by repositioning the spectrometers. The statistics are based on running for one day at each setting under normal JLab operating conditions.

These graphs show statistical errors only. The estimates of the statistical uncertainties were made by acceptance averaging [43] and radiatively folding [44] the PWBA model of Jeschonnek and Donnelly [39]. An alternate 3-pole parameterization of the MMD nucleon form factors [46] and the Argonne V18 *NN* interaction [35] were used. The simulations were done using a realistic acceptance model for the JLab-Hall A high resolution spectrometer pair. A maximum beam energy of 4 GeV, beam current of 100 μA on a 15 cm liquid

TABLE VII: Cuts used to arrive at the statistical uncertainties.

Q^2 (GeV)^2	x	Q^2-cut	x-cut
1	0.5	0.8-1.2	0.4-0.6
	1.0	0.8-1.2	0.8-1.2
	1.5	0.8-1.2	1.3-1.7
	1.95	0.8-1.2	1.9-2.0
2	0.5	1.8-2.2	0.4-0.6
	1.0	1.8-2.2	0.8-1.2
	1.5	1.8-2.2	1.3-1.7
	1.97	1.8-2.2	1.9-2.0
3	0.5	2.6-3.4	0.4-0.6
	1.0	2.6-3.4	0.8-1.2
	1.5	2.6-3.4	1.3-1.7
	1.98	2.6-3.4	1.95-2.0

deuterium target, and measurement time per kinematic setting of 24 hours were assumed. The cuts shown in Table VII were used to restrict the simulations to reasonable intervals around the desired kinematics.

E. The Asymmetry A_ϕ

Next, we present our results for the asymmetry A_ϕ, which is closely related to the transverse-longitudinal response $\tilde{R}_{LT}$; see Eq. (2.14). The numerical results are shown in Figs. 17 - 20. The asymmetry is zero for $\theta^* = 0°$, then becomes negative, with an extremum around $\theta^* = 60°$ for $Q^2 = 0.5$ GeV^2 and $x = 0.5$. The extremum shifts to smaller angles for increasing x and to larger angles for increasing Q^2. Then, the asymmetry changes sign and exhibits another peak around $\theta^* = 140°$ for $Q^2 = 0.5$ GeV^2 and $x = 0.5$. The positive peak shifts to lower angles both for increasing x and Q^2. The appearance of the positive valued part of A_ϕ depends on the presence of the Born graph contribution, the impulse approximation alone would only lead to one negative peak. Accordingly, when both processes start to interfere, i.e. for the highest x values, the minimum tends to wash out, especially for the situations where the peak around $\theta^* = 180°$ has vanished in the cross section.

One can see at first glance that the asymmetry is less sensitive to the differences in the calculations than is the differential cross section, except near $x = 0.5$. Perhaps the most interesting feature of these calculations is the irregular shape of the asymmetry at $x = 0.5$ for $Q^2 = 2$ and 3 GeV^2. At $Q^2 = 2$ GeV^2 both versions of the JD and the C-AV18 calculation develop an extra dip. At $Q^2 = 3$ GeV^2, the results for $x = 0.5$ develop even more structure, with the AA-v/c calculation having the opposite sign near θ^* near 0°, and the C-IIB-noP showing an extra peak around $\theta = 90°$. At $Q^2 = 3$ and $x = 0.5$, A_ϕ could give unique insight both into the effects of relativity and different wave functions. By contrast, at large x and large Q^2 the asymmetry is very small and not measurable with sufficient accuracy.

The uncertainties in A_ϕ were generated by propagating the errors in the cross sections,

where the latter included statistical errors folded in quadrature with an overall 5% systematic uncertainty. Further, to simplify the procedure, the integrated yields for protons within the right and left hemispheres about the momentum transfer direction were assumed to correspond to $\phi = 0$ and $\phi = \pi$. Finally, the values of the cross sections, needed to propagate the errors for A_ϕ, were taken from the point (*i.e.* not acceptance averaged) values; the statistical uncertainties in the cross sections were, of course, determined using the full acceptance.

IV. CONCLUSIONS

In this paper we have estimated the $d(e,e'p)n$ coincidence cross section using the relativistic impulse approximation (RIA). Our calculations span the range $0.5 \leq Q^2 \leq 3$ GeV^2 and x from 0.5 to just less than 2. In this kinematic region, we find that the results are sensitive to different approximate treatments of the single nucleon current, and conclude the following:

- Using equipment already in existence at JLab, it is feasible to measure the unpolarized coincidence cross section over this entire kinematic range. The asymmetry A_ϕ can be measured at small x where it is large.
- The coincidence cross section is sensitive to the theory over the entire kinematic range, and it appears that measurements can be done to an accuracy sufficient to distinguish a large variety of relativistic models from each other, except possibly when *both* x and Q^2 are very large.
- The asymmetry is less sensitive to the theory, except at the smallest value of $x = 0.5$ where measurements can easily distinguish between different theoretical models.

To complete this preliminary study, we must add relativistic final state interactions and interaction currents that are consistent with the RIA. This is certainly feasible at large values of x, where the low relative momentum in the final state makes it possible to use existing relativistic NN interaction models. It may also be feasible at low x, where the large excitation energy deposited into the final state may justify the use of a relativistic generalization of the Glauber approximation.

Acknowledgments

This work was supported in part by the US Department of Energy. The Southeastern Universities Research Association (SURA) operates the Thomas Jefferson National Accelerator Facility under DOE contract DE-AC05-84ER40150. J.A. was also supported by the grant GA CR 202/00/1669.

APPENDIX A: THE DEUTERON WAVE FUNCTION

1. Helicity spinors

Following the conventions of Jacob and Wick [29], the helicity spinors for a particle with four-momentum $p = \{E, \mathbf{p}\}$ are obtained from spinors with four-momentum $\{m, \mathbf{0}\}$

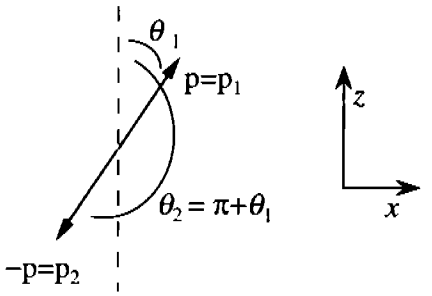

FIG. 21: The definitions of the momenta and angles θ_1 and θ_2.

and spins up or down in the $\hat{z}$ direction. The state is first boosted along the $\hat{z}$-axis until its momentum is $\{E, 0, 0, p\}$ and then is rotated it in the direction of $\mathbf{p}$. The Lorentz transformation that does this is therefore

$$S(\hat{p}, \zeta_p) = \mathcal{R}(\hat{p})\mathcal{B}(\zeta_p) = S(\Lambda(\hat{p}, \zeta_p)) \tag{A1}$$

where $\mathcal{B}$ is the Dirac operator for a pure boost along the z-axis

$$\mathcal{B}(\zeta_p) = e^{\alpha_3 \zeta_p/2} \tag{A2}$$

with $\tanh\zeta_p = p/E$, and $\mathcal{R}$ is the Dirac rotation operator

$$\mathcal{R}(\hat{p}) = \mathcal{R}(\phi, \theta, -\phi) = e^{-i\,\Sigma_3\,\phi/2} e^{-i\,\Sigma_2\,\theta/2} e^{i\,\Sigma_3\,\phi/2} \tag{A3}$$

that takes the momentum from along the $\hat{z}$-axis into its final direction. Using this transformation in the $\hat{x}\hat{z}$ plane ($\phi = 0$), the helicity spinors for particle 1 are defined as in Refs. [24, 47]

$$\begin{aligned}
u(\mathbf{p}, \lambda) &\equiv u_1(\mathbf{p}, \lambda) = S(\hat{p}, \zeta_p)\, u(\mathbf{0}, \lambda) \equiv u_1(\mathrm{p}, \lambda, \theta_1) \\
&= \mathcal{R}_y(\theta_1)\, u_1(\mathrm{p}, \lambda, 0) = \begin{pmatrix} \cosh\frac{1}{2}\zeta_p \\ 2\lambda \sinh\frac{1}{2}\zeta_p \end{pmatrix} \chi_\lambda(\theta_1) \\
v(-\mathbf{p}, \lambda) &\equiv v_1(\mathbf{p}, \lambda) = -(-1)^{\frac{1}{2}-\lambda}\, \mathcal{C}\, u^*(\mathbf{p}, -\lambda) \equiv v_1(\mathrm{p}, \lambda, \theta_1) \\
&= \mathcal{R}_y(\theta_1)\, v_1(\mathrm{p}, \lambda, 0) = \mathcal{R}_y(\theta_1)\, \gamma^5\gamma^0 u_1(\mathrm{p}, \lambda, 0) = \begin{pmatrix} -2\lambda \sinh\frac{1}{2}\zeta_p \\ \cosh\frac{1}{2}\zeta_p \end{pmatrix} \chi_\lambda(\theta_1)
\end{aligned} \tag{A4}$$

where $\mathcal{R}_y(\theta) = \mathcal{R}(0, \theta, 0)$, θ_1 is the polar angle of the vector $\mathbf{p} = \mathbf{p}_1$ (see Fig. 21), and

$$\chi_{\frac{1}{2}}(\theta) = \begin{pmatrix} \cos\frac{1}{2}\theta \\ \sin\frac{1}{2}\theta \end{pmatrix} \qquad \chi_{-\frac{1}{2}}(\theta) = \begin{pmatrix} -\sin\frac{1}{2}\theta \\ \cos\frac{1}{2}\theta \end{pmatrix}. \tag{A5}$$

Note that the $u(\mathbf{p}, \lambda)$ and $v(-\mathbf{p}, \lambda)$ of Ref. [47] are identical to the $u_1(\mathbf{p}, \lambda)$ and $v_1(\mathbf{p}, \lambda)$ of Ref. [24]. Following Jacob and Wick [29], the helicity spinors for particle 2 are defined as

$$u(-\mathbf{p}, \lambda) \equiv u_2(\mathbf{p}, \lambda) = (-1)^{\frac{1}{2}-\lambda}\, \mathcal{R}_y(\theta_1)\, \mathcal{R}_y(\pi)\, \mathcal{B}(\zeta_p)\, u(\mathbf{0}, \lambda) \equiv u_2(\mathrm{p}, \lambda, \theta_2)$$

$$= \mathcal{R}_y(\theta_2)\, u_2(\mathrm{p},\lambda,0) = \mathcal{R}_y(\theta_2)\,(-1)^{\frac{1}{2}-\lambda}\, u_1(\mathrm{p},\lambda,0) = \begin{pmatrix} \cosh\frac{1}{2}\zeta_p \\ 2\lambda\sinh\frac{1}{2}\zeta_p \end{pmatrix} \chi_{-\lambda}(\theta_1)$$

$$v(\mathbf{p},\lambda) \equiv v_2(\mathbf{p},\lambda) = (-1)^{\frac{1}{2}-\lambda}\, C\, u^*(-\mathbf{p},-\lambda) \equiv v_2(\mathrm{p},\lambda,\theta_2)$$

$$= \mathcal{R}_y(\theta_2)\, v_2(\mathrm{p},\lambda,0) = \mathcal{R}_y(\theta_2)\,\gamma^5\gamma^0 u_2(\mathrm{p},\lambda,0) = \begin{pmatrix} -2\lambda\sinh\frac{1}{2}\zeta_p \\ \cosh\frac{1}{2}\zeta_p \end{pmatrix} \chi_{-\lambda}(\theta_1) \quad \text{(A6)}$$

where $\theta_2 = \pi + \theta_1$ is the polar angle of the vector $-\mathbf{p} = \mathbf{p}_2$ (see Fig. 21) and $u(-\mathbf{p},\lambda)$ and $v(\mathbf{p},\lambda)$ are identical to the $u_2(\mathbf{p},\lambda)$ and $v_2(\mathbf{p},\lambda)$ of Ref. [24]. Note that the angular conventions have $0 \le \theta_1 \le \pi$ and have $\pi \le \theta_2 \le 2\pi$. Useful relations, valid on the two-component subspace, are

$$\begin{aligned} \mathcal{R}_y(\theta_2)\,\chi_\lambda(0) &= 2\lambda\,\chi_{-\lambda}(\theta_1) \\ \mathcal{R}_y(\pi)\,\chi_\lambda(\theta) &= 2\lambda\,\chi_{-\lambda}(\theta)\,, \end{aligned} \quad \text{(A7)}$$

and, on the full four-component space, u_1 and u_2 are related by

$$u_2(\mathrm{p},\lambda,\theta_2) = 2\lambda\,\mathcal{R}_y(\pi)\,u_1(\mathrm{p},\lambda,\theta_1)\,. \quad \text{(A8)}$$

[Note that $2\lambda \equiv (-1)^{\frac{1}{2}-\lambda}$.] This last formula is useful for the applications in this paper.

2. Deuteron wave functions in the rest frame

The deuteron wave function (2.27) is manifestly covariant, and we use this feature to simplify the treatment. Applying Eqs. (A4) and (A6) in the deuteron rest frame, the spinor for either particle 1 or 2 can be written in terms of the spinor with the momentum in the $\hat{z}$ direction

$$u_i(\mathbf{p},\lambda) = u_i(\mathrm{p},\lambda,\theta_i) = \mathcal{R}_y(\theta_i)\,u_i(\mathrm{p},\lambda,0)\,. \quad \text{(A9)}$$

Note that this equation holds for particle 2 even though, in applications, we restrict $\theta_2 \ge \pi$. The active rotation of the deuteron helicity vector from an initial direction along the $\hat{z}$-axis to an angle θ with respect to the $\hat{z}$-axis is given in terms of the spin 1 rotation matrices

$$\xi_{\lambda_d}(\theta) = \sum_{\lambda'_d} d^{(1)}_{\lambda_d\lambda'_d}(\theta)\,\xi_{\lambda'_d}(0)\,. \quad \text{(A10)}$$

Substituting (A9) into (2.27), working the operator $\mathcal{R}$ through the rest of the expression, and then using (A10) to realign the deuteron helicity vector in the $\hat{z}$ direction by rotating it through angle $-\theta$, gives

$$\psi^{(i)}_{\lambda,\lambda_d}(p,P) \equiv \psi^{(i)}_{\lambda\mu}(\mathrm{p},\theta_i)\,\xi^\mu_{\lambda_d}(0) = \mathcal{R}_y(\theta_i)\sum_{\lambda'_d}\psi^{(i)}_{\lambda\mu}(\mathrm{p},0)\,\xi^\mu_{\lambda'_d}(0)\,d^{(1)}_{\lambda'_d\lambda_d}(\theta_i) \quad \text{(A11)}$$

where we used $d^{(1)}_{\lambda_d\lambda'_d}(-\theta) = d^{(1)}_{\lambda'_d\lambda_d}(\theta)$. This argument works only in the deuteron rest frame where there is no total three-momentum to be rotated by $\mathcal{R}_y$.

In the *original* reference [30] the on-shell particle was taken to be particle 1 with four-momentum p_1, and the wave function in the deuteron rest frame was expanded in terms

of (on-shell) particle 2 spinors [24]. [Also, be aware that the spinors used in Ref. [30] were quantized along the fixed $\hat{z}$ axis, in for v spinors the notation $-s$ corresponded to spin projection $+s$ in the $\hat{z}$ direction.] In the notation of Eq. (A6) this becomes

$$\psi^{(1)}_{\lambda_1,\lambda_d}(p_1,P) = \sum_{\lambda_2}\left[u_2(\mathrm{p}_1,\lambda_2,\theta_2)\,\psi^{+}_{\lambda_1\lambda_2,\lambda_d}(\mathbf{p}_1) + v_2(\mathrm{p}_1,\lambda_2,\theta_2)\,\psi^{-}_{\lambda_1\lambda_2,\lambda_d}(\mathbf{p}_1)\right]. \tag{A12}$$

Using the fact that $\theta_2 = \pi + \theta_1$, so that $\theta_2 = \pi$ when $\theta_1 = 0$, and using Eq. (A11) gives

$$\begin{aligned}\psi^{(1)}_{\lambda_1,\lambda_d}(p_1,P) \;=\; \sum_{\lambda_2,\lambda'_d}\Big[&u_2(\mathrm{p}_1,\lambda_2,\theta_2)\,\psi^{+}_{\lambda_1\lambda_2,\lambda'_d}(\mathrm{p}_{1z}) \\ &+v_2(\mathrm{p}_1,\lambda_2,\theta_2)\,\psi^{-}_{\lambda_1\lambda_2,\lambda'_d}(\mathrm{p}_{1z})\Big]\,d^{(1)}_{\lambda'_d\lambda_d}(\theta_1)\,,\end{aligned} \tag{A13}$$

where the components $\psi^{\pm}_{\lambda_1\lambda_2,\lambda'_d}(\mathrm{p}_{1z})$ have the relative momentum vector (same as the momentum of particle 1 in the rest system) aligned along the $+\hat{z}$ direction. The $\pm$ components of the wave functions follow from the helicity spinors defined above and the expansions given in Ref. [30]:

$$\begin{aligned}\psi^{+}_{\lambda_1\lambda_2,\lambda_d}(\mathbf{p}) \;&=\; \frac{1}{\sqrt{4\pi}}\chi^{\dagger}_{-\lambda_2}\left[u(\mathrm{p})\,\sigma\cdot\xi_{\lambda_d} + \frac{w(\mathrm{p})}{\sqrt{2}}\left(3\,\hat{\mathbf{p}}\cdot\xi_{\lambda_d}\sigma\cdot\hat{\mathbf{p}} - \sigma\cdot\xi_{\lambda_d}\right)\right]\frac{i\sigma_2}{\sqrt{2}}\,\chi_{\lambda_1} \\ \psi^{-}_{\lambda_1\lambda_2,\lambda_d}(\mathbf{p}) \;&=\; \sqrt{\frac{3}{4\pi}}\chi^{\dagger}_{-\lambda_2}\left[v_s(\mathrm{p})\,\hat{\mathbf{p}}\cdot\xi_{\lambda_d} - \frac{v_t(\mathrm{p})}{\sqrt{2}}\left(\sigma\cdot\hat{\mathbf{p}}\,\sigma\cdot\xi_{\lambda_d} - \hat{\mathbf{p}}\cdot\xi_{\lambda_d}\right)\right]\frac{i\sigma_2}{\sqrt{2}}\,\chi_{\lambda_1}\,.\end{aligned} \tag{A14}$$

Here $u(\mathrm{p})$ and $w(\mathrm{p})$ are the momentum space radial wave functions for the S and D states and $v_t(\mathrm{p})$ and $v_s(\mathrm{p})$ are triplet and singlet P state wave functions, which appear in a manner similar to the lower component wave functions for the Dirac equation. These wave functions are functions of the variable $\mathrm{p} = |\mathbf{p}|$ and satisfy the normalization condition [30]

$$\int_0^\infty \mathrm{p}^2 d\mathrm{p}\left\{u^2(\mathrm{p}) + w^2(\mathrm{p}) + v_t^2(\mathrm{p}) + v_s^2(\mathrm{p})\right\} = 1\,. \tag{A15}$$

The wave functions (A14) can be simplified by specifying the helicity states of the deuteron (in the rest frame). Since the deuteron is a particle 2 in the sense of Jacob and Wick, its helicity states are

$$\xi_{\lambda_d} \equiv \xi^2_{\lambda_d} = (-1)^{s-\lambda_d}\,e^{-i\pi J_y}\,\xi^1_{\lambda_d} = \begin{cases} \frac{1}{\sqrt{2}}(\pm 1,-i,0) & \text{if } \lambda_d = \pm \\ (0,0,1) & \text{if } \lambda_d = 0 \end{cases}. \tag{A16}$$

Note, for future reference, that

$$\mathcal{R}_\pi\,\xi_{\lambda_d} = (-1)^{1-\lambda_d}\,\xi_{-\lambda_d} \tag{A17}$$

where $\mathcal{R}_\pi \equiv \mathcal{R}_y(\pi)$. If $\mathbf{p}$ is in the $+\hat{z}$ direction, it is not difficult to evaluate (A14), giving

$$\begin{aligned}\psi^{+}_{\lambda_1\lambda_2,\lambda_d}(\mathrm{p}_z) \;&=\; \frac{1}{\sqrt{8\pi}}\,\delta_{\lambda_d,\,\lambda_2-\lambda_1}\,f^{+}_{|\lambda_d|}(\mathrm{p}) \\ \psi^{-}_{\lambda_1\lambda_2,\lambda_d}(\mathrm{p}_z) \;&=\; -\frac{2\lambda_1}{\sqrt{8\pi}}\,\delta_{\lambda_d,\,\lambda_2-\lambda_1}\,f^{-}_{|\lambda_d|}(\mathrm{p})\,,\end{aligned} \tag{A18}$$

where

$$f_0^+(\mathrm{p}) = u(\mathrm{p}) + \sqrt{2}\, w(\mathrm{p}) \qquad f_0^-(\mathrm{p}) = \sqrt{3}\, v_s(\mathrm{p})$$
$$f_1^+(\mathrm{p}) = \sqrt{2}\, u(\mathrm{p}) - w(\mathrm{p}) \qquad f_1^-(\mathrm{p}) = \sqrt{3}\, v_t(\mathrm{p}), \tag{A19}$$

Combining the expressions (A13) and (A18) gives

$$\psi^{(1)}_{\lambda_1,\lambda_d}(p_1,P) = \frac{1}{\sqrt{8\pi}} \sum_{\lambda_2} \Big[u_2(\mathrm{p}_1,\lambda_2,\theta_2)\, f^+_{|\lambda_2-\lambda_1|}(\mathrm{p}_1) - 2\lambda_1\, v_2(\mathrm{p}_1,\lambda_2,\theta_2)\, f^-_{|\lambda_2-\lambda_1|}(\mathrm{p}_1) \Big]\, d^{(1)}_{\lambda_2-\lambda_1,\lambda_d}(\theta_1). \tag{A20}$$

One disadvantage of the expansion (A20) is that the four-momentum of particle 2, which is $p_2 = \{M_d - E_{p_1}, -\mathbf{p}_1\}$ in the rest system, is *not* the same as the four-momentum of the spinor u_2, which is $\tilde{p}_2 = \{E_{p_1}, -\mathbf{p}_1\}$. This difference can lead to confusion, especially because the four-momentum $\tilde{p}_2$ is not one of the four-momenta that naturally occurs in the problem. In *this* paper we avoid this confusion, exploit the freedom to expand the off-shell particle in terms spinors with *any* four-momentum, and choose the four-momentum of the on-shell particle (i.e. the spectator) for the expansion. The advantage of this choice is that four-momentum used to describe the off-shell particle is now one of the naturally occurring momenta in the problem. Also, we find that the formalism is simplified if we use $\gamma^5\, u$ instead of v spinors to describe the negative energy states (as in Ref. [47]). With this choice, we find the following expansion for the wave function

$$\psi^{(1)}_{\lambda_1,\lambda_d}(p_1,P) = \sqrt{\frac{3}{8\pi}} \sum_{\lambda_2} \Big[u_1(\mathrm{p}_1,\lambda_2,\theta_1)\, \phi^+_{|\lambda_2+\lambda_1|}(\mathrm{p}_1) - 2\lambda_2\, \gamma^5\, u_1(\mathrm{p}_1,\lambda_2,\theta_1)\, \phi^-_{|\lambda_2+\lambda_1|}(\mathrm{p}_1) \Big]\, d^{(1)}_{-\lambda_2-\lambda_1,\lambda_d}(\theta_1), \tag{A21}$$

where and extra factor of $\sqrt{3}$ has been introduced for convenience. Projecting out the independent components, gives

$$\phi_0^+(\mathrm{p}) = \frac{E_p}{\sqrt{3}\, m} f_0^+(\mathrm{p}) \qquad \phi_0^-(\mathrm{p}) = \frac{1}{\sqrt{3}} \left(\frac{\mathrm{p}}{m} f_0^+(\mathrm{p}) - f_0^-(\mathrm{p}) \right)$$
$$\phi_1^+(\mathrm{p}) = \frac{E_p}{\sqrt{3}\, m} f_1^+(\mathrm{p}) \qquad \phi_1^-(\mathrm{p}) = \frac{1}{\sqrt{3}} \left(\frac{\mathrm{p}}{m} f_1^+(\mathrm{p}) + f_1^-(\mathrm{p}) \right), \tag{A22}$$

where the new wave functions were given in Table III.

Comparison of the expansions (A20) and (A21) underline the fact that *the separation of the wave function into positive and negative energy parts is a matter of convention*; only the total result is independent of this separation.

By a similar argument, we expect the expansion for $\psi^{(2)}$ to be

$$\psi^{(2)}_{\lambda_2\lambda_d}(p_2,P) = \sqrt{\frac{3}{8\pi}} \sum_{\lambda_1} \Big[u_2(\mathrm{p}_2,\lambda_1,\theta_2)\, \phi'^+_{|\lambda_2+\lambda_1|}(\mathrm{p}_2) - 2\lambda_1\, \gamma^5\, u_2(\mathrm{p}_2,\lambda_1,\theta_2)\, \phi'^-_{|\lambda_2+\lambda_1|}(\mathrm{p}_2) \Big]\, d^{(1)}_{\lambda_2+\lambda_1,\lambda_d}(\theta_2-\pi). \tag{A23}$$

One can prove that $\phi^{\pm} = \phi'^{\pm}$ by finding the expansions for $\psi^{(2)}$ directly from those for $\psi^{(1)}$. Using (A23) and orthogonality relations for the spinors gives

$$\begin{aligned}
(3/8\pi)^{1/2}\,\phi'^{+}_{|\Lambda|}(\mathrm{p}_2)\,d^{(1)}_{\Lambda,\lambda_d}(\theta_1) &= \bar{u}_2(\mathrm{p}_2,\lambda_1,\theta_2)\,\psi^{(2)}_{\lambda_2,\lambda_d}(p_2,P) \\
&= \bar{u}_2(\mathrm{p}_2,\lambda_1,\theta_2)\,\Gamma_{\lambda_d}(p_2,P)\,\mathcal{C}\,\bar{u}_2^T(\mathrm{p}_2,\lambda_2,\theta_2) \\
&= 4\lambda_1\lambda_2\,\bar{u}_1(\mathrm{p}_2,\lambda_1,\theta_1)\,\mathcal{R}_\pi\,\Gamma_{\lambda_d}(p_2,P)\,\mathcal{C}\,\mathcal{R}_\pi^{-1}\,\bar{u}_1^T(\mathrm{p}_2,\lambda_2,\theta_1) \\
&= 4\lambda_1\lambda_2(-1)^{1-\lambda_d}\,\bar{u}_1(\mathrm{p}_2,\lambda_1,\theta_1)\,\Gamma_{-\lambda_d}(p_1,P)\,\mathcal{C}\,\bar{u}_1^T(\mathrm{p}_2,\lambda_2,\theta_1) \\
&= (-1)^{\Lambda-\lambda_d}\,\bar{u}_1(\mathrm{p}_2,\lambda_1,\theta_1)\,\Gamma_{-\lambda_d}(p_1,P)\,\mathcal{C}\,\bar{u}_1^T(\mathrm{p}_2,\lambda_2,\theta_1)\,, \quad \text{(A24)}
\end{aligned}$$

where $\Lambda = \lambda_1 + \lambda_2$, $\Gamma_{\lambda_d}(p,P) \equiv \Gamma_\mu(p,P)\,\xi^\mu_{\lambda_d}(P)$, $R_y(\pi)\,p_2 = p_1$, and we used the relations (A8) and (A17). However, from (A21)

$$\begin{aligned}
(3/8\pi)^{1/2}\,\phi^{+}_{|\Lambda|}(\mathrm{p}_1)\,d^{(1)}_{\Lambda,\lambda_d}(\theta_2-\pi) &= (3/8\pi)^{1/2}\,(-1)^{\Lambda-\lambda_d}\,\phi^{+}_{|\Lambda|}(\mathrm{p}_1)\,d^{(1)}_{-\Lambda,-\lambda_d}(\theta_1) \\
&= (-1)^{\Lambda-\lambda_d}\,\bar{u}_1(\mathrm{p}_1,\lambda_2,\theta_1)\,\psi^{(1)}_{\lambda_1,-\lambda_d}(p_1,P) \\
&= (-1)^{\Lambda-\lambda_d}\,\bar{u}_1(\mathrm{p}_1,\lambda_2,\theta_1)\,\Gamma_{-\lambda_d}(p_1,P)\,\mathcal{C}\,\bar{u}_1^T(\mathrm{p}_1,\lambda_1,\theta_1)\,. \quad \text{(A25)}
\end{aligned}$$

Since this equation is symmetric under the interchange of λ_1 and λ_2, and $\mathrm{p}_1 = \mathrm{p}_2$ in the c.m. system, the two equations (A24) and (A25) are equal, and $\phi^+ = \phi'^+$. A similar argument holds of ϕ^-.

The wave functions used in this paper were obtained by solving the Spectator equation using a kernel adjusted to fit the NN data below 350 MeV lab energy [24].

3. Boosting helicity spinors

In order to boost the spectator equation wave functions it is necessary to have expressions for the pure boosts of the helicity spinors. Indeed, for the applications to elastic deuteron electromagnetic form factors and the response functions for deuteron electrodisintegration, it is only necessary to study the case where the boosts are made along the z-axis. Since the Dirac spinors for arbitrary momentum are defined in terms of a Lorentz transformation of the rest frame spinors, it is useful to define the four-momentum in the particle rest frame as

$$\tilde{p} = (m, \mathbf{0}). \quad \text{(A26)}$$

Three basic Lorentz transformations are required in the following discussion. In the notation of Eq. (A1), these are:

$$\begin{aligned}
p &= S(\hat{p},\zeta_p)\,\tilde{p} \equiv \mathcal{R}(\hat{p})\mathcal{B}(\zeta_p)\,\tilde{p} \\
p' &= S(\hat{p}',\zeta_{p'})\,\tilde{p} \equiv \mathcal{R}(\hat{p}')\mathcal{B}(\zeta_{p'})\,\tilde{p} \\
p' &= \mathcal{B}(\zeta_z)\,p \quad \text{(A27)}
\end{aligned}$$

The first Lorentz transformation connects the particle rest frame with the initial frame of the particle and is composed of a pure boost along the z-axis $\mathcal{B}(\zeta_p)$ followed by a rotation into the direction of the initial particle direction $\mathcal{R}(\hat{p})$. The second Lorentz transformation connects the particle rest frame with the final frame of the particle and is also composed of a pure boost along the z-axis followed by a rotation. The third Lorentz transformation connects the initial and final particle frames with a pure boost along the z-axis.

Now consider the boost of a helicity spinor [either u_1 of Eq. (A4) or $u_2(\mathbf{p},\lambda)$ of Eq. (A6)] along the z-axis

$$\begin{aligned}\mathcal{B}(\zeta_z)\,u_i(\mathbf{p},\lambda) &= \mathcal{B}(\zeta_z)\,S(\hat{p},\zeta_p)\,u_i(\mathbf{0},\lambda)\\ &= S(\hat{p}',\zeta_{p'})\,S^{-1}(\hat{p}',\zeta_{p'})\,\mathcal{B}(\zeta_z)\,S(\hat{p},\zeta_p)\,u_i(\mathbf{0},\lambda)\\ &= S(\hat{p}',\zeta_{p'})\,S\left(\Lambda^{-1}(\hat{p}',\zeta_{p'})B(\zeta_z)\Lambda(\hat{p},\zeta_p)\right)u_i(\mathbf{0},\lambda) \qquad \text{(A28)}\end{aligned}$$

where $S(\hat{p},\zeta_p) = S(\Lambda(\hat{p},\zeta_p))$ is the representation of the Lorentz transformation $\Lambda(\hat{p},\zeta_p)$ and the group composition property of the Lorentz transformations has been used in writing the final step. Since

$$\Lambda^{-1}(\hat{p}',\zeta_{p'})B(\zeta_z)\Lambda(\hat{p},\zeta_p)\,\tilde{p} = \tilde{p}, \qquad \text{(A29)}$$

this combination of Lorentz transformations must be equivalent to a rotation,and is referred to as the Wigner rotation. In this case, where the boost is along the z-axis and the momenta are in the $\hat{x}\hat{z}$ plane, the Wigner rotation is a rotation about the $\hat{y}$ axis, denoted $\mathcal{R}_y(\omega_i)$. The boosted spinor can therefore be written

$$\begin{aligned}\mathcal{B}(\zeta_z)\,u_i(\mathbf{p},\lambda) &= S(\hat{p}',\zeta_{p'})\,\mathcal{R}_y(\omega_1)\,u_i(\mathbf{0},\lambda) = S(\hat{p}',\zeta_{p'})\sum_{\lambda'}u_i(\mathbf{0},\lambda')\,d^{(1/2)}_{\lambda'\lambda}(\omega_i)\\ &= \sum_{\lambda'}u_i(\mathbf{p}',\lambda')\,d^{(1/2)}_{\lambda'\lambda}(\omega_i)\,. \qquad \text{(A30)}\end{aligned}$$

Since γ^5 and $\mathcal{C}\,\gamma^0$ both commute with the boost, and since the boost is real, (A30) also holds for $\gamma^5\,u_i(\mathbf{p},\lambda)$ and $\mathcal{C}\,\bar{u}_i^T(\mathbf{p},\lambda)$.

In this paper $\mathcal{B}(\zeta_z)$ will be chosen to be the boost from the c.m. frame where $P^* = \{D_0,0,0,-q_0\}$ to the lab frame where $P = \{M_d,0,0,0\}$. This is accomplished by a boost in the positive $\hat{z}$ direction with $\tanh\zeta_z = q_0/D_0$. In the notation we have introduced, the basic equations are

$$\mathcal{B}(\zeta_z)\,\mathcal{C}\,\bar{u}_i^T(\mathbf{p}_i^*,\lambda) = \sum_{\lambda'}\mathcal{C}\,\bar{u}_i^T(\mathbf{p}_i,\lambda')\,d^{(1/2)}_{\lambda'\lambda}(\omega_i)\,, \qquad \text{(A31)}$$

and the inverse relations

$$\mathcal{B}^{-1}(\zeta_z)\,\mathcal{C}\,\bar{u}_i^T(\mathbf{p}_i,\lambda) = \sum_{\lambda'}\mathcal{C}\,\bar{u}_i^T(\mathbf{p}_i^*,\lambda')\,d^{(1/2)}_{\lambda'\lambda}(-\omega_i)\,, \qquad \text{(A32)}$$

where the unstarred variables are in the deuteron rest frame (the lab frame) and the starred variables are in the c.m. frame of the electrodisintegration process.

The Wigner rotation angles can be computed from the standard relations

$$\mathcal{B}^{-1}(\zeta_z)\,\mathcal{R}_y(\theta_i)\,\mathcal{B}(\zeta_{p_i}) = \mathcal{R}_y(\theta_i^*)\,\mathcal{B}(\zeta_p)\mathcal{R}_y(\mp\omega_i)\,, \qquad \text{(A33)}$$

where the upper sign holds for $i = 1$ and the lower for $i = 2$ [the change in sign is a consequence of the phase relation in Eq. (A8)], and $\theta_1^* = \theta^*$ and $\theta_2^* = \theta^* + \pi$ [recall Table I; the form of θ_2^* is a consequence of the extra rotation by π in Eq. (A8)]. Writing the rotation and boost operators in closed form, Eq. (A33) can be written

$$\begin{aligned}&\left[\cosh\tfrac{1}{2}\zeta_z - \alpha_3\sinh\tfrac{1}{2}\zeta_z\right]\left(\cos\tfrac{1}{2}\theta_i - i\Sigma_2\sin\tfrac{1}{2}\theta_i\right)\left[\cosh\tfrac{1}{2}\zeta_{p_i} - \alpha_3\sinh\tfrac{1}{2}\zeta_{p_i}\right]\\ &\quad= \left(\cos\tfrac{1}{2}\theta_i^* - i\Sigma_2\sin\tfrac{1}{2}\theta_i^*\right)\left[\cosh\tfrac{1}{2}\zeta_p - \alpha_3\sinh\tfrac{1}{2}\zeta_p\right]\left(\cos\tfrac{1}{2}\tilde{\omega} + i\Sigma_2\sin\tfrac{1}{2}\tilde{\omega}\right), \qquad \text{(A34)}\end{aligned}$$

where $\tilde{\omega}$ is a shorthand for either ω_1 or $-\omega_2$, depending on the case under consideration. This operator relation can be separated into four independent equations relating $\tilde{\omega}$ to the lab variables $\{p_i,\, \theta_i\}$ to the c.m. variables $\{p, \theta_i^*\}$. A convenient form of these equations is

$$\begin{aligned}
C_{-+} \cos\tfrac{1}{2}\theta_i &= \sqrt{2M_d(E+m)}\, \cos\tfrac{1}{2}(\theta_i^* - \tilde{\omega}) \\
C_{--} \cos\tfrac{1}{2}\theta_i &= \sqrt{2M_d(E-m)}\, \cos\tfrac{1}{2}(\theta_i^* + \tilde{\omega}) \\
C_{++} \sin\tfrac{1}{2}\theta_i &= \sqrt{2M_d(E+m)}\, \sin\tfrac{1}{2}(\theta_i^* - \tilde{\omega}) \\
C_{+-} \sin\tfrac{1}{2}\theta_i &= \sqrt{2M_d(E-m)}\, \sin\tfrac{1}{2}(\theta_i^* + \tilde{\omega})
\end{aligned} \tag{A35}$$

where

$$C_{ab} = \sqrt{(D_0 + M_d)(E_i + am)} + b\sqrt{(D_0 - M_d)(E_i - am)}\,, \tag{A36}$$

with $E = \sqrt{m^2 + p^2}$ and $E_i = \sqrt{m^2 + p_i^2}$. The following identities, derived from these equations, are very useful:

$$\begin{aligned}
\frac{E}{m}\sin\theta_i^*\cos\tilde{\omega} - \cos\theta_i^*\sin\tilde{\omega} &= \frac{E_i}{m}\sin\theta_i \\
\frac{E}{m}\sin\theta_i^*\sin\tilde{\omega} + \cos\theta_i^*\cos\tilde{\omega} &= \cos\theta_i \\
-\frac{E}{m}\cos\theta_i^*\sin\tilde{\omega} + \sin\theta_i^*\cos\tilde{\omega} &= \frac{D_0}{M_d}\sin\theta_i \\
\frac{E}{m}\cos\theta_i^*\cos\tilde{\omega} + \sin\theta_i^*\sin\tilde{\omega} &= \frac{D_0\, E_i}{M_d\, m}\cos\theta_i - \frac{q_0\, p_i}{M_d\, m} \\
-p\cos\tilde{\omega} &= \frac{q_0}{M_d}E_i\cos\theta_i - \frac{D_0}{M_d}p_i \\
p\sin\tilde{\omega} &= \frac{m}{M_d}\,q_0\sin\theta_i
\end{aligned} \tag{A37}$$

4. Boosting the deuteron wave function

In order to calculate the response functions for deuteron electrodisintegration it is necessary boost the deuteron wave functions from the center of momentum frame of the final state proton-neutron pair to the rest (lab) frame of the deuteron (where the decomposition of the wave functions onto S, D, and P states has been defined). If the system is quantized such that the three-momentum transfer $\mathbf{q}$ lies along the z-axis, then the deuteron wave functions in the c.m. must be boosted to the rest frame by a pure active boost $\mathcal{B}(\zeta_z)$ in the $\hat{z}$ direction with $\tanh\zeta_x = q_0/D_0$, as defined in the previous section.

The rest frame wave functions are obtained by applying the operator $\mathcal{B} = \mathcal{B}(\zeta_z)$ to the wave functions (2.27), which gives

$$\begin{aligned}
\mathcal{B}\,\psi^{(i)}_{\lambda\lambda_d}(p_i^*,\, P^*) &= \mathcal{B}\,\frac{m + \not{P}^* - \not{p}_i^*}{m^2 - (P^* - p_i^*)^2}\, N_d\, \Gamma_{\lambda_d}(p_i^*, P^*)\, \mathcal{C}\, \bar{u}_i^T(\mathbf{p}_i^*, \lambda) \\
&= \left\{\mathcal{B}\,\frac{m + \not{P}^* - \not{p}_i^*}{m^2 - (P^* - p_i^*)^2}\,\mathcal{B}^{-1}\right\}\left\{\mathcal{B}\, N_d\, \Gamma_{\lambda_d}(p_i^*, P^*)\,\mathcal{B}^{-1}\right\}\left[\mathcal{B}\,\mathcal{C}\,\bar{u}_i^T(\mathbf{p}_i^*, \lambda)\right] \\
&= \sum_{\lambda'}\frac{m + \not{P} - \not{p}_i}{m^2 - (P - p_i)^2}\, N_d\, \Gamma_{\lambda_d}(p_i, P)\, \mathcal{C}\, \bar{u}_i^T(\mathbf{p}_i, \lambda')\; d^{(1/2)}_{\lambda'\lambda}(\omega_i)
\end{aligned}$$

$$= \sum_{\lambda'} \psi^{(i)}_{\lambda'\lambda_d}(p_i, P)\; d^{(1/2)}_{\lambda'\lambda}(\omega_i)\,, \tag{A38}$$

where, in the next to last step, we used the boost properties of the helicity spinors (A31) and fact that the propagator and $\Gamma_{\lambda_d}(p_i, P)$ are Lorentz scalars. Note that there is no Wigner rotation of the deuteron helicity vector because the boost is in the same direction as its momentum (but the components of the vector ξ_0 do change). The wave function in the c.m. frame can therefore be written in terms of the rest frame wave function

$$\psi^{(i)}_{\lambda\lambda_d}(p_i^*, P^*) = \sum_{\lambda'} \mathcal{B}^{-1}\, \psi_{\lambda'\lambda_d}(p, P)\; d^{(1/2)}_{\lambda'\lambda}(\omega_i)\,. \tag{A39}$$

Using the representations (A21) or (A23), and the boost formula (A39) and (A30), the wave function in the c.m. frame becomes

$$\begin{aligned}
\psi^{(i)}_{\lambda_i,\lambda_d}(p_i^*, P^*) \;&=\; \sqrt{\frac{3}{8\pi}} \sum_{\lambda_j'\lambda_i'} \mathcal{B}^{-1}\, \Big[u_i(\mathbf{p}_i, \lambda_j')\, \phi^+_{|\Lambda|}(\mathrm{p}_i) - 2\lambda_j'\, \gamma^5\, u_i(\mathbf{p}_i, \lambda_j')\, \phi^-_{|\Lambda|}(\mathrm{p}_i)\Big] \\
&\qquad\qquad \times d^{(1)}_{\mp\Lambda,\,\lambda_d}(\tilde\theta_i)\; d^{(1/2)}_{\lambda_i'\lambda_i}(\omega_i) \\
&=\; \sqrt{\frac{3}{8\pi}} \sum_{\lambda_j'\lambda_i'\lambda} \Big[u_i(\mathbf{p}_i^*, \lambda)\, \phi^+_{|\Lambda|}(\mathrm{p}_i) - 2\lambda_j'\, \gamma^5\, u_i(\mathbf{p}_i^*, \lambda)\, \phi^-_{|\Lambda|}(\mathrm{p}_i)\Big] \\
&\qquad\qquad \times d^{(1)}_{\mp\Lambda,\,\lambda_d}(\tilde\theta_i)\; d^{(1/2)}_{\lambda_i'\lambda_i}(\omega_i)\; d^{(1/2)}_{\lambda_j'\lambda}(\omega_i)\,,
\end{aligned} \tag{A40}$$

where $\Lambda = \lambda_i' + \lambda_j'$, $\tilde\theta_1 = \theta_1$ and $\tilde\theta_2 = \theta_2 - \pi$, and the upper(lower) sign in the Λ index of $d^{(1)}$ is for $i = 1(2)$. Note that the notation is mixed in the last equation : the momentum of the spinors is expressed in the c.m. frame and the variables of the ϕ's and $d^{(1)}$ are in the deuteron rest frame.

APPENDIX B: THE HADRONIC MATRIX ELEMENT

1. The plane wave matrix elements

Using Eq. (A40), the current matrix element (2.25), in the c.m. frame, becomes

$$\begin{aligned}
&\Big\langle \lambda_1\lambda_2 \Big| J_{\lambda_\gamma}(q) \Big| \lambda_d \Big\rangle = \sqrt{\frac{3}{16\pi}}\, \frac{1}{N_d} \sum_{\lambda_1'\lambda_2'\lambda} \\
&\Big\{ \bar u_1(\mathbf{p}_1^*, \lambda_1)\, j^{(1)}_{\lambda_\gamma}(p_1^*, p_1^* - q^*) \Big[u_2(\mathbf{p}_2^*, \lambda)\, \phi^+_{|\Lambda|}(\mathrm{p}_2) - 2\lambda_1'\, \gamma^5\, u_2(\mathbf{p}_2^*, \lambda)\, \phi^-_{|\Lambda|}(\mathrm{p}_2)\Big]\; \Xi_2 \\
&- \bar u_2(\mathbf{p}_2^*, \lambda_2)\, j^{(2)}_{\lambda_\gamma}(p_2^*, p_2^* - q^*) \Big[u_1(\mathbf{p}_1^*, \lambda)\, \phi^+_{|\Lambda|}(\mathrm{p}_1) - 2\lambda_2'\, \gamma^5\, u_1(\mathbf{p}_1^*, \lambda)\, \phi^-_{|\Lambda|}(\mathrm{p}_1)\Big]\; \Xi_1 \Big\}\,,
\end{aligned} \tag{B1}$$

where

$$\begin{aligned}
\Xi_2 \;&=\; d^{(1)}_{\Lambda,\,\lambda_d}(\theta_2 - \pi)\; d^{(1/2)}_{\lambda_2'\lambda_2}(\omega_2)\; d^{(1/2)}_{\lambda_1'\lambda}(\omega_2) \\
\Xi_1 \;&=\; d^{(1)}_{-\Lambda,\,\lambda_d}(\theta_1)\; d^{(1/2)}_{\lambda_1'\lambda_1}(\omega_1)\; d^{(1/2)}_{\lambda_2'\lambda}(\omega_1)\,.
\end{aligned} \tag{B2}$$

and Λ and the Wigner rotation angles ω_i were defined above.

The matrix elements of the single nucleon current operator, in the c.m. system, are defined to be

$$j^{(i)\,\rho}_{\lambda_i\,\lambda;\lambda_\gamma}(\mathrm{p},\theta^*,q_0) = \begin{cases} \bar{u}_i(\mathbf{p}_i^*,\lambda_i)\, j^{(i)}_{\lambda_\gamma}(p_i^*,p_i^*-q^*)\, u_j(\mathbf{p}_j^*,\lambda) & \text{if } \rho=+ \\ \bar{u}_i(\mathbf{p}_i^*,\lambda_i)\, j^{(i)}_{\lambda_\gamma}(p_i^*,p_i^*-q^*)\, \gamma^5\, u_j(\mathbf{p}_j^*,\lambda) & \text{if } \rho=- \end{cases} . \tag{B3}$$

These are calculated in the next section. Using this notation, the current matrix elements (B1) can be written in the following compact notation

$$\begin{aligned} \left\langle \lambda_1\lambda_2 \left| J_{\lambda_\gamma}(q) \right| \lambda_d \right\rangle &= (J_{\lambda_\gamma})^{\lambda_d}_{\lambda_1\,\lambda_2}(p_1^*,p_2^*,q^*) \\ &= \sqrt{\frac{3}{16\pi}}\,\frac{1}{N_d}\sum_{\lambda\rho}\sum_{\lambda_1'\lambda_2'}\Big\{ \eta_\rho(2\lambda_1')\, j^{(1)\,\rho}_{\lambda_1'\,\lambda;\lambda_\gamma}(\mathrm{p},\theta^*,q_0)\,\phi^\rho_{|\Lambda|}(\mathrm{p}_2)\, d^{(1)}_{\Lambda,\lambda_d}(\theta_2-\pi)\, d^{(1/2)}_{\lambda_2'\lambda_2}(\omega_2)\, d^{(1/2)}_{\lambda_1'\lambda}(\omega_2) \\ &\quad -\eta_\rho(2\lambda_2')\, j^{(2)\,\rho}_{\lambda_2'\,\lambda;\lambda_\gamma}(\mathrm{p},\theta^*,q_0)\,\phi^\rho_{|\Lambda|}(\mathrm{p}_1)\, d^{(1)}_{-\Lambda,\lambda_d}(\theta_1)\, d^{(1/2)}_{\lambda_1'\lambda_1}(\omega_1)\, d^{(1/2)}_{\lambda_2'\lambda}(\omega_1)\Big\}, \end{aligned} \tag{B4}$$

where $\eta_\rho(x)$ is the phase defined in Eq. (2.35). The unpolarized cross section will be calculated from this matrix element after the matrix elements of the nucleon current have been discussed.

2. The single nucleon current

In the spectator formalism used in this paper, the NN interaction kernel has a form factor $h(p^2)$ ($h(m^2)=1$) attached to each off-shell nucleon which enters of leaves the interaction. Alternatively, this form factor can be removed from the kernel and attached to the nucleon propagators, which then have the form

$$\tilde{S}_F(p) = \frac{h^2(p^2)}{m-\not{p}} \tag{B5}$$

Gauge invariance [32] will be insured if we introduce a *reduced* nucleon current $j^\mu_R(p',p)$

$$j^\mu(p',p) = \quad h' j^\mu_R(p',p) h\,, \tag{B6}$$

where $h = h(p^2)$ and $h' = h(p'^2)$, which satisfies the Ward-Takahashi identity using the dressed propagator

$$q_\mu j^\mu_R(p',p) = \tilde{S}_F^{-1}(p) - \tilde{S}_F^{-1}(p')\,. \tag{B7}$$

A simple choice for the reduced current which satisfies this identity is [25, 32, 48]

$$\begin{aligned} j^\mu_R(p',p) = \quad & F_0(F_1(Q^2)-1)\tilde{\gamma}^\mu + F_0F_2(Q^2)\,\frac{i\,\sigma^{\mu\nu}q_\nu}{2m} + F_0\,\gamma^\mu \\ & +G_0(F_3(Q^2)-1)\,\Lambda_-(p')\tilde{\gamma}^\mu\Lambda_-(p) + G_0\,\Lambda_-(p')\gamma^\mu\Lambda_-(p)\,, \end{aligned} \tag{B8}$$

where $F_{1,2}(Q^2)$ are the on-shell nucleon form factors, $F_3(Q^2)$ is a completely unknown form factor describing the off-shell structure of the nucleon (subject to the constraint that $F_3(0) =$

1), $\Lambda_-(p) = (m - \not{p})/(2m)$, $\tilde{\gamma}^\mu = \gamma^\mu - q^\mu \not{q}/q^2$ and F_0 and G_0 are functions of p^2 and p'^2 completely determined by the WT identity:

$$\begin{aligned} F_0 &= \frac{1}{h'^2}\,\frac{m^2 - p'^2}{p^2 - p'^2} + \frac{1}{h^2}\,\frac{m^2 - p^2}{p'^2 - p^2} \\ G_0 &= \left(\frac{1}{h'^2} - \frac{1}{h^2}\right)\frac{4m^2}{p'^2 - p^2}\,. \end{aligned} \tag{B9}$$

Since the final nucleon is always on-shell in the RIA approximation, $p'^2 = m^2$ and the terms multiplied by $\Lambda_-(p')$ vanish, giving

$$j^\mu_R(p', p) = \frac{1}{h^2}\left\{F_1(Q^2)\tilde{\gamma}^\mu + F_2(Q^2)\,\frac{i\,\sigma^{\mu\nu}q_\nu}{2m} + \frac{q^\mu \not{q}}{q^2}\right\}. \tag{B10}$$

Furthermore, the terms proportional to q^μ vanish when the current is contracted with the photon helicity vectors. Hence, the current for use in the RIA reduces to the traditional current divided by h

$$j^\mu(p', p) = \frac{1}{h(p^2)}\left\{F_1(Q^2)\gamma^\mu + F_2(Q^2)\,\frac{i\,\sigma^{\mu\nu}q_\nu}{2m}\right\} \qquad \left(\text{when } p'^2 = m^2\right). \tag{B11}$$

Even when one of the particles is off-shell the only modification to the on-shell current which survives is the appearance of the factor of $1/h$.

The photon helicity states in the c.m. frame, as defined in Ref. [21], are

$$\begin{aligned} \varepsilon_{\pm 1} &= \frac{1}{\sqrt{2}}\,(0, \mp 1, -i, 0) \\ \varepsilon_0 &= \frac{1}{Q}\,(q_0, 0, 0, \nu_0)\,. \end{aligned} \tag{B12}$$

Hence, the single nucleon current operator, defined in Eq. (2.26) and (B11), is

$$j^{(i)}_{\lambda_\gamma}(p_i^*, p_i^* - q^*) = F_1(Q^2)\;\not{\varepsilon}_{\lambda_\gamma} - F_2(Q^2)\frac{\not{\varepsilon}_{\lambda_\gamma}\not{q}}{2m}, \tag{B13}$$

where the factor of $1/h$ has been omitted (it is absorbed into the wave function). As discussed above and in Ref. [21], the results are simplified if we consider the symmetric and anti-symmetric combinations of the transverse helicity amplitudes, which are found from

$$\begin{aligned} \varepsilon_s &= \frac{1}{2}\,(\varepsilon_1 - \varepsilon_{-1}) = \frac{1}{\sqrt{2}}\,(0, -1, 0, 0) \\ \varepsilon_a &= \frac{1}{2}\,(\varepsilon_1 + \varepsilon_{-1}) = \frac{1}{\sqrt{2}}\,(0, 0, -i, 0)\,. \end{aligned} \tag{B14}$$

Using the explicit form of the spinors given in Eqs. (A4) and (A6) we can show that the current matrix elements have the form

$$j^{(i)\,\rho}_{\lambda'\lambda;\,g}(\mathrm{p}, \theta^*, q_0) = \begin{cases} \delta_{\lambda',\,-\lambda}\; j^{(i)\rho}_{1g} + 2\lambda'\,\delta_{\lambda',\lambda}\; j^{(i)\rho}_{2g} & \text{for } \{\rho, g\} = (+,0), (+,s), (-,a) \\ 2\lambda'\,\delta_{\lambda',\,-\lambda}\; j^{(i)\rho}_{1g} + \delta_{\lambda',\lambda}\; j^{(i)\rho}_{2g} & \text{for } \{\rho, g\} = (-,0), (-,s), (+,a)\,. \end{cases} \tag{B15}$$

where $g = \{0, s, a\}$ replaces the helicity. If the proton (particle 1) matrix elements are calculated first, the neutron elements follow from

$$\begin{aligned} j^{(2)+}_{\lambda'\lambda;g}(\mathrm{p}, \theta^*, q_0) &= \bar{u}_2(\mathrm{p}, \lambda', \theta^* + \pi)\, j^{(2)}_g(p_2^*, p_2^* - q^*)\, u_1(\mathrm{p}, \lambda, \theta^*) \\ &= -4\lambda'\lambda\, \bar{u}_1(\mathrm{p}, \lambda', \theta^*)\, \mathcal{R}_\pi j^{(2)}_g(p_2^*, p_2^* - q^*)\, \mathcal{R}_\pi^{-1}\, u_2(\mathrm{p}, \lambda, \theta^* + \pi) \\ &= -4\lambda'\lambda\, \eta'(g)\, \bar{u}_1(\mathrm{p}, \lambda', \theta^*)\, j^{(2)}_g(p_1^*, p_1^* - \hat{q}^*)\, u_2(\mathrm{p}, \lambda, \theta^* + \pi) \\ &= -4\lambda'\lambda\, \eta'(g)\, j^{(1)+}_{\lambda'\lambda;g}(\mathrm{p}, \theta^*, -q_0)\,, \end{aligned} \tag{B16}$$

where the rotation by π about the $\hat{y}$ axis has changed $p_2^* \to p_1^*$, $q^* \to \hat{q}^* = (\nu_0, 0, 0, -q_0)$, $\varepsilon_0 \to -(-q_0, 0, 0, \nu_0)$ [so that the effect on the $g = 0$ amplitude is to change the phase and to change $q_0 \to -q_0$], and therefore the phase $\eta'(g)$, arising from the rotation of the photon helicity vectors, is negative (for $g = 0$ or s) or positive (for $g = a$). The change in the operator $j^{(2)}_g \to j^{(1)}_g$ corresponds to the replacement of the neutron form factors with proton form factors. The effect of the phase $-4\lambda'\lambda$ is an additional change in the sign of all j_2 type elements. Combining all of these effects allows us to obtain $j^{(2)+}_{\lambda'\lambda;g}(\mathrm{p}, \theta^*, q_0)$ from $j^{(1)+}_{\lambda'\lambda;g}(\mathrm{p}, \theta^*, q_0)$ by changing proton to neutron form factors, $q_0 \to -q_0$, $j_{1(0,s)} \to -j_{1(0,s)}$, $j_{2(0,s)} \to j_{2(0,s)}$, $j_{1a} \to j_{1a}$, and $j_{2a} \to -j_{2a}$. These phase changes are recorded through the factor δ shown in Table IV.

3. The hadronic structure functions

Substituting the form (B15) for the current into the expressions (B4) allows the sum over λ to be carried out. If $g = 0$ or s the result is

$$\begin{aligned} &(J_g)^{\lambda_d}_{\lambda_1\lambda_2}(p_1^*, p_2^*, q^*) \\ &= \sqrt{\frac{3}{16\pi}}\, \frac{1}{N_d} \sum_\rho \sum_{\lambda_1'\lambda_2'} \Big\{ \eta_\rho(4\lambda_1\lambda_1') \left[j^{(1)\rho}_{1g}\, \phi^\rho_{|\Lambda|}(\mathrm{p}_2)\, d^{(1/2)}_{\lambda_1' -\lambda_1}(\omega_2) + 2\lambda_1\, j^{(1)\rho}_{2g}\, \phi^\rho_{|\Lambda|}(\mathrm{p}_2)\, d^{(1/2)}_{\lambda_1'\lambda_1}(\omega_2) \right] \mathcal{Y}_2 \\ &\qquad -\eta_\rho(4\lambda_2\lambda_2') \left[j^{(2)\rho}_{1g}\, \phi^\rho_{|\Lambda|}(\mathrm{p}_1)\, d^{(1/2)}_{\lambda_2' -\lambda_2}(\omega_1) + 2\lambda_2\, j^{(2)\rho}_{2g}\, \phi^\rho_{|\Lambda|}(\mathrm{p}_1)\, d^{(1/2)}_{\lambda_2'\lambda_2}(\omega_1) \right] \mathcal{Y}_1 \Big\}, \end{aligned} \tag{B17}$$

where

$$\begin{aligned} \mathcal{Y}_2 &= d^{(1/2)}_{\lambda_2'\lambda_2}(\omega_2)\, d^{(1)}_{\Lambda, \lambda_d}(\theta_2 - \pi) \\ \mathcal{Y}_1 &= d^{(1/2)}_{\lambda_1'\lambda_1}(\omega_1)\, d^{(1)}_{-\Lambda, \lambda_d}(\theta_1)\,. \end{aligned} \tag{B18}$$

If $g = a$ the phase $2\lambda_1$ in the first square bracket multiplies $j^{(1)\rho}_{1g}$ instead of $j^{(1)\rho}_{2g}$, and the phase $2\lambda_2$ in the second square bracket multiplies $j^{(2)\rho}_{1g}$ instead of $j^{(2)\rho}_{2g}$. This different phase insures that there is no interference between J_a and the other components of the current; J_a contributes only quadratically in the term $J_a\, J_a^\dagger$.

The unpolarized hadronic structure functions are now obtained by squaring the current (B17), summing over final hadron helicities and averaging over the initial deuteron helicity, and multiplying by the kinematic factors given in Eq. (2.38). The structure functions $R^{(\mathrm{II})}$ are identically zero in the RIA. The others are proportional to

$$\left\langle J_g\, J^\dagger_{g'} \right\rangle = \sum_{\lambda_1\lambda_2\lambda_d} (J_g)^{\lambda_d}_{\lambda_1\lambda_2}(p_1^*, p_2^*, q^*) (J^\dagger_{g'})^{\lambda_d}_{\lambda_1\lambda_2}(p_1^*, p_2^*, q^*) \tag{B19}$$

This generates three terms: the proton contribution (proportional to $[j^{(1)}]^2$), the neutron contribution (proportional to $[j^{(2)}]^2$), and an interference term (proportional to $j^{(1)} \times j^{(2)}$).

The proton and neutron terms simplify easily. The sum over λ_d and λ_2 (for the proton term) or λ_1 (for the neutron term) collapses the sum over λ_1' and λ_2' (associated with J_g and the sum over λ_1'' and λ_2'' (associated with $J_{g'}^\dagger$) reducing the "diagonal" terms to

$$\left\langle J_g\, J_{g'}^\dagger \right\rangle\Big|_i = \frac{3}{16\pi\, N_d^2} \sum_{\substack{\lambda_1'\lambda_2' \\ \lambda}} \Big\{ \left[-4\lambda_1'\lambda\, j_{1g}^{(i)+}\, \phi_{|\Lambda|}^+(\mathrm{p}_j) + j_{1g}^{(i)-}\, \phi_{|\Lambda|}^-(\mathrm{p}_j) \right] d_{-\lambda_1'\lambda}^{(1/2)}(\omega_j) + \left[2\lambda\, j_{2g}^{(i)+}\, \phi_{|\Lambda|}^+(\mathrm{p}_j) - 2\lambda_1'\, j_{2g}^{(i)-}\, \phi_{|\Lambda|}^-(\mathrm{p}_j) \right] d_{\lambda_1'\lambda}^{(1/2)}(\omega_j) \Big\} \times \Big\{ g \to g' \Big\} \quad \text{(B20)}$$

where $i = 1$ (for the proton) or 2 (for the neutron), $j = 1$ or 2 (but $j \neq i$), and we used $d_{\lambda_1' -\lambda}^{(1/2)}(\omega_i) = -4\lambda_1'\lambda\, d_{-\lambda_1'\lambda}^{(1/2)}(\omega_i)$. Next, using the identities

$$\begin{aligned} \sum_\lambda d_{-\lambda_1'\lambda}^{(1/2)}(\omega_j) d_{-\lambda_1'\lambda}^{(1/2)}(\omega_j) &= 1 = \sum_\lambda d_{\lambda_1'\lambda}^{(1/2)}(\omega_j) d_{\lambda_1'\lambda_1}^{(1/2)}(\omega_j) \\ \sum_\lambda 2\lambda\, d_{a\lambda}^{(1/2)}(\omega_j) d_{b\lambda}^{(1/2)}(\omega_j) &= d_{-ab}^{(1/2)}(\pi - 2\omega_j) = 2b\, d_{ab}^{(1/2)}(2\omega_j) \\ \sum_\lambda d_{\lambda_1'\lambda}^{(1/2)}(\omega_j) d_{-\lambda_1'\lambda}^{(1/2)}(\omega_j) &= 0\,, \end{aligned} \quad \text{(B21)}$$

and $(2\lambda)^2 = 1$, gives

$$\left\langle J_g\, J_{g'}^\dagger \right\rangle\Big|_i = \frac{3}{16\pi\, N_d^2} \sum_{\lambda_1'\lambda_2'} \Big\{ J_{gg'}^{(i)+} \left[\phi_{|\Lambda|}^+(\mathrm{p}_j) \right]^2 + J_{gg'}^{(i)-} \left[\phi_{|\Lambda|}^-(\mathrm{p}_j) \right]^2 + \left(J_{gg'}^{(i)c} \cos\omega_j + J_{gg'}^{(i)s} \sin\omega_j \right) \left[\phi_{|\Lambda|}^+(\mathrm{p}_j)\, \phi_{|\Lambda|}^-(\mathrm{p}_j) \right] \Big\} \quad \text{(B22)}$$

where the currents $J_{gg'}$ were given in Eq. (2.39). Since these currents do not depend on the helicities, we may complete the sums using

$$\sum_{\lambda_1'\lambda_2'} \phi_{|\Lambda|}^\rho(\mathrm{p}_j)\, \phi_{|\Lambda|}^{\rho'}(\mathrm{p}_j) = 2 \left[\phi_0^\rho(\mathrm{p}_j)\, \phi_0^{\rho'}(\mathrm{p}_j) + \phi_1^\rho(\mathrm{p}_j)\, \phi_1^{\rho'}(\mathrm{p}_j) \right]. \quad \text{(B23)}$$

This gives the result reported in Eq. (2.38).

The interference term does not simplify as nicely. The sums over λ_d, λ_1, and λ_2 can be carried out, but there are no delta functions to collapse the remaining four sums. The result is

$$\left\langle J_g\, J_{g'}^\dagger \right\rangle\Big|_{12} = \frac{3}{16\pi\, N_d^2} \sum_{\substack{\lambda_1'\lambda_2' \\ \lambda_1''\lambda_2''}} d_{\Lambda -\Lambda'}^{(1)}(\theta_2 - \pi - \theta_1) \left[J_g^{(1)}\, J_{g'}^{(2)} + J_{g'}^{(1)}\, J_g^{(2)} \right] \quad \text{(B24)}$$

where $\Lambda = \lambda_1' + \lambda_2'$, $\Lambda' = \lambda_1'' + \lambda_2''$, and

$$\begin{aligned} J_g^{(1)} &= \left[-2\lambda_1'\, j_{1g}^{(1)+}\, d_{\lambda_1'\lambda_1''}^{(1/2)}(\delta_+) + j_{2g}^{(1)+}\, d_{-\lambda_1'\lambda_1''}^{(1/2)}(\delta_+) \right] \phi_{|\Lambda|}^+(\mathrm{p}_2) \\ &\quad + \left[j_{1g}^{(1)-}\, d_{-\lambda_1'\lambda_1''}^{(1/2)}(\delta_-) - 2\lambda_1'\, j_{2g}^{(1)-}\, d_{\lambda_1'\lambda_1''}^{(1/2)}(\delta_-) \right] \phi_{|\Lambda|}^-(\mathrm{p}_2) \\ J_{g'}^{(2)} &= \left[-2\lambda_2''\, j_{1g'}^{(2)+}\, d_{\lambda_2''\lambda_2'}^{(1/2)}(\delta_+) + j_{2g'}^{(2)+}\, d_{-\lambda_2''\lambda_2'}^{(1/2)}(\delta_+) \right] \phi_{|\Lambda'|}^+(\mathrm{p}_1) \\ &\quad + \left[j_{1g'}^{(2)-}\, d_{-\lambda_2''\lambda_2'}^{(1/2)}(-\delta_-) - 2\lambda_2''\, j_{2g'}^{(2)-}\, d_{\lambda_2''\lambda_2'}^{(1/2)}(-\delta_-) \right] \phi_{|\Lambda'|}^-(\mathrm{p}_1). \end{aligned} \quad \text{(B25)}$$

APPENDIX C: KINEMATIC SINGULARITY IN THE LAB CROSS SECTIONS

In Sec. II B it was shown that, if $x > 1$, the lab angle, θ_1, reaches a maximum value in the first quadrant, leading to the condition (2.20). In this Appendix we show that this condition generates a true singularity in the lab cross section [suggested by Eq. (2.21)], but that, because of the finite resolution of any detector, all observable cross sections remain finite.

Mathematically, this singularity arises from a zero in the recoil factor $\mathcal{R}$ defined in Eq. (2.8). The denominator of Eq.(2.8) vanishes if

$$E_W \, \mathrm{p}_1 = E_1 \, q_L \cos\theta_1 \,, \tag{C1}$$

where $E_W = M_d + \nu = \sqrt{W^2 + q_L^2}$ is the energy of the final np pair in the lab frame. We will first show that the condition that this denominator vanish is identical to the condition (2.20).

To see this, it is convenient differentiate $\cos\theta_1$ with respect to θ^*. Using Eq. (2.17) gives

$$\begin{aligned}
\frac{d\cos\theta_1}{d\theta^*} = \frac{d}{d\theta^*}\left(\frac{\mathrm{p}_1^z}{\mathrm{p}_1}\right) &= \frac{\mathrm{p}E_W \sin\theta^*}{\mathrm{p}_1 W} - \frac{\mathrm{p}_1^z}{2\mathrm{p}_1^3}\left[\frac{E_W}{W} q_L \mathrm{p}\sin\theta^* + \frac{q_L^2}{W^2} 2\mathrm{p}^2 \cos\theta^* \sin\theta^*\right] \\
&= \frac{\mathrm{p}\sin\theta^*}{\mathrm{p}_1^2 W}\left\{E_W \mathrm{p}_1 - q_L \cos\theta_1 \left[\frac{1}{2}E_W + \frac{q_L}{W}\mathrm{p}\cos\theta^*\right]\right\} \\
&= \frac{\mathrm{p}\sin\theta^*}{\mathrm{p}_1^2 W}\left\{E_W \mathrm{p}_1 - q_L \cos\theta_1 E_1\right\} \,,
\end{aligned} \tag{C2}$$

where, in the last step we used

$$E_1 = \frac{1}{2}E_W + \frac{q_L}{W}\mathrm{p}\cos\theta^* \,, \tag{C3}$$

easily obtained form the same boost that gave Eq. (2.17). Equation (C2) shows that the two conditions (2.20) and (C1) are equivalent (except when $\sin\theta^* = 0$, when there is no singularity).

It is instructive to see how the cosine,

$$z_L = \cos\theta_1 = \frac{\mathrm{p}_1^z}{\sqrt{\mathrm{p}_1^{z\,2} + \mathrm{p}^2 \sin^2\theta^*}} = \frac{q_L W + 2\mathrm{p}E_W \, z}{\sqrt{q_L^2 W^2 + 4q_L \mathrm{p} W E_W \, z + 4\mathrm{p}^2 q_L^2 \, z^2 + 4\mathrm{p}^2 W^2}} \,, \tag{C4}$$

of the proton lab angle, θ_1, varies with $z = \cos\theta^*$. For fixed x and Q^2, z_L depends only on z as given by Eq. (C4). As an example, Fig. 22 shows how z_L varies with z for selected values of x when $Q^2 = 3$. The value of z at which z_L is a minimum, denoted z_{crit} can be computed from Eq. (C4). In the approximation that $m_n = m_p = m$ we obtain

$$z_{crit} = -\frac{\sqrt{(W^2 + q_L^2)(W^2 - 4m^2)}}{W q_L} \,. \tag{C5}$$

Moreover, solving Eq. (C1) for z gives the *same* value, and hence we recover again the observation that the singularity occurs at the kinematic boundary of $\cos\theta_1$.

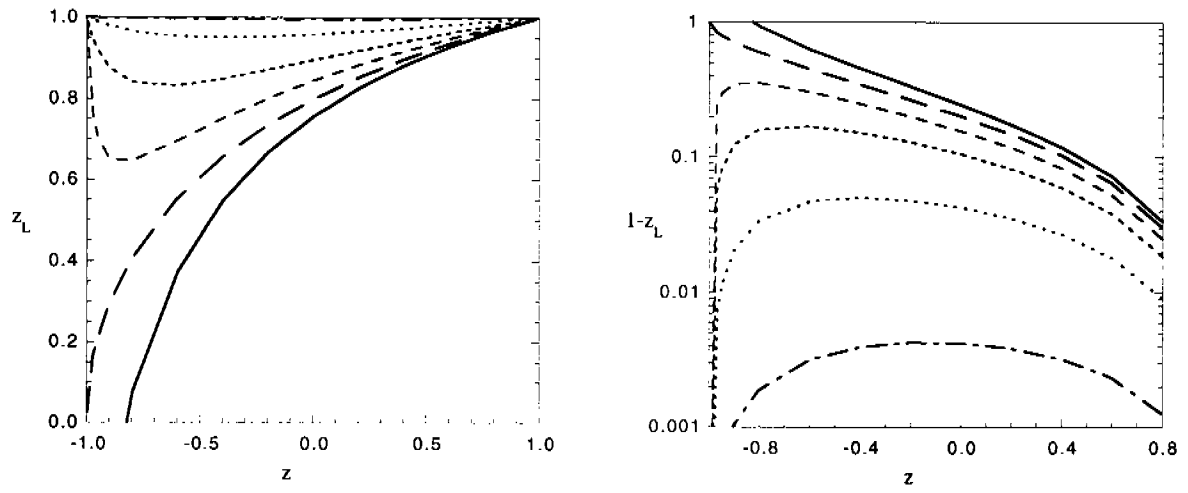

FIG. 22: The left panel shows $z_{_L} = \cos\theta_1$ as a function of $z = \cos\theta^*$ and the right panel shows $1 - z_{_L}$. In all cases $Q^2 = 3$ GeV^2, $M_d = 2$ GeV, $m = 1$ GeV, and the lines show $x = 0.5$ (solid), $x = 1.0$ (very long dashes), $x = 1.25$ (long dashes), $x = 1.5$ (dashed), $x = 1.8$ (dotted), and $x = 1.98$ (dot-dashed).

The values of E_1, p_1 and $z_{_L}$ at the critical point can be found using the additional constraint that follows from energy conservation. Energy conservation gives the following general formula for $z_{_L}$:

$$z_{_L} = \frac{q_{_L}^2 + m_n^2 - m_p^2 + 2E_1(M_d + \nu) - (M_d + \nu)^2}{2\mathrm{p}_1 q_{_L}} = \frac{2E_W E_1 - \tilde{W}^2}{2\mathrm{p}_1 q_{_L}}\,, \tag{C6}$$

where we have defined $\tilde{W}^2 = W^2 - m_n^2 + m_p^2$. For fixed electron kinematics, Eqs. (C1) and (C6), taken together, give the proton energy E_0, proton momentum p_0 and angle z_0 at which the denominator (C1) is singular:

$$E_0 = \frac{2m_p^2\, E_W}{\tilde{W}^2}\,, \quad \mathrm{p}_0 = \frac{m_p}{\tilde{W}^2}\sqrt{4E_W^2\, m_p^2 - \tilde{W}^4}\,, \quad z_0 = \frac{\sqrt{4E_W^2\, m_p^2 - \tilde{W}^4}}{2m_p q_{_L}}\,. \tag{C7}$$

Of course, the value of E_0 must be physical, i.e. the denominator has to be positive and $E_0 \geq m_p$. The first condition leads to the constraint

$$W^2 > m_n^2 - m_p^2\,, \tag{C8}$$

which is always satisfied, while the second one requires

$$Q^2 \geq 2\nu(m_n - \epsilon_d) - \epsilon_d(2m_n - \epsilon_d) \simeq \frac{Q^2}{x}\,, \tag{C9}$$

where $M_d = m_p + m_n - \epsilon_d$ and in the last step we put $m_n \simeq m_p \simeq m$, $\epsilon_d \simeq 0$, and $\nu = Q^2/(2mx)$. This is the mathematical proof that the differential cross section is singular if and only if $x > 1$.

We conclude this discussion by showing that, even though the cross section is singular, the physical observables obtained from it are not. Because *any* measuring apparatus must necessarily have a *finite* resolution, all physical measurements must necessarily *average* the differential cross section (2.1) over this finite resolution. At the kinematic boundary this average is

$$\left\langle \frac{d^5\sigma}{d\Omega' dE' d\Omega_1} \right\rangle_{\epsilon} \equiv \frac{1}{z_0\epsilon} \int_{z_0}^{z_0(1+\epsilon)} \left(\frac{d^5\sigma}{d\Omega' dE' d\Omega_1} \right) dz_{_L}\,. \tag{C10}$$

This average will be finite only if the singularity is integrable, and this will now be shown explicitly. That it must be so follows from general physical considerations, and also from the behavior of the differential cross section in the c.m. frame, where there is a smooth, non-singular behavior for all kinematical conditions. In the lab frame, for fixed electron kinematics, the z_L dependent part of the integrand is contained in the kinematic factors

$$\mathrm{p_1}\,\mathcal{R}\left\{\tilde{R}_L^{(\mathrm{I})}+\ldots\right\}=\frac{W\mathrm{p_1^2}}{E_W\,\mathrm{p_1}-E_1\,q_L\,z_L}\left\{\tilde{R}_L^{(\mathrm{I})}+\ldots\right\} \tag{C11}$$

At first glance, if we assume that the factor $\mathrm{p_1}\,\mathcal{R}$ is an analytical function of z_L, Eq. (C1) suggests that the singularity will be a simple pole, which is not integrable. However, it is easy to show that the dependence of $\mathrm{p_1}\,\mathcal{R}$ on z_L is not analytic. Begin by using (C3) to rewrite Eq. (C4)

$$z_L=\frac{aE_1-b}{\mathrm{p_1}}\ ,\ a=\frac{E_W}{q_L}\ ,\ b=\frac{\tilde{W}^2}{2q_L}\,, \tag{C12}$$

and solve this equation for $\mathrm{p_1}$ as a function of z_L (recalling that a and b depend only on the electron variables and are not functions of z_L). The result is

$$\mathrm{p_1}=\frac{z_Lb+a\sqrt{b^2+(z_L^2-a^2)m_p^2}}{a^2-z_L^2}=\frac{z_Lb+am_p\sqrt{z_L^2-z_0^2}}{a^2-z_L^2}\,, \tag{C13}$$

where we used (C7) to express z_0 in terms of a and b

$$z_0=\frac{\sqrt{a^2m_p^2-b^2}}{m_p}\ . \tag{C14}$$

From (C13) we obtain the following expression for the energy E_1

$$E_1=\frac{m_pz_L\sqrt{z_L^2-z_0^2}+ba}{a^2-z_L^2}\ . \tag{C15}$$

Substituting (C13) and (C15) into the recoil factor we obtain

$$\mathrm{p_1}\,\mathcal{R}=\frac{W\mathrm{p_1^2}}{E_W\,\mathrm{p_1}-E_1\,q_L\,z_L}=\frac{W\mathrm{p_1^2}}{m_p\,q_L\sqrt{z_L^2-z_0^2}}\,. \tag{C16}$$

From this it is clear that in the vicinity of the end point singularity at z_0, the cross section Eq. (C10) behaves as $1/\sqrt{z_L^2-z_0^2}$ and the singularity is integrable.

---

[1] M. Croissiaux, Phys. Rev. **127**, 613 (1962).
[2] S. Frullani and J. Mougey, Advances in Nuclear Physics, **14**, 1 (1984).
[3] M. Bernheim *et al.*, Nucl. Phys. **A365**, 349 (1981).
[4] S. Turck-Chieze *et al.*, Phys. Lett. **142B**, 145 (1984).
[5] H. Breuker *et al.*, Nucl. Phys. **A455**, 641 (1986).

[6] K.I. Blomqvist *et al.*, Phys. Lett. B **424**, 33 (1998).
[7] M. van der Schaar *et al.*, Phys. Rev. Lett. **68**, 776 (1992).
[8] T. Tamae *et al.*, Phys. Rev. Lett. **59**, 2919 (1987).
[9] M. van der Schaar *et al.*, Phys. Rev. Lett. **66**, 2855 (1991).
[10] F. Frommberger *et al.*, Phys. Lett. B **339**, 17 (1994).
[11] J.E. Ducret *et al.*, Phys. Rev. C **49**, 1783 (1994).
[12] H.J. Bulten *et al.*, Phys. Rev. Lett. **74**, 4775 (1995).
[13] D. Jordan *et al.*, Phys. Rev. Lett. **76**, 1579 (1996).
[14] A. Pellegrino *et al.*, Phys. Rev. Lett. **78**, 4011 (1997).
[15] W.-J. Kasdorp *et al.*, Phys. Lett. B **393**, 42 (1997).
[16] Z.-L. Zhou *et al.*, Phys. Rev. Lett. **87**, 172301 (2001).
[17] G. Beck and H. Arenhövel, Few-Body Syst. **13**, 165 (1992);
T. Wilbois, G. Beck and H. Arenhövel, Few-Body Syst. **15**, 39 (1993);
G. Beck, T. Wilbois, and H. Arenhövel, Few-Body Syst. **17**, 91 (1994).
[18] L. Durand, III, Phys. Rev. **123**, 1393 (1961).
[19] I. McGee, Phys. Rev. **158**, 1500 (1967); *ibid.* **161**, 1640 (1967).
[20] J. Tjon, Few-Body Syst. Suppl, **5**, 5 (1992).
[21] V. Dmitrašinović and Franz Gross, Phys. Rev. **C40**, 2479 (1989); Phys. Rev. **C43**, 1495(E) (1991).
[22] G.R. Goldstein and M.J. Moravcsik, Nucl. Instrum. Methods A **240**, 43 (1985).
[23] H. Arenhövel, W. Leidemann, E. L. Tomusiak, Few-Body Syst. **15**, 109 (1993).
V. Dmitrasinovic and F. Gross, Few Body Syst. **20**, 41 (1996).
[24] F. Gross, J. W. Van Orden, and K. Holinde, Phys. Rev. C **45**, 2094 (1992).
[25] J. W. Van Orden, N. Devine, and Franz Gross, Phys. Rev. Lett. **75**, 4369 (1995).
[26] F. Gross, invited talk published in the proceedings of the *topical workshop on Two-Nucleon Emission Reactions*, edited by O. Benhar and A. Fabrocini, ETS Editrice, Pisa (1990), p. 242.
F. Gross, Czech J. Phys. **B39**, 871 (1989).
[27] R. J. Glauber, in Lectures in Theoretical Physics, edited by W. Brittin and L. G. Dunham (Interscience, New York, 1959), Vol. I;
S. Jeschonnek and T. W. Donnelly, Phys. Rev. **C59**, 2676 (1999);
A. Bianconi, S. Jeschonnek, N. N. Nikolaev, and D. G. Zakharov, Phys. Lett. **B343**, 13 (1995);
L. L. Frankfurt, M. M. Sargsian, and M. I. Strikman, Phys. Rev. **C56**, 1124 (1997).
[28] I. Fachruddin, C. Elster, and W. Glockle, preprint nucl-th/0104027.
[29] M. Jacob and G. C. Wick, Ann. Phys. (N.Y.) **7**, 404 (1959).
[30] W. W. Buck and Franz Gross, Phys. Rev. D **20**, 2361 (1979).
[31] R. Blankenbecler and L.F. Cook, Jr., Phys. Rev. **119**, 1745 (1960).
[32] F. L. Gross and D. O. Riska, Phys. Rev. C **36**, 1928 (1987).
[33] Z. Batiź and F. Gross, Phys. Rev. C **58**, 2963 (1998).
[34] S. Jeschonnek and J. W. Van Orden, Phys. Rev. C **62**, 044613 (2000).
[35] R. B. Wiringa, V. G. J. Stoks, and R. Schiavilla, Phys. Rev. **C51**, 38 (1995).
[36] J. Adam, Jr., H. Arenhövel, Nucl. Phys. **A598**, 462 (1996); Nucl. Phys. **A 614**, 289 (1997).
[37] J. L. Friar, B. F. Gibson and G. L. Payne, Phys. Rev. **C30**, 441 (1984).
[38] J. L. Friar, Ann. Phys. (N.Y.) **81** (1973) 332; Nucl. Phys. **A264**, 455 (1976).
[39] J. E. Amaro and T. W. Donnelly, Ann. Phys. **263**, 56 (1998);
S. Jeschonnek and T. W. Donnelly, Phys. Rev. C **57**, 2438 (1998).
[40] F. Ritz, H. Göller, T. Wilbois, and H. Arenhövel, Phys. Rev. **C55**, 2214 (1997).

H. Arenhövel, W. Leidemann, E. L. Tomusiak, Phys. Rev. **C52**, 1232 (1995).
[41] R. A. Krajcik and L. L. Foldy, Phys. Rev. **D10**, 1777 (1974).
[42] J. E. Amaro, M. B. Barbaro, J. A. Caballero, T. W. Donnelly, and A. Molinari, Nucl. Phys. **A643**, 349 (1998)
[43] P.E. Ulmer, computer program MCEEP, *Monte Carlo for (e,e'p) Experiments*, JLAB Technical Note # 91-101 (1991).
[44] E. Borie and D. Drechsel, Nucl. Phys. **A167**, 369 (1971).
[45] S. Jeschonnek and T. W. Donnelly, Phys. Rev. C **57**, 2438 (1998).
[46] J.W. Van Orden, private communication; P. Mergell, Ulf-G. Meissner and D. Drechsel, Nucl. Phys. **A596**, 367 (1996).
[47] A. Stadler, F. Gross, and M. Frank, Phys. Rev. **C56**, 2396 (1997).
[48] Y. Surya and F. L. Gross, Phys. Rev. **C53**, 2422 (1996).